FATIGUE AT HIGH TEMPERATURE

STP 459

AMERICAN SOCIETY FOR TESTING AND MATERIALS

FATIGUE AT HIGH TEMPERATURE

A symposium
presented at the
Seventy-first Annual Meeting
AMERICAN SOCIETY FOR
TESTING AND MATERIALS
San Francisco, Calif., 23-28 June, 1968

ASTM SPECIAL TECHNICAL PUBLICATION 459

List price $11.25

AMERICAN SOCIETY FOR TESTING AND MATERIALS
1916 Race Street, Philadelphia, Pa. 19103

Library of Congress Catalog Card Number: 72-89673
SBN 8031-0016-7

NOTE

The Society is not responsible, as a body,
for the statements and opinions
advanced in this publication.

Printed in Lutherville-Timonium, Md.
November 1969

Foreword

This Special Technical Publication contains most of the papers presented at a Symposium on Fatigue at High Temperature held in San Francisco, Calif., during the Seventy-first Annual Meeting of ASTM, 23-28 June 1968. The topic was chosen because of its current timeliness and interest to those seeking answers to pressing questions regarding elevated temperature material behavior. The sponsor of this symposium was the Task Group on Fatigue under Cyclic Strain, now Subcommittee VIII of the E-9 Committee on Fatigue. L. F. Coffin, Jr., General Electric Company Research and Development Center, presided as symposium chairman.

Related
ASTM Publications

Electron Fractography, STP 436 (1968), $11.00

Fatigue Crack Propagation, STP 415 (1967), $30.00

Contents

Introduction

The origin of interest in the subject of fatigue at high temperature is far from academic. High temperature is becoming a way of life with more and more of our engineering structures, and the means for accounting for the many effects which high temperature introduces must find its way into design criteria. Information generated on this subject can be applied in many areas in our advancing technology. Examples include the aircraft gas turbine, diesel engine, steam turbine, nuclear reactor, land-based gas turbine, and many other important applications. In each of these cases it is the design objective to provide reliable performance with a minimum of down time and cost of repair. Fatigue is encountered in these applications in several ways. One source is vibration as a consequence of rotation, or of fluid motion, and failure may result after a large number of stress cycles. Another source of fatigue is a consequence of start and stop operation, and is identified generally as thermal or low-cycle fatigue. Here strain is the controlling variable, induced mostly by temperature effects, such as thermal mismatch, temperature transients, etc.

In conjunction with these effects, high temperature introduces a number of complications. Included are:

(*a*) Gaseous or liquid environments introduce surface reactions which interact strongly with fatigue cracks to accelerate crack initiation, growth, and failure.

(*b*) Long hold-time periods between cycles introduce creep effects which interact with fatigue, often by changing the mode of crack propagation from the more ductile transgranular mode to the more brittle intergranular type.

(*c*) The material may change its properties with long times at temperature due to aging and phase instability effects or to creep damaging mechanisms.

(*d*) Thermal cycling introduces complications regarding predictions of stresses and strains and uncertainty regarding the interaction of temperature cycling and strain cycling.

These complications serve as a basis for identifying problem areas for fatigue investigation. It is clear that many disciplines are involved here, including those of the surface chemist, metallurgist, and mechanical engineer. In the papers that are included in this Special Technical Publication some of these problem areas are brought into focus. Particular attention is given to the effect of hold time, that is, where the strain is held constant for fixed intervals of time during the cyclic strain program.

It will become apparent, in reading over these papers, that testing technique is an important element in elevated temperature fatigue studies. Control of atmosphere, measurement of strain, control of the test to follow some predetermined strain-time program, and temperature control are some of the special areas where much attention has been given. Some insight into the current state of the art of mechanical testing is provided in close examination of the several papers.

On behalf of the E-9 Committee on Fatigue, I would like to thank the many authors for their willingness to contribute to this symposium. It is only through their efforts that this publication has come into being.

L. F. Coffin, Jr.
Mechanical engineer, Metallurgy and Ceramics Laboratory, General Electric Company Research and Development Center, Schnectady, N.Y.; symposium chairman.

J. T. Berling[1] *and T. Slot*[2]

Effect of Temperature and Strain Rate on Low-Cycle Fatigue Resistance of AISI 304, 316, and 348 Stainless Steels

REFERENCE: Berling, J. T. and Slot, T., "**Effect of Temperature and Strain Rate on Low-Cycle Fatigue Resistance of AISI 304, 316, and 348 Stainless Steels,**" *Fatigue at High Temperature*, *ASTM STP 459*, American Society for Testing and Materials, 1969, pp. 3–30.

ABSTRACT: Results are reported of strain-controlled, low-cycle fatigue experiments conducted on annealed AISI 304, 316, and 348 stainless steels at temperatures of 430, 650, and 816 C with strain rates of approximately 4×10^{-3}, 4×10^{-4}, and 4×10^{-5} s^{-1}. The investigation generally shows that fatigue life measured in terms of sustained loading cycles is affected adversely by the increase in temperature and by the decrease in strain rate. The test results were generated with servo-controlled, hydraulic testing machines using inductively heated hourglass-type specimens. Cyclic stress-strain data are compared with monotonic stress-strain data obtained from tension tests performed at the same temperatures and strain rates.

KEY WORDS: fatigue (materials), elevated temperature, cyclic loads, strain measurement, stress-strain diagrams, stainless steel, evaluation, tests

Nomenclature

Δ	Symbol denoting double amplitude (range)
ϵ_t	Axial strain $= \epsilon_p + \epsilon_e$
ϵ_p	Plastic component of axial strain
ϵ_e	Elastic component of axial strain
ϵ_d	Diametral strain (transverse strain) $= \epsilon_{dp} + \epsilon_{de}$
ϵ_{dp}	Plastic component of diametral strain $= -\nu_p \epsilon_p$
ϵ_{de}	Elastic component of diametral strain $= -\nu_e \epsilon_e$
$\dot{\epsilon}_t$	Axial strain rate
$\dot{\epsilon}_d$	Diametral strain rate
ϵ_f	Tensile ductility $= \log_e(A_o/A_f) = \log_e[1/(1 - RA)]$

[1] Test engineer, Nuclear Systems Programs, General Electric Co., Cincinnati, Ohio. 45215.

[2] Manager, Structures and Materials Laboratory, Knolls Atomic Power Laboratory, General Electric Co., Schenectady, N. Y. 12305.

σ	Axial stress
σ_u	Tensile strength
ν_e	Poisson's ratio for elastic deformation
ν_p	Poisson's ratio for plastic deformation (0.5)
E	Modulus of elasticity
A_o	Initial area of cross section
A_f	Area of cross section after fracture
RA	Reduction of area $= (A_o - A_f)/A_o$
c, m	Material constants (Coffin-Manson formula)
N_f	Number of loading cycles to complete fracture (fatigue life)
N_0, N_5	Number of cycles defined in paper (fatigue life)
f	Loading frequency
T	Temperature
T_m	Melting temperature
t	Time

In the last several years there has been a marked increase in the research effort aimed at a better understanding of the time-dependent mechanical and metallurgical behavior of structural materials under cyclic loading conditions at temperatures in the creep range. Evidence of such effort is found in the program of this symposium, which includes several papers concerned with the effects of strain rate and hold time on the fatigue resistance of various materials at elevated temperatures. Other recent investigations of these effects were reported at the International Conference on Thermal and High-Strain Fatigue [*1*],[3] London, June 1967, and at the National Metals Congress of the Society for Metals, Cleveland, Oct. 1967. Papers concerned with current work in the area of high-temperature fatigue were presented also at a recent meeting of the Society for Experimental Stress Analysis, Ottawa, May 1967 [*2, 3*].

A number of investigations on the effect of strain rate has shown that low-cycle fatigue resistance at elevated temperature tends to be affected adversely by a reduction in strain rate or in loading frequency [*4-16*]. It is the purpose of the present paper to report test results obtained on three austenitic steels that also exhibit a decrease in fatigue life with a decrease in strain rate. Specifically, the results are presented of strain-controlled fatigue tests performed on annealed AISI 304, 316, and 348 stainless steel at temperatures of 430 C (800 F), 650 C (1200 F), and 816 C (1500 F), with strain rates of approximately 4×10^{-3}, 4×10^{-4}, and 4×10^{-5} s^{-1}. The number of cycles to fracture in these tests ranged from 100 to 100,000.

The work reported was carried out in the course of a research program on low-cycle fatigue properties of temperature-resistant materials being spon-

[3] The italic numbers in brackets refer to the list of references appended to this paper.

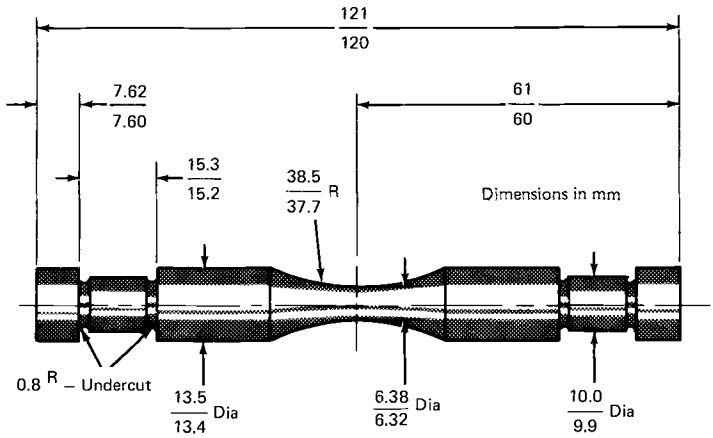

FIG. 1—*Dimensions of low-cycle fatigue specimen.*

sored by the U. S. Atomic Energy Commission (USAEC)[4] at the Nuclear Systems Programs Department[5] of the General Electric Co. This program was originally proposed to the USAEC by the Subcommittee on Plastic Fatigue Strength of the Pressure Vessel Research Committee and by the Task Force on Fatigue of the Special Committee to Review Code Stress Basis of the American Society of Mechanical Engineers.

Testing Procedure

An earlier paper [*3*] by Slot and Stentz dealt with the experimental methods and testing facility developed for carrying out the aforementioned research program. The testing procedure consists essentially of subjecting a round specimen with a gage section in the shape of an hourglass to programmed push-pull loading on a servo-controlled, hydraulic testing machine. In Fig. 1, a sketch is shown of the specimen geometry. The "buttonheads" of the specimen are clamped in fixtures of the die-set type, such that they are in a state of compression throughout the fatigue test. The fixtures were designed to maintain the axial alignment of the ends of the specimen during the test without reliance on the precision and rigidity of the testing machines. Heating of the specimen is accomplished by means of an induction coil that surrounds the gage section. The geometry of the coil was chosen to give a flat axial temperature profile in the gage section, while leaving sufficient room for transverse strain measurements to be made at the minimum diameter with a specially-developed strain sensor.

[4] Fuels and Materials Branch, Division of Reactor Development and Technology, Contract AT(40-1)-2847.

[5] Formerly, Nuclear Materials and Propulsion Operation.

The strain sensor furnishes an electronic signal proportional to the change in diameter, and a load cell in series with the specimen supplies a signal proportional to the load on the specimen. A computer network was developed that combines the two signals to provide an instantaneous signal proportional to the axial strain at the minimum diameter. The testing machines, therefore, can be operated with closed loop control of either diametral strain, axial strain, or stress in the specimen. It is also possible to program plastic strain instead of total strain. The mode of cycling also can be varied with respect to wave form, frequency, and the duration of hold periods in each cycle. A photograph of one of several fatigue testing machines being used in the research program is shown in Fig. 2. The plexiglas enclosure permits a test to be conducted in an inert gas environment instead of in air.

All fatigue tests reported here were performed in air and with diametral strain as the controlled test parameter. A triangular cyclic mode was chosen whereby the diametral strain varied linearly between two equal and opposite limits (zero mean strain). The frequency of loading was selected in accordance with desired magnitudes for strain range and strain rate through the relationship $f = \dot{\epsilon}_d/(2\Delta\epsilon_d)$. The axial strain was determined from the measured stress and diametral strain with the aid of the relation $\epsilon_t = (\sigma/E)(1 - \nu_e/\nu_p) - \epsilon_d/\nu_p$. This relation is obtained by elimination of ϵ_p from the basic relationships $\epsilon_t = \epsilon_p + \epsilon_e$ and $\epsilon_d = -\nu_p\epsilon_p - \nu_e\epsilon_e$, where $\epsilon_e = \sigma/E$. Values for E and ν_e were measured, and ν_p was assumed to be 0.5 on the basis of the constant volume condition associated with plastic deformation.

Most of the fatigue tests exhibited cyclic strain hardening in the early part of the test with a resulting increase in the stress range. However, after relatively few loading cycles the stress range reached a stationary value. In some tests, notably those at 430 C on AISI 316 and to a lesser extent those on AISI 304, strain hardening was followed by strain softening before the stress range became stationary. Cyclic strain hardening and softening actually produced only insignificant variation in the axial strain range, for these effects were most pronounced at high strain ranges, where the strain range was composed predominantly of plastic strain, so that changes in the elastic strain range had little effect on the conversion from diametral to axial strain. The value of the stress range at the halfway mark in the test ($N_f/2$) was used to compute the axial strain range.

Materials Characterization

The materials used in the manufacture of test specimens was supplied in the form of $\frac{5}{8}$-in. (16-mm) diameter rods by the Pacific Northwest Laboratory, which coordinates the procurement of materials for certain USAEC sponsored research programs [*17*]. Table 1 gives the chemical composition of the three stainless steels, and Table 2 provides a summary of the fabrication

FIG. 2—*Servo-controlled hydraulic fatigue testing machine.*

TABLE 1—*Chemical composition of three stainless steels used in test program.*[a]

Material	Heat	C	Mn	Si	Cr	Ni	Mo	Co	Sn	Cu	S	P	Nb	N_2
AISI 304.....	55 697 [*17a*]	0.051	0.83	0.47	18.30	9.50	0.18	...	0.004	0.21	0.012	0.020	...	0.034
AISI 316.....	65 808 [*17b*]	0.086	1.73	0.52	18.16	13.60	2.47	0.074	0.040	0.078	0.006	0.010	...	0.050
AISI 348.....	55 700 [*17a*]	0.04	1.67	0.51	17.52	9.67	0.06	0.018	0.009	0.06	0.009	0.014	0.58	0.037

[a] In weight percent.

TABLE 2—*Material and specimen fabrication history.*

Material	Vendor Processing	GE-NSP Processing	Grain Structure	Average ASTM Grain Size	Average VHN Hardness
AISI 304 [*17a*].....	billets 49 cm² cross-sectional area, rolled at 1180 C to rods 16 mm in diameter; rods coiled, annealed 60 min at 1066 C and water quenched; sections cut from coil, straightened, and cut to 1.5 m lengths; stress relieved 30 min at 1010 C and water quenched	specimens ground to hourglass configuration; surface of gage section longitudinally polished; annealed for 30 min at 1092 C in argon, cooling rate approximately 100 C/min	equiaxed	3 to 5	139
AISI 316 [*17b*].....	billets 7 cm² cross-sectional area, rolled at 1204 C to rods 16 mm in diameter; rods coiled, annealed 60 min at 1066 C, and water quenched; sections cut from coil, straightened, and cut to 1.5 m lengths	specimen blanks annealed 30 min at 1070 C in air and water quenched; specimens ground to hourglass configuration; surface of gage section longitudinally polished; stress relieved 60 min at 760 C in argon, cooling rate approximately 100 C/min	equiaxed	3 to 5	171
AISI 348 [*17a*].....	processing same as that used for AISI 304 stainless steel	processing same as that used for AISI 304 stainless steel specimens	duplex; fine grained core surrounded by a coarse-grained outer layer	fine 9 to 10 coarse 3 to 5	155

history of materials and specimens. Fatigue specimens were manufactured by centerless grinding, followed by longitudinal polishing of the gage section.

Tension tests performed on the rod material yielded the mechanical properties listed in Table 3. The temperatures and strain rates employed in these tests were the same as those in the fatigue experiments. (Some tensile data obtained at room temperature are included also in the table.)

The values reported for the modulus of elasticity (E) were measured on tension specimens having a cylindrical gage section, 0.25 in. (6.3 mm) round by 1 in. (25 mm) long. The specimens were tested on a closed-loop, servo-controlled, hydraulic testing machine equipped with a high-temperature furnace. Axial strain in the gage section was measured using a microformer-type extensometer with high-temperature extension arms. Loading of the specimens was limited in these tests to the elastic range, to permit accurate measurement of the effect of temperature and strain rate on a single specimen. As indicated in Table 3, no effect of strain rate on the value of E could be detected. Increasing the temperature had the effect of decreasing the modulus.

Regular fatigue specimens (Fig. 1) were used in conjunction with induction heating to obtain the values of Poisson's ratio (ν_e), the tensile strength (σ_u), and the reduction of area (RA). Poisson's ratio was determined with the aid of the diametral strain sensor used in the fatigue experiments [3]. Measurements on a single specimen tested in the elastic range produced no evidence of a strain rate effect on Poisson's ratio of the materials. However, it is apparent from Table 3 that its value did vary with temperature.

A modified version of the strain sensor was used for the measurement of diametral strain in tension tests carried to fracture. On account of the large deformation encountered in these tests, they were programmed in such a way that the true axial strain at the minimum diameter increased at the desired rate. (In the fatigue tests, the strain amplitudes were small enough to permit programming on the basis of engineering stress and strain.) The tensile strength was obtained by dividing the maximum load recorded in the test by the original cross-sectional area, the latter corrected for thermal expansion. Measurements of the reduction of area after fracture provided the fracture ductility values (ϵ_f) in Table 3, through the relation: $\epsilon_f = \log_e [1/(1 - RA)]$.

Inspection of the information in Table 3 shows that a hundredfold decrease in strain rate produced increases in the tensile strength at 430 C and decreases at 650 and 816 C. The table also shows that the decrease in strain rate generally resulted in lower values for the fracture ductility. However, a slight increase is noted for AISI 304 at 430 C and for AISI 348 at 816 C. In all but one case is the fracture ductility a minimum at 650 C, given the same strain rate. The exception is AISI 348, which exhibited for the highest strain rate a minimum at 430 C and a maximum at 816 C.

Fatigue Test Results

The objective of the fatigue tests was to determine the number of loading cycles to fracture as a function of temperature, strain amplitude, and strain rate for each of the three stainless steels. In interpreting the results of low-cycle fatigue tests, a suitable criterion for defining fatigue failure would be the number of cycles required to initiate a propagating crack. However, fatigue life based on such a criterion is difficult to measure in practice, even on a laboratory specimen when it is tested at elevated temperature in an oxidizing environment. For practical reasons, therefore, the authors chose to define fatigue life as the number of loading cycles to that point in the test where, due to the presence of one or more cracks, the load range had decreased by a certain percentage from its stationary value. Accordingly, the fatigue life defined in this paper as N_5 refers to the number of cycles required to produce a load range reduction of five percent. This particular number of cycles is determined readily from a continuous strip-chart recording of the load history in the test. The number of cycles sustained to complete fracture is called N_f.

In view of the large number of tests to be reported in this paper, it is practical only to present the fatigue test data in the form of diagrams, such as is done in Figs. 3 through 11. A compilation of numerical test data is available from a separate document [*18*]. That document also contains measured values of N_0, the number of cycles to the point in the test where the load range first starts to taper off.

The fatigue test results plotted in Fig. 3 show the correlation between total strain range ($\Delta\epsilon_t$) and fatigue life (N_5) at three temperatures for a strain rate of 4×10^{-3} s^{-1}, the highest strain rate employed. Diagrams (*a*), (*b*), and (*c*) of Fig. 3 include data for each of the steels and pertain to temperatures of 430, 650, and 816 C, respectively. Diagram (*d*) of Fig. 3 is a composite of the other three diagrams without distinction of material. This diagram is illustrative of a significant decrease in fatigue life with increase in temperature. It appears from diagram (*b*) that at 650 C, AISI 348 stainless steel has better fatigue resistance than the other two steels.

In Figs. 4 through 6, test results pertaining to the highest and lowest strain rates are compared with fatigue curves obtained by application of empirical formulas developed by Manson and Halford [*19*, *20*, *21*]. The curves shown for 430 C correspond to the equation $\Delta\epsilon_t = (3.5\ \sigma_u/E)N_f^{-0.12} + \epsilon_f^{0.6}N_f^{-0.6}$, where the values of σ_u, ϵ_f, and E are from Table 3. This equation was shown by Manson [*19*] to fit low-temperature fatigue data for many materials. Utilizing again the mechanical properties listed in Table 3, the curves shown for 650 and 816 C were determined by the procedure of Manson and Halford [*20*, *21*]. The equation for $\Delta\epsilon_t$ cited above was used to obtain the

TABLE 3—*Tensile properties of AISI 304, 316, and 348 stainless steel.*

Material	Temperature, deg C	$T\ ^{\circ}K$ / $T_m\ ^{\circ}K$	Strain Rate, $\dot{\epsilon}_t$, s^{-1}	Elastic Constants: E, 10^6 psi	E, 10^3 kg/mm²	ν_e	Ultimate Tensile Strength, σ_u: psi	σ_u: kg/mm²	Reduction of Area, RA, %	Tensile Ductility, ϵ_f, %
AISI 304.....	20	0.172	4×10^{-3}	28.7	20.2	0.264	...	...	...	...
	20	0.172	4×10^{-4}	28.7	20.2	0.264	...	...	...	...
	20	0.172	4×10^{-5}	28.7	20.2	0.264	...	...	...	..
	430	0.414	4×10^{-3}	23.4	16.5	0.282	62 400	43.9	64	102
	430	0.414	4×10^{-4}	23.4	16.5	0.282	...	...	...	...
	430	0.414	4×10^{-5}	23.4	16.5	0.282	64 600	45.4	64	103
	650	0.543	4×10^{-3}	21.6	15.2	0.315	45 600	32.1	42	55
	650	0.543	4×10^{-4}	21.6	15.2	0.315	...	..	...	...
	650	0.543	4×10^{-5}	21.6	15.2	0.315	35 000	24.6	33	41
	816	0.641	4×10^{-3}	18.8	13.2	0.323	25 000	17.6	51	71
	816	0.641	4×10^{-4}	18.8	13.2	0.323	...	...	..	...
	816	0.641	4×10^{-5}	18.8	13.2	0.323	13 400	9.4	32	39
AISI 316.....	20	0.177	4×10^{-3}	30.1	21.2	0.295	...	...	...	...
	20	0.177	4×10^{-4}	30.1	21.2	0.295	...	...	...	...

	20	0.177	4×10^{-5}	30.1	21.2	0.295	...	...	...	...
	430	0.424	4×10^{-3}	24.0	16.9	0.315	67 200	47.2	62	97
	430	0.424	4×10^{-4}	24.0	16.9	0.315	...	...	...	...
	430	0.424	4×10^{-5}	24.0	16.9	0.315	73 200	51.5	61	93
	650	0.557	4×10^{-3}	21.9	15.4	0.326	55 700	39.2	59	89
	650	0.557	4×10^{-4}	21.9	15.4	0.326	...	...	...	...
	650	0.557	4×10^{-5}	21.9	15.4	0.326	43 200	30.4	32	39
	816	0.657	4×10^{-3}	18.4	12.9	0.321	33 800	23.8	62	95
	816	0.657	4×10^{-4}	18.4	12.9	0.321	...	...	...	...
	816	0.657	4×10^{-5}	18.4	12.9	0.321	21 000	14.8	50	69
AISI 348.....	20	0.174	4×10^{-3}	28.2	19.8	0.250	...	...	...	...
	20	0.174	4×10^{-4}	28.2	19.8	0.250	...	...	...	...
	20	0.174	4×10^{-5}	28.2	19.8	0.250	...	...	...	...
	430	0.417	4×10^{-3}	23.8	16.7	0.275	59 600	41.9	66	109
	430	0.417	4×10^{-4}	23.8	16.7	0.275	...	...	...	...
	430	0.417	4×10^{-5}	23.8	16.7	0.275	65 600	46.1	57	86
	650	0.547	4×10^{-3}	21.8	15.3	0.295	46 700	32.8	69	116
	650	0.547	4×10^{-4}	21.8	15.3	0.295	...	...	...	...
	650	0.547	4×10^{-5}	21.8	15.3	0.295	40 800	28.7	40	52
	816	0.646	4×10^{-3}	19.0	13.4	0.340	25 900	18.2	83	175
	816	0.646	4×10^{-4}	19.0	13.4	0.340	...	...	...	...
	816	0.646	4×10^{-5}	19.0	13.4	0.340	17 800	12.5	84	183

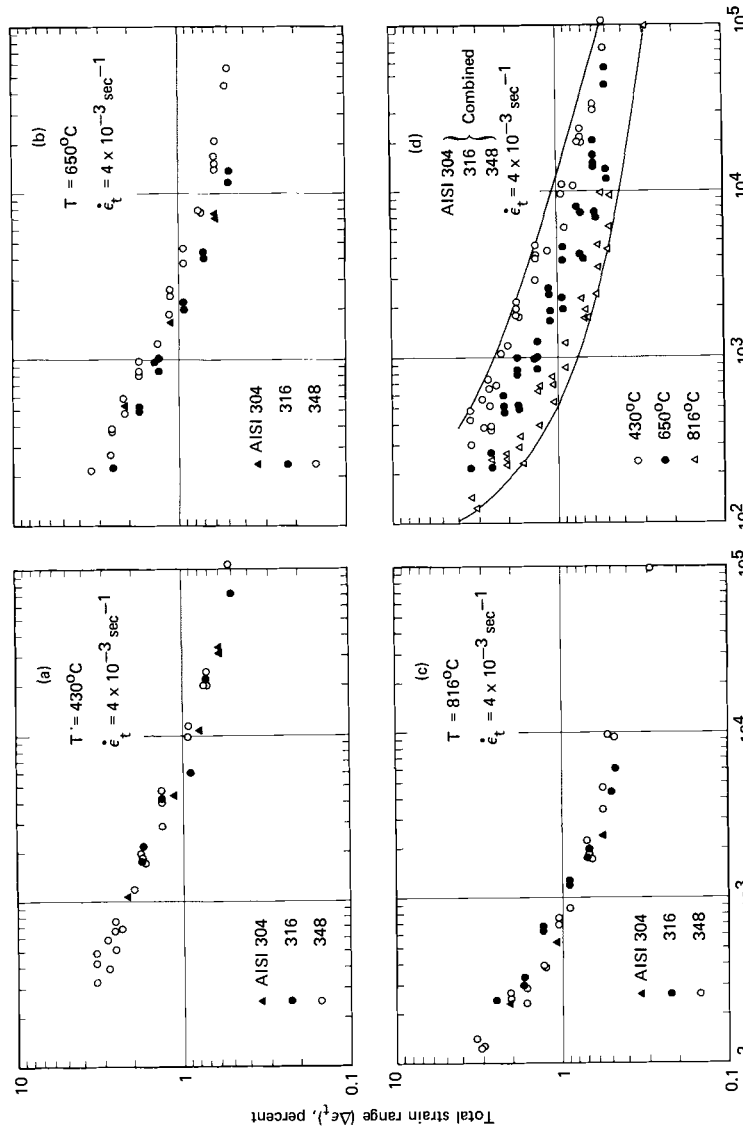

FIG. 3—*Fatigue test results for three stainless steels, three temperatures, one strain rate.*

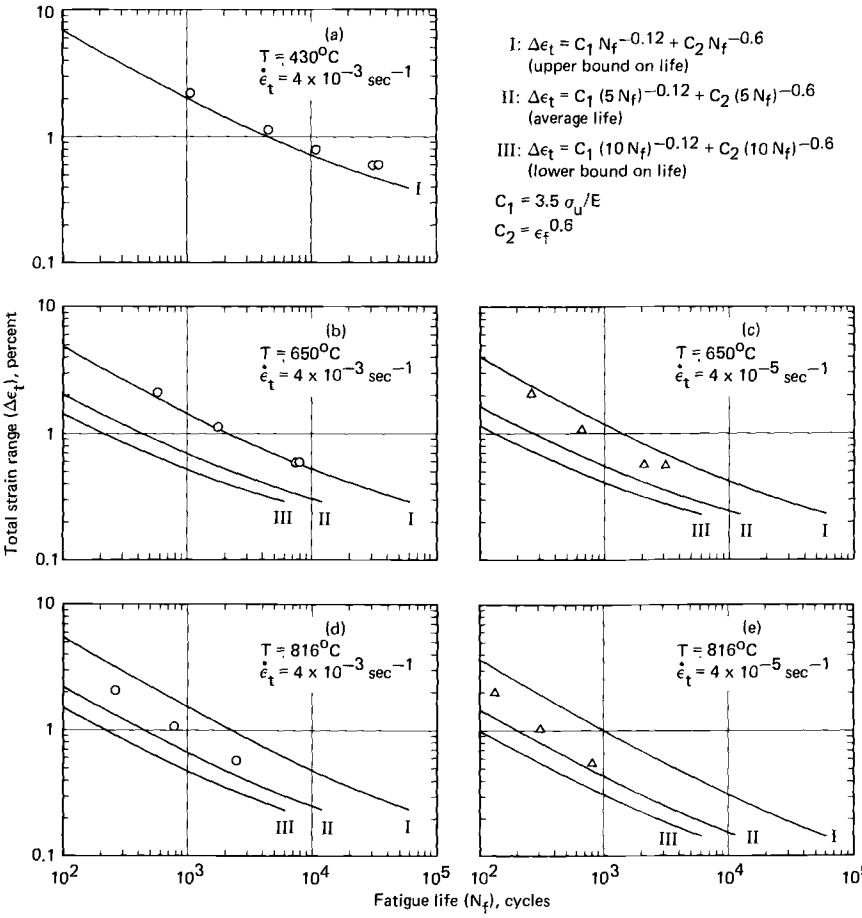

FIG. 4—*Comparison of fatigue test results for AISI 304 stainless steel with fatigue curves predicted by Manson-Halford procedure.*

curves representing an upper bound on fatigue life. The curves representing average life and a lower bound on life were determined from the upper bound of life by multiplication of the number of cycles by factors of ½ and 1/10, respectively. It appears that for the materials considered here, the Manson procedure predicts the 430 C data quite satisfactorily. For the 650 and 816 C data, the Manson-Halford procedure is somewhat conservative in the sense that the measured fatigue lives tend to be greater than predicted by the average life curves.

A different treatment of the fatigue data obtained for all three strain rates is the basis for Figs. 7 through 10. There, the plastic portion of the strain range is plotted as a function of the fatigue life defined by N_5 for all three

strain rates. The straight lines in the log-log diagrams represent the Coffin-Manson relation: $\Delta\epsilon_p = cN_5^{-m}$, where c and m are material constants and N_5 has been substituted for N_f [*22, 23*]. To obtain a best fit of the straight lines through the data points, least-squares analyses were performed with log $\Delta\epsilon_p$ as the independent variable and log N_5 as the dependent variable. However, tests with more than 50,000 cycles to failure were excluded from the least-squares estimates of constants c and m. For the purpose of comparison, similar analyses were made on the basis of the relation $\Delta\epsilon_p = cN_f^{-m}$. The two sets of values for constants c and m corresponding to N_5 and N_f are shown in Table 4. In several instances, the least-squares analyses are based on only a small number of data points, so that from a statistical point of view the

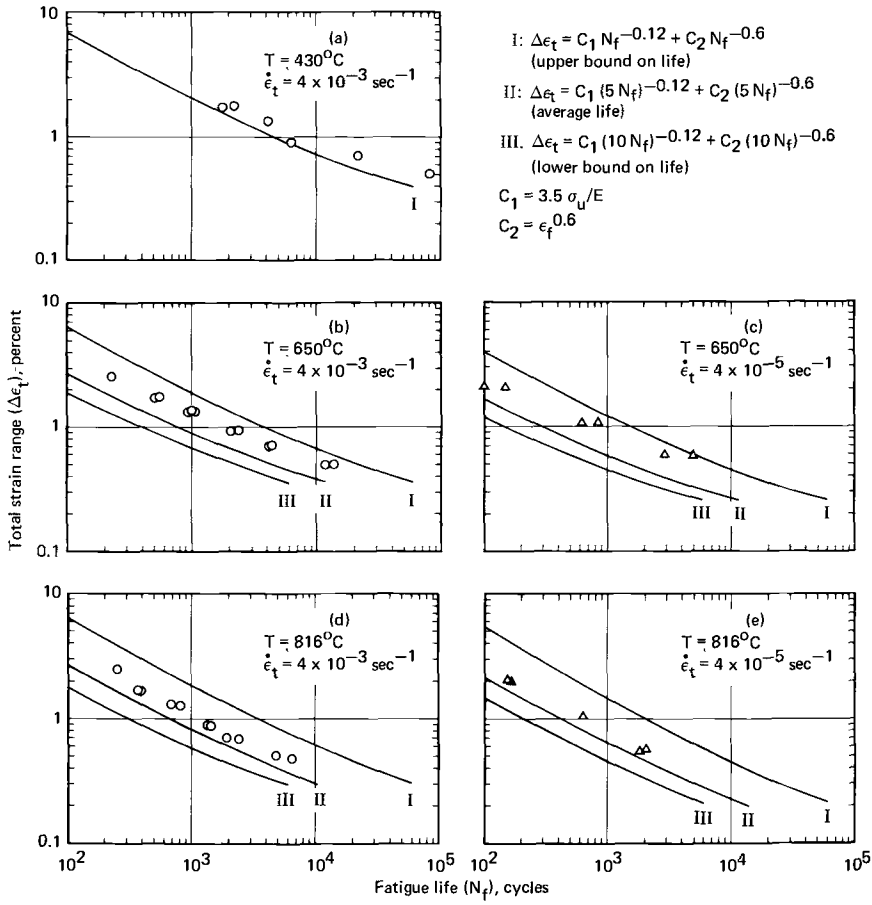

FIG. 5—*Comparison of fatigue test results for AISI 316 stainless steel with fatigue curves predicted by Manson-Halford procedure.*

TABLE 4—*Values of* c *and* m *in Coffin-Manson equation:* $\Delta\epsilon_p = c\ N_f^{-m}$ or $\Delta\epsilon_p = c\ N_5^{-m}$.

Material	Temperature, deg C	Strain Rate, $\dot{\epsilon}_t$, s^{-1}	Material Constants Based on Fatigue Life, N_f		Material Constants Based on Fatigue Life, N_5		Tensile Ductility, ϵ_f, %
			c	m	c	m	
AISI 304.....	430	4×10^{-3}	39.2	0.455	38.9	0.455	102
	650	4×10^{-3}	89.2	0.628	84.7	0.626	55
	650	4×10^{-4}	79.4	0.673	87.9	0.698	...
	650	4×10^{-5}	84.1	0.699	86.5	0.738	41
	816	4×10^{-3}	97.7	0.717	70.7	0.688	71
	816	4×10^{-4}	71.7	0.734	60.3	0.727	...
	816	4×10^{-5}	121.0	0.864	54.4	0.778	39
AISI 316.....	430	4×10^{-3}	54.1	0.493	58.6	0.503	97
	650	4×10^{-3}	50.4	0.586	47.5	0.582	89
	650	4×10^{-4}	51.7	0.633	47.1	0.631	...
	650	4×10^{-5}	19.5	0.500	17.4	0.492	39
	816	4×10^{-3}	90.4	0.691	81.8	0.690	95
	816	4×10^{-4}	169.1	0.804	106.3	0.760	...
	816	4×10^{-5}	56.9	0.665	38.4	0.629	69
AISI 348.....	430	4×10^{-3}	39.5	0.446	38.1	0.443	109
	650	4×10^{-3}	34.8	0.478	33.1	0.475	116
	650	4×10^{-4}	34.7	0.515	32.4	0.514	...
	650	4×10^{-5}	29.6	0.528	29.7	0.544	52
	816	4×10^{-3}	38.6	0.551	28.3	0.524	175
	816	4×10^{-4}	73.3	0.668	40.4	0.606	...
	816	4×10^{-5}	84.3	0.714	34.2	0.607	183

values of c and m cannot be very precise. However, the straight lines obtained appear to fit the data reasonably well in most cases. Considering the effect of strain rate at the test temperatures of 650 and 816 C, it is noted that the value of constant m, which determines the slope of the straight-line relationships, in general increases with a decrease in strain rate. However, in the case of AISI 316, a decrease in the value of m is noted with a decrease in strain rate from 4×10^{-4} to 4×10^{-5} s^{-1}.

Another way of presenting the test data concerned with the effect of strain rate on fatigue life is shown in Fig. 11. In this figure, fatigue life (N_5) is plotted versus diametral strain rate ($\dot{\epsilon}_d$) for two temperatures and three diametral strain ranges. Only the data obtained for AISI 304 and 348 stainless steels are presented in this fashion, as the data for AISI 316 were not generated by the same systematic procedure. Figure 11, as well as the preceding diagrams, supply ample evidence that the elevated-temperature fatigue life of the three materials concerned is significantly dependent on the rate of straining, at least when tested in the annealed condition.

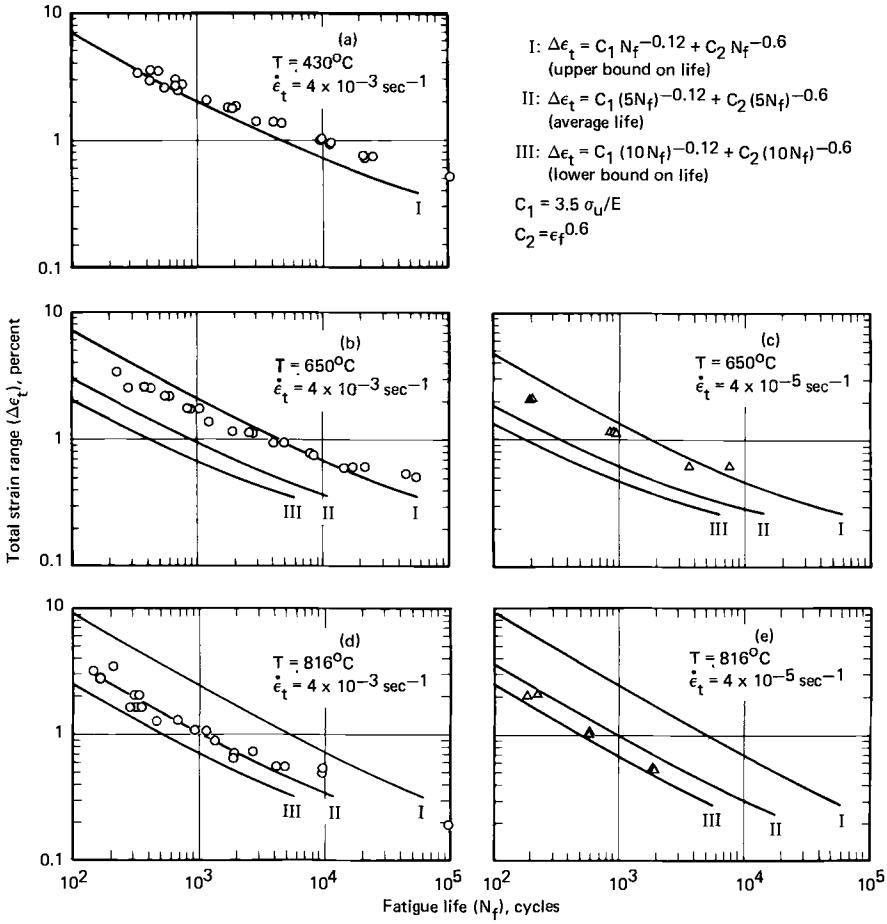

FIG. 6—*Comparison of fatigue test results for AISI 348 stainless steel with fatigue curves predicted by Manson-Halford procedure.*

As stated in the beginning, most of the fatigue tests exhibited cyclic hardening during the early part of the tests. Typically, the stress range reached a saturation value in relatively few cycles after which it remained stationary until cracks developed. Exceptions to this behavior were noted for AISI 304 and 316 at 430 C. In this case, cyclic hardening was followed by cyclic softening before the stress range reached a stationary value. Some typical results for AISI 316 are presented in Fig. 12.

In Figs. 13 through 15, the relationship between cyclic stress and cyclic strain is considered for the fastest strain rate. Each of the diagrams contains two sets of data, distinguished by open and closed circles. The open circles

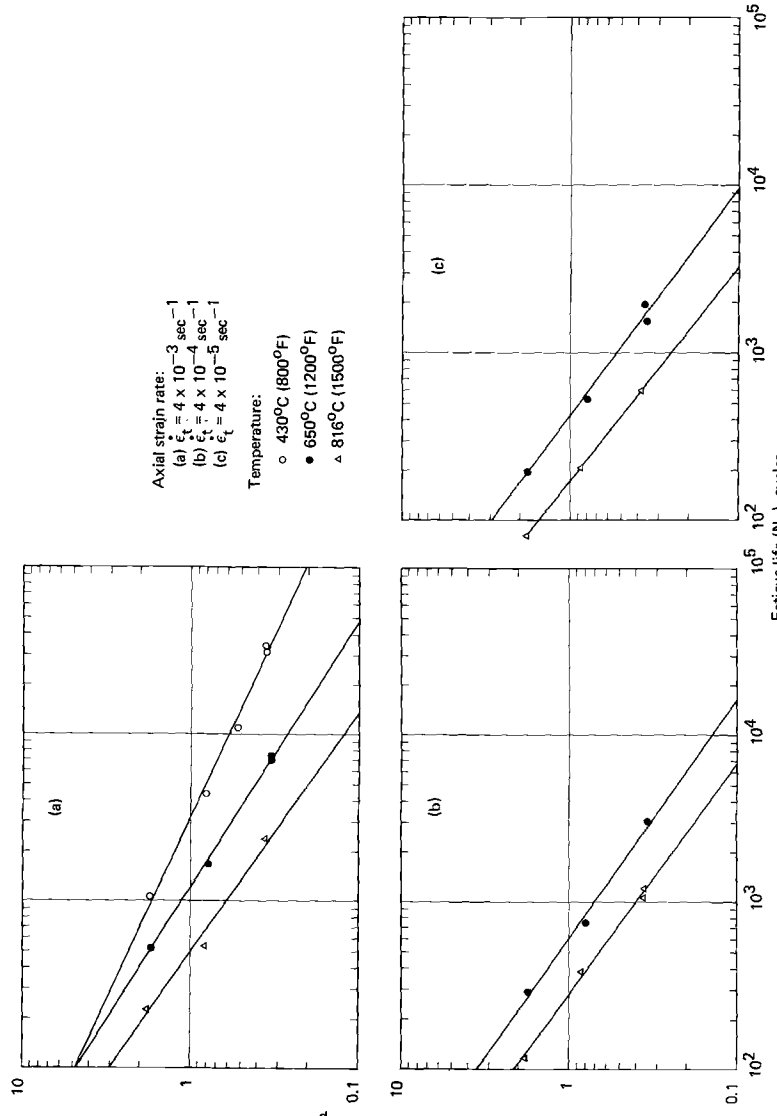

FIG. 7—*Plastic strain range versus fatigue life for AISI 304 stainless steel.*

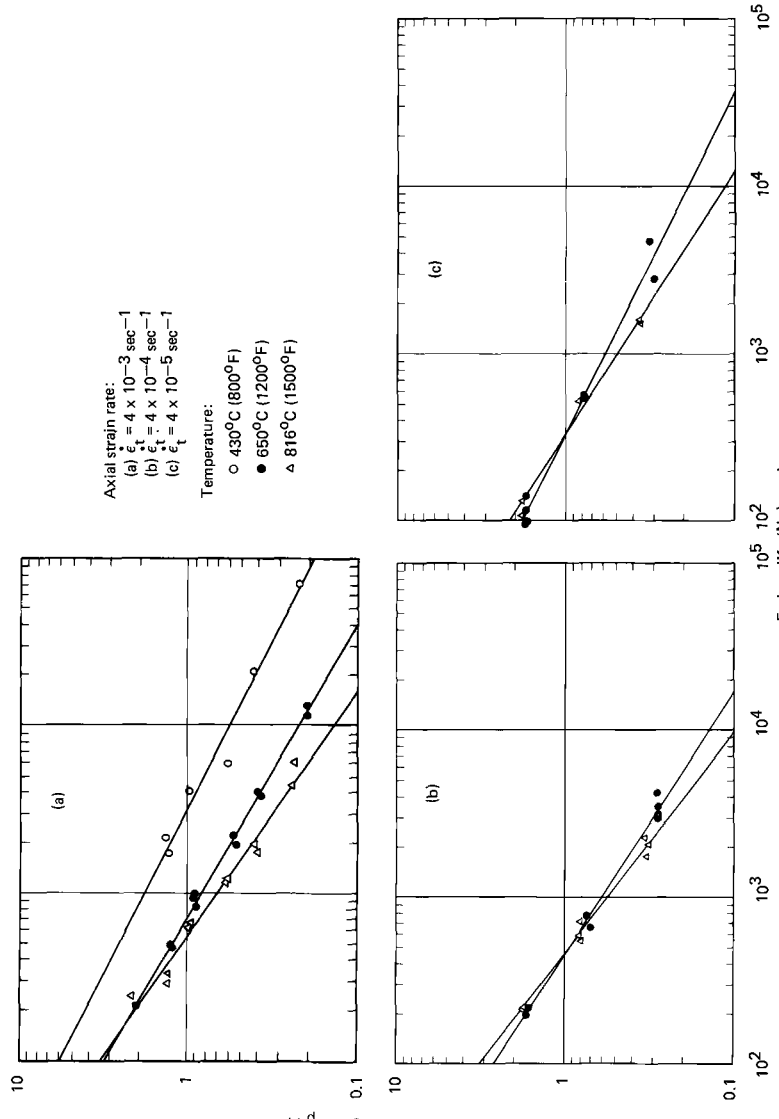

FIG. 8—*Plastic strain range versus fatigue life for AISI 316 stainless steel.*

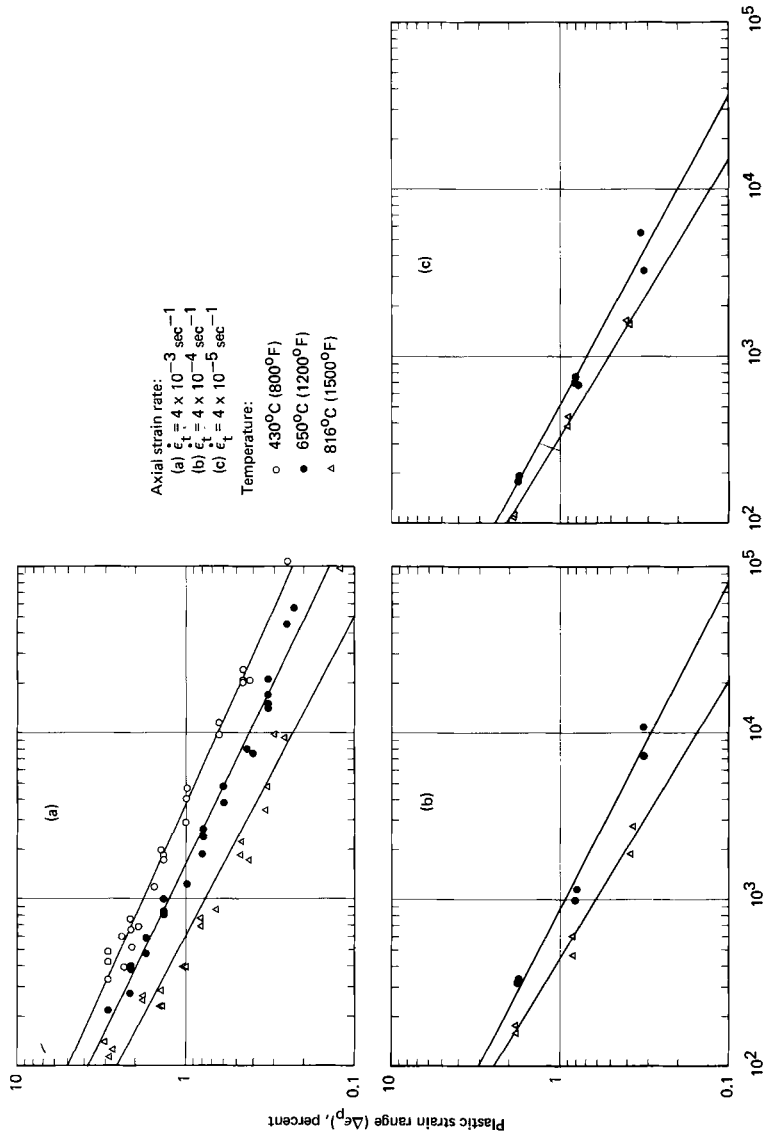

FIG. 9—*Plastic strain range versus fatigue life for AISI 348 stainless steel.*

correspond to the values of $\Delta\sigma/2$ and $\Delta\epsilon_t/2$ determined in individual fatigue tests (one point per test). The closed circles represent test results obtained with a single specimen. Employing the same strain rate as in the fatigue tests, the specimen was loaded cyclically for a relatively short number of cycles at each of several successively higher strain levels. Each point shown gives the stress amplitude reached in 50 to 100 cycles at the particular strain level. It is noted that the cyclic stress-strain curves obtained by joining these data points tend to be in general agreement with those drawn through the results of the completed fatique tests. Thus, testing a single specimen in the indicated manner appears to be an expedient method for generating a good first

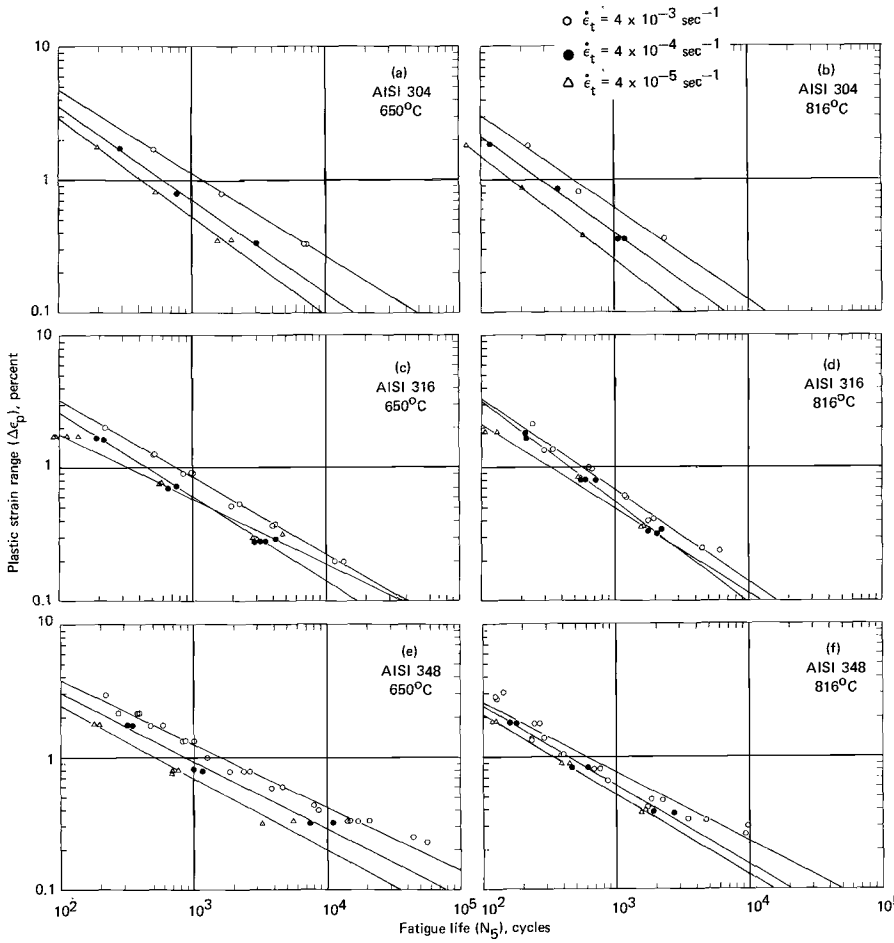

FIG. 10—*Plastic strain range versus fatigue life for AISI 304, 316, and 348 stainless steel.*

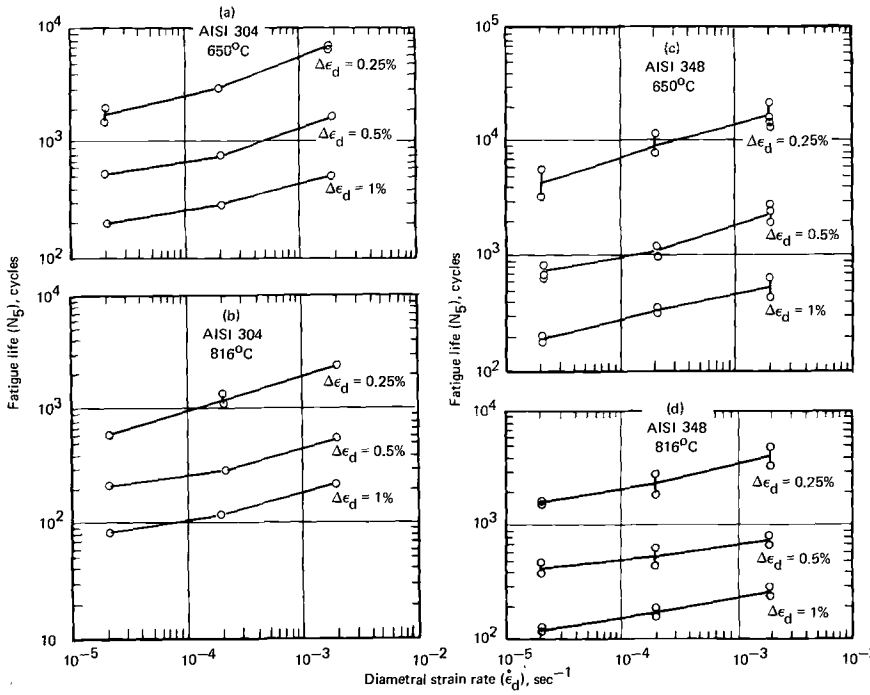

FIG. 11—*Effect of strain rate on low-cycle fatigue life of AISI 304 and 348 stainless steels at 650 and 816 C.*

approximation for the cyclic stress-strain curve pertaining to the strain rate of interest.

In most cases, the single specimen data fall somewhat below the data from the fatigue tests. The reverse is noted for AISI 304 and 316 at 430 C. There, the closed circles essentially represent maximum values reached by the stress amplitude because of cyclic hardening. However, as mentioned previously, cyclic hardening at this temperature is followed by strain softening, and the open circles reflect the subsequent steady-state condition. Better agreement is found with the maximum value of the stress range in the fatigue tests, shown in Fig. 14 by the open triangles.

For comparison with the cyclic data, the monotonic true stress-true strain curves obtained in tension tests at the same strain rate are shown also in Figs. 13 through 15. It is evident that the differences between the monotonic and cyclic stress-strain diagrams are quite pronounced for all three materials. The same observation holds for the lower strain rates employed in the test program [*18*].

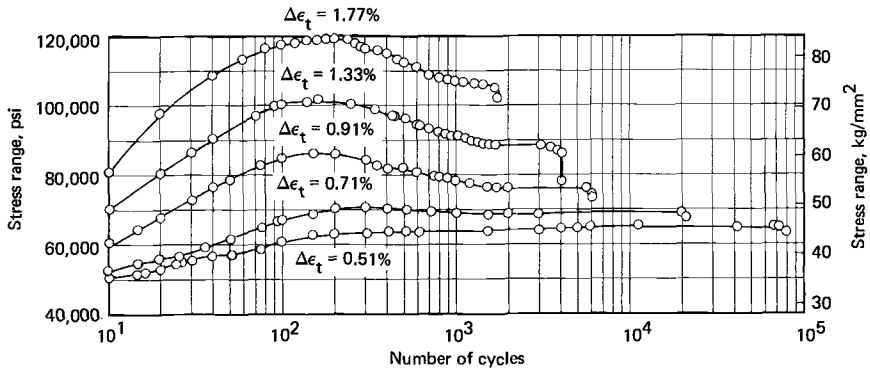

FIG. 12—*Stress range versus cycles obtained for AISI 316 stainless steel at 430 C with axial strain rate of* 4×10^{-3} s^{-1}.

A summary is presented in Table 5 of metallographic observations made of the fracture area in representative fatigue specimens. A detailed account of metallographic and fractographic studies is beyond the intended scope of the present paper.

Discussion

This paper has been concerned with the results of an elevated-temperature investigation of the time-dependent, low-cycle fatigue behavior of three stainless steels, AISI 304, 316, and 348. It can be stated in summary that the fatigue life measured in terms of the sustained number of loading cycles (not in terms of the elapsed time) generally was found to be affected adversely by an increase in temperature from 430 to 650 to 816 C and by a decrease in strain rate from approximately 4×10^{-3} s^{-1} to strain rates lower by factors of 10 to 100. Although tests concerned with the effect of strain rate were not performed at temperatures below 650 C, it should not be concluded that there is no effect of strain rate at lower temperatures. For instance, torsional fatigue tests conducted by Miller [*24*] on a 2½ nickel-chromium-molybdenum steel at room temperature showed a distinct influence of strain rate on the number of cycles to fracture as a function of plastic strain.

An attempt was made in this paper to interpret the fatigue data on the basis of the well-known Coffin-Manson relation, which has been shown to be descriptive for many materials tested at temperatures below the creep range. This relation predicts a straight-line relationship between the logarithm of the plastic strain range and the logarithm of the number of cycles to failure, as shown in Figs. 7 through 10. On inspection of these diagrams it appears that at elevated temperatures the assumption of such a straight-line relationship is not supported fully by the test data. However, from a practical point

TABLE 5—*Fracture mode characterization of AISI 304, 316, and 348 stainless steel low-cycle fatigue specimens.*

Material	Test Temperature, deg C	Axial Strain Range, $\Delta\epsilon_t$, %	Axial Strain Rate, ϵ_t, s^{-1}	Cycles to 5 Percent Reduction in Load, N_5	Mode of Crack Initiation	Intergranular Crack Length from Point of Initiation, mm	Mode of Crack Propagation to the Shear Point[a]
AISI 304...	650	2.08	4×10^{-5}	194	I	0.3	I and T
	650	2.10	4×10^{-4}	287	I	0.1	T and I
	650	2.10	4×10^{-3}	524	T	...	T and I
	650	0.57	4×10^{-5}	1 533	I	0.6	I and T
	650	0.58	4×10^{-4}	3 009	I	0.2	T and I
	650	0.59	4×10^{-3}	7 176	T	...	T and I
	816	2.06	4×10^{-5}	80	I	4.0	I and T
	816	2.05	4×10^{-4}	117	I	1.2	I and T
	816	2.06	4×10^{-3}	226	I	1.0	I and T
	816	0.56	4×10^{-5}	591	I	0.7	I and T
	816	0.56	4×10^{-4}	1 055	I	0.8	I and T
	816	0.57	4×10^{-3}	2 346	I	0.8	I and T
AISI 316...	650	2.11	4×10^{-5}	93	I	0.6	I
	650	2.15	4×10^{-4}	193	I	0.4	I and T
	650	2.56	4×10^{-3}	219	I	0.2	T
	650	1.10	4×10^{-5}	562	T	...	T and I
	650	1.16	4×10^{-4}	649	T	...	T
	650	0.94	4×10^{-3}	2 227	T	...	T
	650	0.59	4×10^{-5}	4 663	T	...	T
	650	0.61	4×10^{-4}	2 926	T	...	T
	650	0.50	4×10^{-3}	13 394	T	...	T
	816	2.06	4×10^{-5}	107	I	0.8	I and T
	816	2.07	4×10^{-4}	215	I	0.5	I and T
	816	2.50	4×10^{-3}	241	I	0.2	T
	816	1.06	4×10^{-5}	524	I	1.0	I
	816	1.08	4×10^{-4}	590	I	0.4	I and T
	816	0.89	4×10^{-3}	1 199	T	...	T
	816	0.55	4×10^{-5}	1 530	I	1.0	I
	816	0.59	4×10^{-4}	2 046	I	0.3	I and T
	816	0.48	4×10^{-3}	5 984	T	...	T
AISI 348...	650	2.14	4×10^{-5}	193	I	0.2	T
	650	2.15	4×10^{-4}	320	I	0.1	T
	650	2.16	4×10^{-3}	585	I	0.1	T
	650	0.61	4×10^{-5}	5 464	I	0.4	T
	650	0.61	4×10^{-4}	10 948	I	0.2	T
	650	0.61	4×10^{-3}	15 010	I	0.1	T
	816	2.02	4×10^{-5}	122	I	<0.1	T
	816	2.04	4×10^{-4}	158	I	<0.1	T
	816	2.06	4×10^{-3}	266	I	<0.1	T
	816	0.54	4×10^{-5}	1 613	I	<0.1	T
	816	0.54	4×10^{-4}	2 714	I	<0.1	T
	816	0.57	4×10^{-3}	4 656	I	<0.1	T

[a] I = intergranular; T = transgranular; where both modes are given, the predominant mode is listed first.

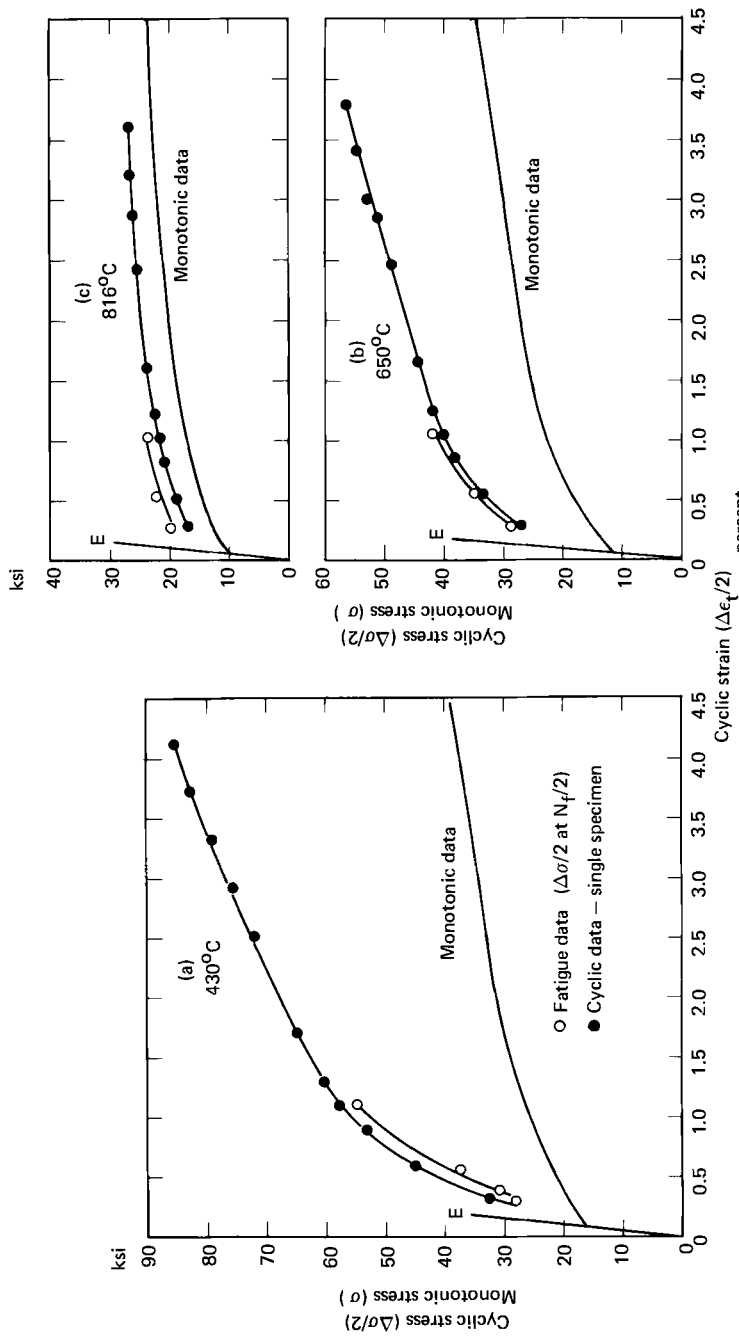

FIG. 13—*Cyclic and monotonic stress-strain diagrams for AISI 304 stainless steel at 430, 650, and 816 C (axial strain rate 0.004 s^{-1}).*

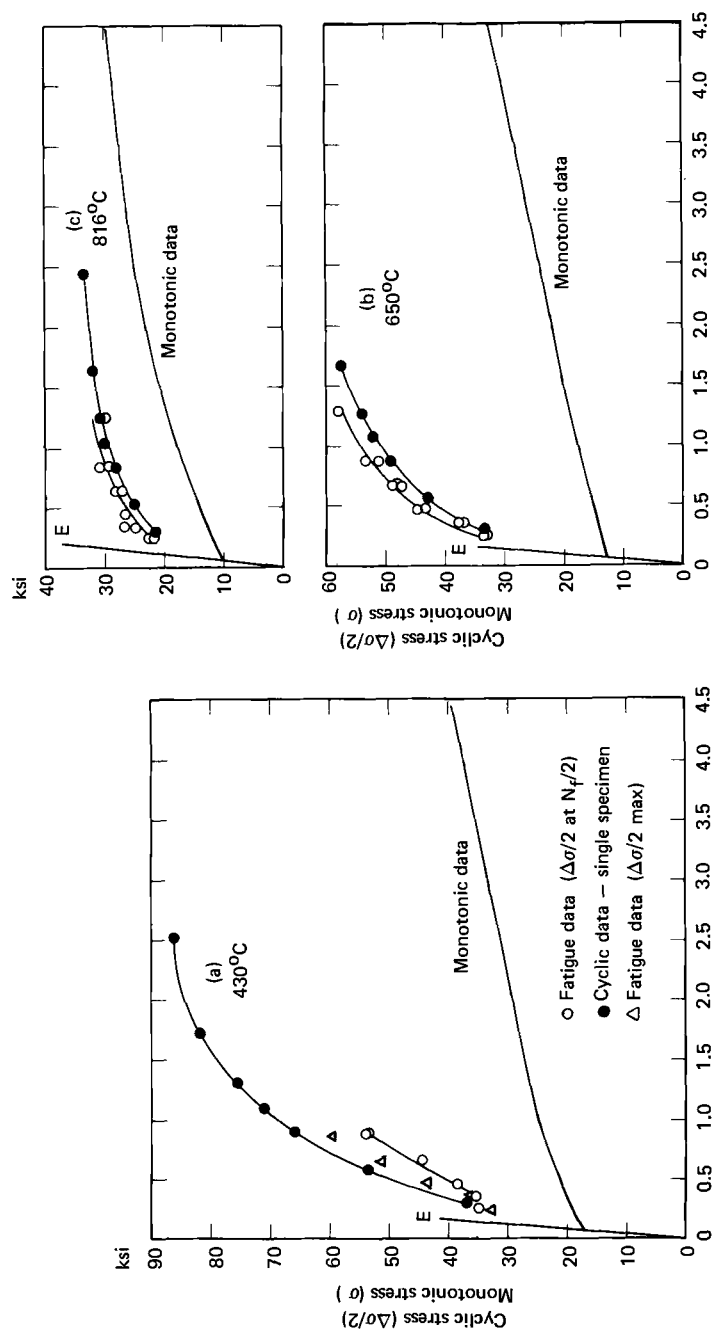

FIG. 14—*Cyclic and monotonic stress-strain diagrams for AISI 316 stainless steel at 430, 650, and 816 C (axial strain rate 0.004 s^{-1}).*

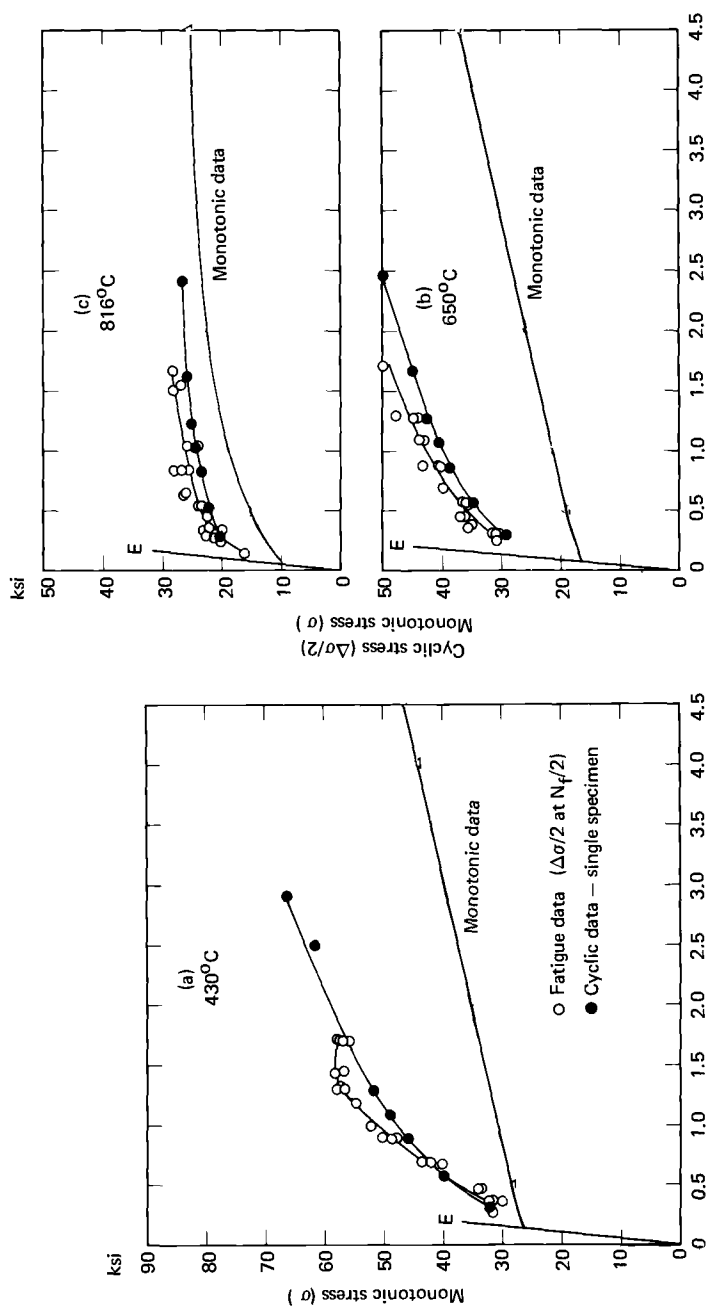

FIG. 15—*Cyclic and monotonic stress-strain diagrams for AISI 348 stainless steel at 430, 650, and 816 C (axial strain rate 0.004 s^{-1}).*

of view the empirical relation may be still useful when applied to a limited range of cycles to failure.

It was noted also in the paper that the test data obtained at 650 and 816 C with the highest and lowest strain rates were within lower and upper bounds on fatigue life established by means of an empirical procedure suggested by Manson and Halford. Manson and Halford have found the procedure to satisfy many test data involving numerous materials [*20*, *21*]. However, it must be recognized that the two bounds on life are a full decade apart.

The experimental methods by which the data in the paper were generated reflect the importance that was attached to precise control of testing conditions. Push-pull loading of solid round specimens was chosen to achieve a uniform strain distribution in the region of fracture. Moreover, the use of an hourglass gage section in conjunction with transverse strain measurement at the minimum diameter assured accurate local control of temperature and strain [*3*]. Finally, by maintaining a constant strain rate during the loading cycle and throughout the test the effects of temperature, strain amplitude, and strain rate were separated readily. In this connection, the authors have reason to believe on the basis of preliminary test results that, in testing for the effect of hold periods on fatigue resistance, the rate of strain reversal between hold periods cannot be ignored as a test parameter. Consequently, a well-defined cyclic loading mode should be an important objective in investigations concerned with material behavior under hold-time conditions.

Acknowledgments

The authors gratefully acknowledge the valuable technical assistance received from their colleagues D. G. Salyards, R. H. Stentz, D. H. Stratton, and E. W. Filer.

References

[*1*] *Proceedings of International Conference on Thermal and High-Strain Fatigue*, organized by Institute of Metals and by Iron and Steel Institute, London, 6–7 June 1967; Monograph and Report Series No. 32, The Metals and Metallurgy Trust, London, 1967.

[*2*] Tuppeny, W. H., ed., "High-Temperature Low-Cycle Fatigue," Society for Experimental Stress Analysis, Westport, Conn., 1968. (Papers by Coffin, L. F., Jr., Lawton, C. W., Manson, S. S., and Benham, P. P.).

[*3*] Slot, T. and Stentz, R. H., "Experimental Procedures for Low-Cycle Fatigue Research at High Temperatures," *Experimental Mechanics*, Vol. 8, March 1968.

[*4*] Eckel, J. F., "The Influence of Frequency on the Repeated Bending Life of Acid Lead," *Proceedings*, American Society for Testing and Materials, Vol. 51, 1951.

[*5*] Gohn, G. R. and Ellis, W. C., "The Fatigue Test as Applied to Lead Cable Sheath," *Proceedings*, American Society for Testing and Materials, Vol. 51, 1951.

[*6*] Swindeman, R. W., "The Interrelation of Cyclic and Monotonic Creep Rupture," *Proceedings of Joint International Conference on Creep*, The Institution of Mechanical Engineers, 1963, Paper No. 32.

[*7*] Coffin, L. F., Jr., "Cyclic Strain and Fatigue Study of a 0.1% C, 2% Mo Steel," *Transactions*, American Institute of Mining, Metallurgical, and Petroleum Engineers, Vol. 230, 1964.

[8] Coffin, L. F., Jr., "Cyclic Strain and Fatigue Behavior of Metals in the Creep Range," *Proceedings International Conference on Fracture*, Sendai, Japan, 1965, Japan Society for Strength and Fracture of Materials.

[9] Forrest, P. G. and Armstrong, K. B., "Investigation of the Thermal Fatigue Behavior of Nickel-Chromium-Based Alloys," *Journal of the Institute of Metals*, Vol. 94, 1965.

[10] Tilly, G. P., "Fracture Behavior of Two Creep-Resistant Materials Subjected to Cyclic Loading at Elevated Temperature," *Proceedings*, Institution of Mechanical Engineers, Vol. 180, Part I, 1965–1966.

[11] Price, A. T. and Elder, W. J., "High Strain Fatigue and Crack Propagation in Type 316 Steel," *Journal of the Iron and Steel Institute*, Vol. 204, 1966.

[12] Kusumoto, S., "Effects of Strain Rate on High Temperature Low-Cycle Torsional Fatigue Strength of 1 Cr-1 Mo-1/4 V Cast Steel," Hitachi Research Laboratory Report, Hitachi Ltd., Japan, April 1967.

[13] Coles, A. et al, "The High Strain Fatigue Properties of Low-Alloy Creep Resisting Steels," see Ref *1*.

[14] Dawson, R. A. T. et al, "High-Strain Fatigue of Austenitic Steels," see Ref *1*.

[15] Raraty, L. E. and Suhr, R. W., "Correlation of the Fatigue Properties of Magnox AL80 in Terms of the Plastic Strain Range," *Journal of the Institute of Metals*, Vol. 94, 1966.

[16] Tilly, G. P., "Influence of Static and Cyclic Loads on the Deformation Behavior of an Alloy Steel at 600 C," see Ref. *1*.

[17] (*a*) Claudson, T. T., "Fabrication History of Alloys Used in the Irradiation Effects on Structural Materials Program," Pacific Northwest Laboratory, BNML-CC-236, Richland, Wash., Oct. 1965. (*b*) Private communication with Gurwell, W. E., Pacific Northwest Laboratory, 30 Oct. 1968.

[18] Berling, J. T. and Slot, T., "Effect of Temperature and Strain Rate on Low-Cycle Fatigue Resistance of AISI 304, 316, and 348 Stainless Steels," General Electric Report GEMP-642, June 1968, Cincinnati, Ohio.

[19] Manson, S. S., *Thermal Stress and Low-Cycle Fatigue*, McGraw-Hill, New York, 1966.

[20] Manson, S. S. and Halford, G., "A Method of Estimating High Temperature Low Cycle Fatigue Behavior of Materials," see Ref *1*.

[21] Halford, G. R. and Manson, S. S., "Application of a Method of Estimating High Temperature Low Cycle Fatigue Behavior of Materials," paper presented at National Metals Congress, American Society for Metals, Cleveland, 19 Oct. 1967, NASA TM X-52357.

[22] Coffin, L. F., Jr., "A Study of Cyclic Thermal Stresses on a Ductile Material," Knolls Atomic Power Laboratory Report No. KAPL-853, Schenectady, N. Y., June 1953.

[23] Manson, S. S., "Behavior of Materials Under Conditions of Thermal Stress," NACA TN-2933, National Advisory Committee for Aeronautics, 1953.

[24] Miller, K. J., "The Effect of Strain Rate on Low-Endurance Torsional Fatigue in an Alloy Steel (En 25)," see Ref *1*.

R. W. Swindeman[1]

Low-Cycle Fatigue Study of Columbium Alloy D-43

REFERENCE: Swindeman, R. W., **"Low-Cycle Fatigue Study of Columbium Alloy D-43,"** *Fatigue at High Temperature, ASTM STP 459*, American Society for Testing and Materials, 1969, pp. 31-41.

ABSTRACT: A machine was developed to study the low-cycle fatigue characteristics of refractory metals in vacuum at high temperatures. Operating capability included temperatures up to 1400 C, loads to 4.45×10^4 N (10 ksi), and frequencies from static to 10 Hz. The machine operated in a push-pull mode and was stroke controlled.

To minimize material required for testing, grips were designed to operate at nearly the same temperature as the specimen. A typical specimen geometry was a rod, 76 mm long with a test section 12.7 mm long and 5.18 mm in diameter.

A series of tests was performed on a columbium alloy, D-43, at temperatures ranging from 20 to 1204 C and cyclic plastic strains from 0.3 to 4 percent. Data at 20, 871, and 1093 C revealed that D-43 conformed to the Coffin-Manson equation, wherein cycles to failure was related to plastic strain range by a power function.

The plastic strain resistance was found to increase with increasing temperature and to exhibit a maximum around 871 C. Up to 1024 C cyclic strain resistance remained better than or equivalent to that at room temperature.

Posttest examination of specimen revealed ductile, transgranular failures at all temperatures.

KEY WORDS: columbium alloys, vacuum, fatigue (materials), high temperature, cyclic loads, evaluation, tests

The need for space power-conversion systems has stimulated the development of refractory metal technology. A considerable number of new alloys have appeared within the last ten years, and the qualification of these materials for engineering applications requires a substantial effort. Since these materials are expected to see service at temperatures in the creep range, most of the emphasis in regard to mechanical testing has been on the creep- and stress-rupture properties for times up to 10,000 h [*1*].[2] However, failures resulting from cyclic thermal and mechanical stresses are common in high-temperature

[1] Metallurgist, Metals and Ceramics Div., Oak Ridge National Laboratory, Oak Ridge, Tenn. 37830, operated by Union Carbide Corp. for the U.S. Atomic Energy Commission.

[2] The italic numbers in brackets refer to the list of references appended to this paper.

structures, so we consider it important that the capability for fatigue testing of refractory metals at high temperatures be developed. Honeycutt et al [*2*] have described a testing system which operates in the high-cycle range, but virtually no information on low-cycle fatigue is available. We chose to work in this area and to initiate our program by testing D-43. This is one of the stronger materials in the columbium alloy group [*3*, *4*].

Equipment

In developing a machine for low-cycle fatigue testing a number of decisions were necessary which involved a compromise between cost, capability, and convenience. The system which evolved is shown schematically in Fig. 1.

The vacuum system incorporated a 750-dm^3/s oil diffusion pump coupled to a liquid nitrogen cold trap. This combination was capable of maintaining chamber pressure at less than 10^{-7} torr (1.33×10^{-5} N/m^2) at room temperature and less than 10^{-6} torr (1.33×10^{-4} N/m^2) at 1200 C. Although these pressures do not simulate the hard vacuum of space, we were able to prevent changes in the chemical composition of the specimen by: (1) using specimens with a low surface-to-volume ratio, (2) wrapping each test specimen with protective tantalum foil, and (3) minimizing the test time.

We chose a 51-mm-diameter tungsten mesh furnace for heating in order to allow flexibility in specimen design. This furnace, designed for service to 2000 C, was powered by a 20-kVA 440-V supply through a 7-V stepdown

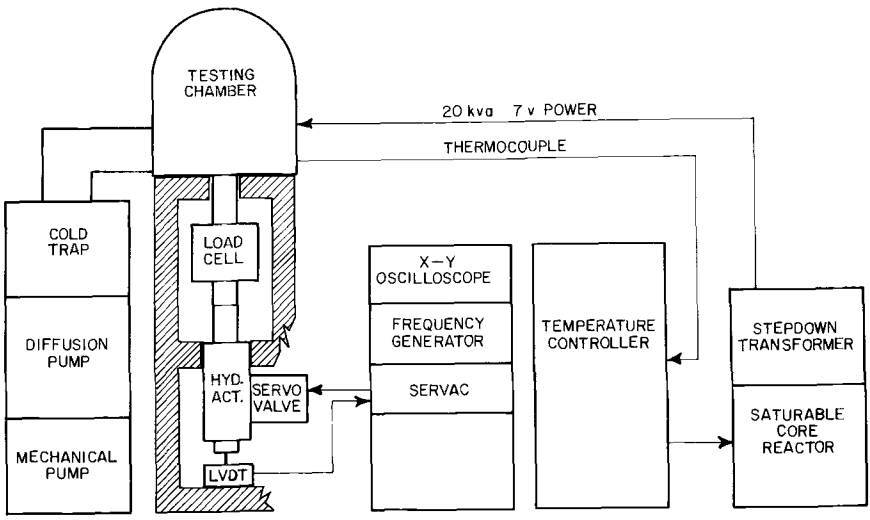

FIG. 1—*Schematic drawing showing the major components of the high-temperature fatigue machine.*

transformer and regulated by a saturable core reactor (SCR). The specimen temperature was controlled by a Leeds and Northrup AZAR unit, coupled to the SCR, and sensed by platinum versus Pt-10Rh thermocouples tied to the specimen. There was no detectable thermal gradient along the specimen gage length.

The loading system was assembled from components purchased from the MTS Corporation or manufactured locally. The former consisted of: (1) a hydraulic pump providing a pressure of 6.89×10^7 N/m^2 (3 ksi) at a rate of 6.3×10^{-4} m^3/s (10 gallons per minute (gpm)), (2) a hydraulic control manifold, (3) a Servac model 401.1 servo-controller, and (4) a 4.45×10^4 N (10 ksi) hydraulic actuator coupled with a 3.15×10^{-4} m^3/s (5 gpm) servo-valve.

The hydraulic actuator was bolted to a sturdy frame, of our own design, and connected to a 4.45-N (10-ksi) load cell. The active pull rod extended from this load cell through a linear bearing and entered the bottom of the testing chamber. The chamber-to-pull rod seal was maintained by a metal bellows.

The chamber of the testing machine is shown in Fig. 2. The photograph shows the specimen mounted in the grips and half of the furnace and radiation shields in position. The upper grip was bolted to the static pull rod and the lower grip to the active pull rod. These pull rods were centered within 0.025 mm and were spaced approximately 266 mm apart. The bellows allowed a stroke of ± 65 mm.

In order to minimize material required for specimens we designed a hot grip, shown in Fig. 3. The four parts were fabricated from a tantalum alloy, T-111.[3] The outer hollow cylinder carried the tensile load while the inner rod carried the compressive load. The tapered split sleeve provided a rigid grip on the specimen. One tapered sleeve was machined to match threaded-end specimens and another sleeve to match tapered-end specimens. The tight grip presented a disassembly problem because these materials self-welded at elevated temperatures. We had some success using a colloidal alumina coating on the contacting parts but found that spraying the surfaces with tungsten disulfide was more effective.

The specimen designs are shown in Fig. 4. The threaded-end specimen was used in a few tests at room temperature but was abandoned in favor of the tapered-end specimen because the latter produced much better alignment and did not tend to work loose during testing. Even the tapered-end specimen gave rise to some misalignment when mounted in the grips. The deviation from the center line through the specimen axis amounted to about 0.1 mn. at the grip extremities.

[3] Nominal composition tantalum-8 percent tungsten-2 percent hafnium.

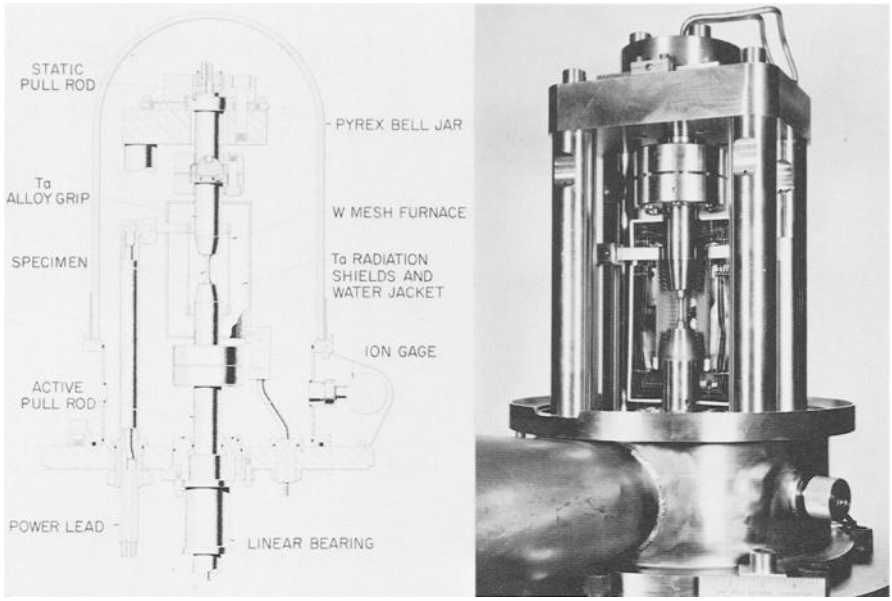

FIG. 2—*Schematic drawing and photograph of the vacuum chamber of the high-temperature fatigue machine.*

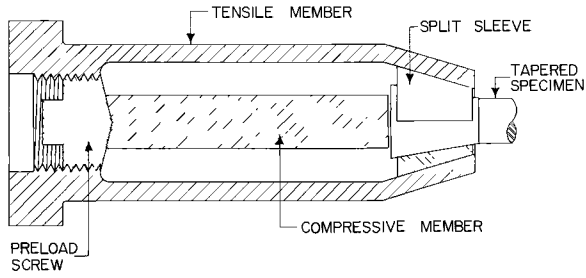

FIG. 3—*High-temperature grip design.*

Material

The D-43 alloy was received as 15.5-mm-diameter rod stock. The heat treatment stated by the vendor was 1 h at 1427 C, which produced an ASTM grain size of 7 to 8. The compositional specifications, Oak Ridge National Laboratory (ORNL) interstitial analysis, and a typical posttest analysis are given in Table 1. Tensile data generated on the fatigue specimens are given in Table 2.

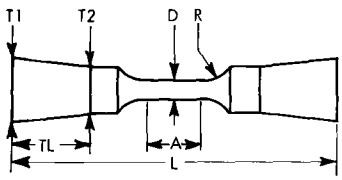

TAPERED END SPECIMEN

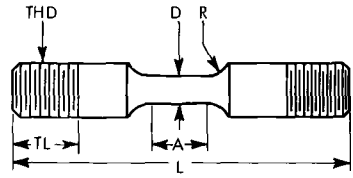

THREADED END SPECIMEN

DIMENSIONS OF TEST SPECIMENS

		Tapered End Specimen		Threaded End Specimen	
		(in.)	(mm)	(in.)	(mm)
D	- Diameter	0.200 ± 0.0005	5.18 ± 0.013	0.250 ± 0.001	6.35 ± 0.025
A	- Length of reduced section	0.500 ± 0.005	12.7 ± 0.13	0.500 ± 0.005	12.7 ± 0.13
R	- Rad of fillet, min	3/8	~9.5	1/4	~6.4
L	- Overall length	3	~76.2	3-1/8	~79.3
TL	- Taper or thread length	0.700 ± 0.001	17.780 ± 0.025	5/8	~15.9
T1	- Taper diameter, max	0.601 ± 0.001	15.27 ± 0.025	-	-
T2	- Taper diameter, min	0.401 ± 0.001	10.19 ± 0.025	-	-
THD	- Thread	-	-	1/2-13 UNC-2A	-

FIG. 4—*Specimen designs.*

TABLE 1—*Composition of D-43.*

Element	Tungsten, weight %	Zirconium, weight %	Carbon, ppm	Oxygen, ppm	Nitrogen, ppm	Hydrogen, ppm
Specification.....	8 to 11	0.9 to 1.3	800 to 1100	20 to 40	30 to 40	4 to 6
ORNL analysis (pretest).....	...	...	1000	90	61	9
ORNL analysis (1093 C test).....	...	...	960	88	27	...

TABLE 2—*Tensile properties of D-43.*[a]

Temperature, deg C	0.2% Offset Yield Strength		Ultimate Tensile Strength		Reduction, in Area, %
	ksi	MN/m^2	ksi	MN/m^2	
20.....	57	393	77	530	68
871.....	35	241	54	372	76
1093.....	31	214	44	303	82

[a] 0.05 in./min extension rate (approximately 768 mm/s).

Test Procedure

All tests were performed in a fully reversed axial mode with a triangular stroke-time wave. The outputs from the load cell and control transducer were displayed on an x-y oscilloscope, and the actuator stroke was adjusted to maintain the width of the load-stroke hysteresis loop at the desired level. We assumed that the loop width was a measure of the plastic strain being introduced into the specimen. This was confirmed at room temperature by using an averaging extensometer attached to the specimen shoulders. The length of the uniform diameter of the specimen was the basis for calculating the nominal plastic strain range, ϵ_p. This practice ignored any plastic strain component which occurred in the fillets and also any component associated with bending and buckling in the specimen.

The testing frequency depended on the plastic strain range. At the 1 percent level and above, the frequency was the reciprocal of the strain. For example, at 2 percent ϵ_p the frequency was 0.5 Hz. Below 1 percent ϵ_p the frequency was never more than 2 Hz. The reasons for these frequency selections were to minimize self-heating in the specimens at high strains, to reduce testing time at high temperature and low strains, and to maintain a triangular stroke-time wave.

Results

The variation in fatigue life, N_f, with nominal plastic strain range, ϵ_p, is shown in Fig. 5 for three temperatures, 20, 871, and 1093 C. Some air test data at 20 C are included, and there is an indication that at this temperature life in vacuum is greater than air at the lowest strain level. Vacuum data at 20 C indicate a power relationship between life and strain range. The slope of the line is about -0.54. Parallel lines pass through the data at the three temperatures; however, life at 871 C is about five times greater than at 20 C, while at 1093 C it is about 50 percent greater.

Stress amplitudes versus life data at the three temperatures are shown in Fig. 6. These stress amplitudes correspond to the values at $\frac{1}{2} N_f$. The 20 C data show very little stress decrease for lives beyond 10^3 cycles and are well above the 0.2 percent yield strength of 393 MN/m^2 (see Table 2). Data at 871 and 1093 C reveal a decrease in stress amplitude with life extending to at least 10^5 cycles.

The variation in fatigue life with test temperature is summarized in Table 3 for ϵ_p values near 1 percent. These results show life increasing with temperature and reaching a maximum around 871 C. The stress amplitude necessary to produce 1 percent strain decreases over this same temperature range.

The appearance of specimens after testing varied with the temperature, strain range, and stress amplitude. At 20 C, an S-shaped buckle developed

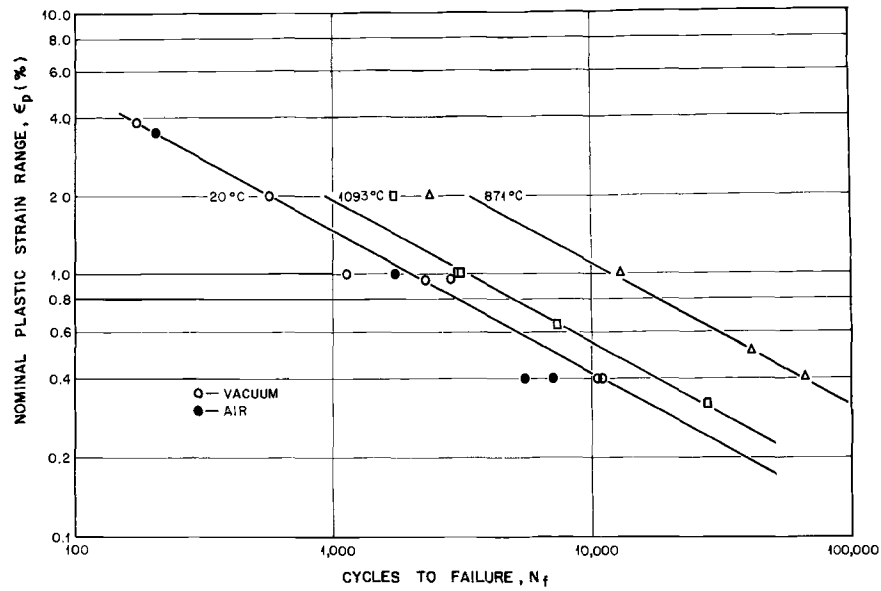

FIG. 5—*Strain fatigue data for D-43 at 20, 871, and 1093 C.*

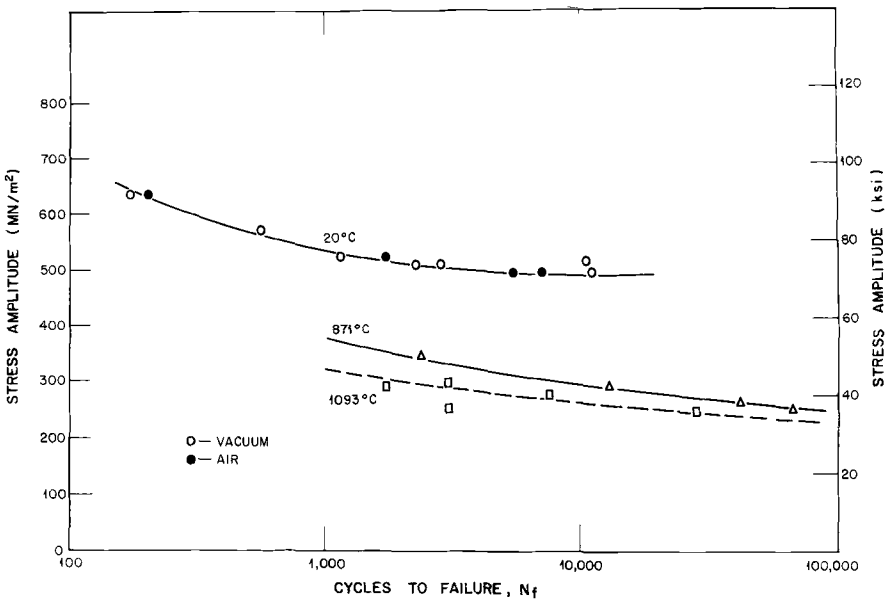

FIG. 6—*Stress-fatigue data for D-43 at 20, 871, and 1093 C.*

TABLE 3—*Effect of temperature on the life of D-43 tested near 1 percent plastic strain range.*

Temperature, deg C	Stress Amplitude at One-Half Life		Life, cycles
	ksi	MN/m^2	
20[a]	75	517	2100
300	55	379	6100
537	48	331	6900
760[a]	44	303	7600
871	42	289	13,100
982	40	276	8400
1093[b]	40	276	3100
1204	28	193	8900

[a] Average of three tests.
[b] Average of two tests.

and surface disturbances were pronounced in the two concave regions of the buckle. Cracks developed in these regions and also near the fillets. As the testing temperature increased, buckling diminished, and the locations of the initiated cracks become more random.

Failures initiated normal to the stress axis but eventually progressed in a shear mode after reaching a critical size. The relative area of the normal crack strongly depended upon the stress amplitude and ranged from less than 10 percent at 634 MN/m^2 (3.5 percent ϵ_p at 20 C) to greater than 90 percent at 248 MN/m^2 (0.32 percent ϵ_p at 1093 C). Typical fracture surfaces are shown in Fig. 7.

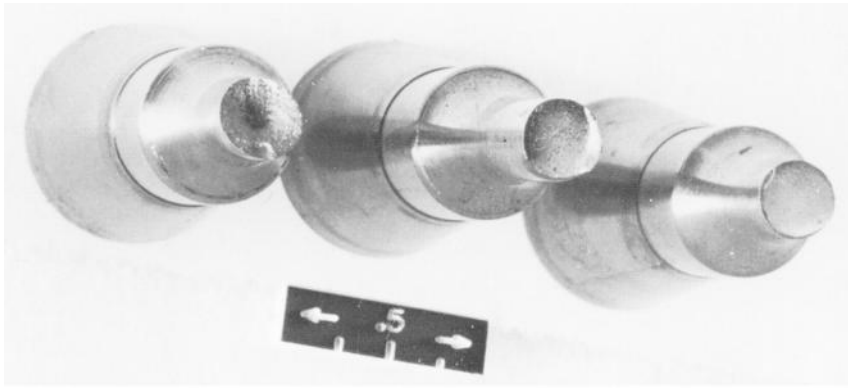

FIG. 7—*Three fatigue specimens after testing. Rupture surfaces show an increase in the area of the normal crack with decreasing stress amplitude.* (left) *20 C, 0.4 percent* ϵ_p, *11,000 cycles, 496* MN/m^2 *stress amplitude.* (center) *537 C, 1 percent* ϵ_p, *6900 cycles, 331* MN/m^2. (right) *1093 C, 1 percent* ϵ_p, *3100 cycles, 296* MN/m^2. *Failures initiated near the top of the photograph.*

Examination of crack surfaces up to ×200 revealed dimple formation as the most prominent feature at all temperatures. Severe rubbing obscured most of the detail near the crack initiation point, but dimples were prevalent in this area also.

Metallographic studies on secondary cracks revealed transgranular failures at all temperatures. A typical section taken from a specimen tested at 982 C is shown in Fig. 8.

Discussion

The strain fatigue of D-43 conforms to the behavior suggested by the Coffin-Manson equation in which the life is related to the plastic strain range according to the equation:

$$\epsilon_p = CN_f^{-\alpha} \quad \ldots\ldots\ldots\ldots\ldots\ldots\ldots\ldots\ldots\ldots (1)$$

where:

C and α = material constants.

The best value for α seems to be about 0.54, which is greater than 0.5, the value proposed by Tavernelli and Coffin [5], and less than 0.6, the value suggested by Manson [6]. The D-43 data, however, are based on a gage length defined as 12.7 mm when, in actual fact, the effective gage length may vary with the strain range. Furthermore, strain concentrations in the buckled regions impose mean and cyclic strain components which may influence both the slope and the position of the observed ϵ_p versus N_f curve.

The increase in life with increasing temperature may be due partly to a decrease in buckling. It seems likely that some of the increase is a real effect. Although we have no experimental evidence for establishing the cause, factors such as rewelding of the crack interfaces or mproved work-hardening capability could exert such an influence.

The loss in plastic strain resistance between 871 and 1093 C is more difficult to understand. Since these temperatures are in the creep range, we expect that integranular cracking or void formation might produce a decrease in strain resistance. However, investigation of the primary and secondary cracks revealed no distinguishable differences in the fracture mode at the two temperatures. Even under creep conditions at 1093 C, when intergranular voids have been observed in D-43, fractures occur by necking and shear.[4]

One possible explanation is that the work-hardening capability of D-43 decreases at 1093 C, and this contributes to strain concentration in areas where favorable dimensional and temperature gradients occur. It could be, however, that the drop in strain resistance is associated with aging processes

[4] Stephenson, R. L., Oak Ridge National Laboratory, unpublished work.

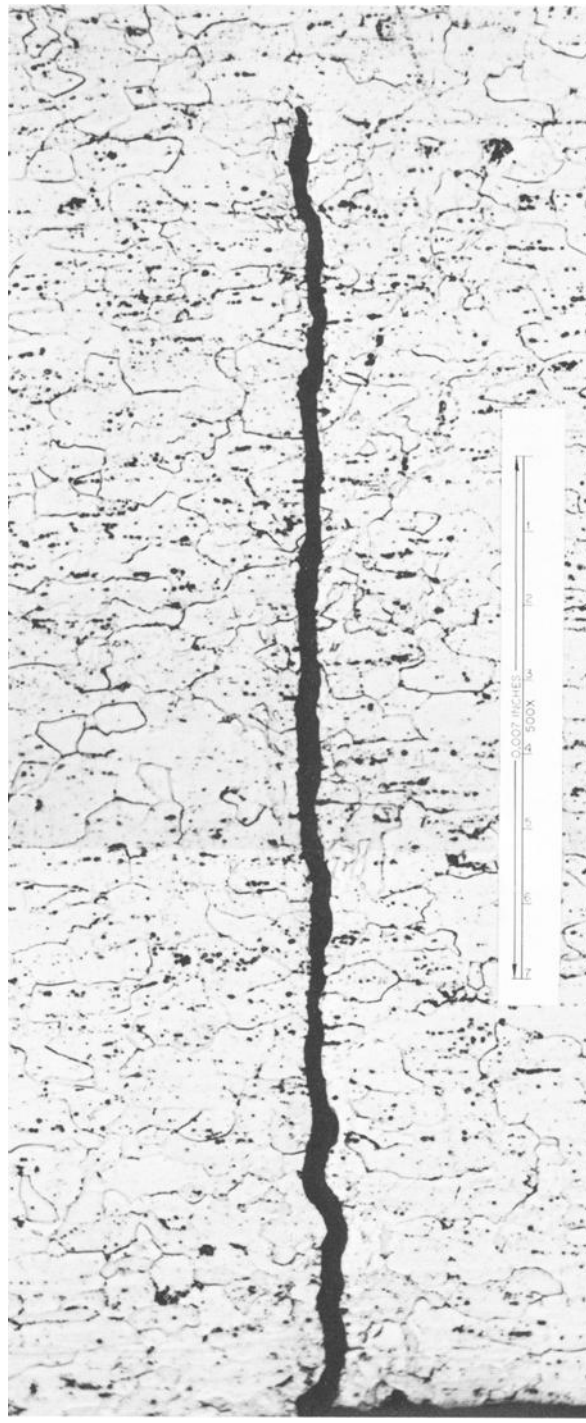

FIG. 8—*Secondary fatigue crack in a specimen cycled at 1 percent* ϵ_p *and 982 C. Failed after 8400 cycles. This crack is typical of all elevated-temperature failures* (×500). *Etchant: 30 lactic acid, 10 hydrofluoric acid, 10 nitric acid.*

which occur in D-43 [7-8]. In this regard, further work is desirable to establish the effect of frequency or strain rate on the plastic strain resistance. Before undertaking this subject it would be desirable to develop a more sophisticated strain measuring and control capability.

Conclusions

1. The low-cycle fatigue behavior of D-43 conforms to the power relationship between plastic strain range and life.
2. The strain resistance at temperatures up to 1204 C is equivalent to or better than that at room temperature.
3. The fatigue crack, once developed, is transgranular at all temperatures and may be characterized as ductile fracture.

Acknowledgments

The author acknowledges the assistance of R. Becker for his work on the machine design and W. Johnson who assisted in assembly of the instrument and controls systems. A special thanks is deserved by F. L. Beeler who participated in all phases of the program and who performed all of the testing.

References

[1] Sawyer, J. C. and Steigerwald, E. A., "Generation of Long Time Creep Data of Refractory Alloys at Elevated Temperatures," Final Report, National Aeronautics and Space Administration, 6 June 1967.

[2] Honeycutt, C. R. et al, "Elevated-Temperature Fatigue of TZC Molybdenum Alloy Under High Frequency and High-Vacuum Conditions," *Transactions*, American Society for Metals, Vol. 60, No. 450, Sept. 1967.

[3] Stephenson, R. L., "Comparative Creep-Rupture Properties of B-66 and D-43 Alloys," *Fourth Symposium on Refractory Metals*, Metallurgical Society, American Institute of Mining, Metallurgical, and Petroleum Engineers, French Lick, Ind., 3–5 Oct. 1965 (to be published in the proceedings).

[4] McCoy, H. E., Jr., "An Evaluation of the Creep Properties of Cb-753 and a Comparison of this Alloy with Several Other Niobium-Base Alloys," ORNL-TM-1347, Oak Ridge National Laboratory, Jan. 1966.

[5] Tavernelli, J. F. and Coffin, L. F., Jr., "A Compilation and Interpretation of Cyclic Strain Fatigue Tests," *Transactions*, American Society for Metals, Vol. 51, No. 438, 1959.

[6] Manson, S. S., "Fatigue: A Complex Subject—Some Simple Approximations," *Experimental Mechanics*, Vol. 5, No. 193, 1965.

[7] Stephenson, R. L., "Effect of Heat Treatment on the Creep-Rupture Properties of D-43 Alloy," ORNL-TM-1587, Oak Ridge National Laboratory, Sept. 1966.

[8] Lessmann, G. G., "Effect of 1000 Hour Thermal Exposures on Tensile Properties of Refractory Metal Alloys," NASA-CR-72095, National Aeronautics and Space Administration.

R. L. Stegman[1] *and* P. *Shahinian*[1]

Effect of Temperature on the Fatigue of Nickel at Varying Oxygen Pressures

REFERENCE: Stegman, R. L. and Shahinian, P., **"Effect of Temperature on the Fatigue of Nickel at Varying Oxygen Pressures,"** *Fatigue at High Temperature, ASTM STP 459*, American Society for Testing and Materials, 1969, pp. 42–58.

ABSTRACT: The fatigue of high-purity nickel in reversed bending has been studied as a function of oxygen pressure at temperatures of 20, 300, 425, and 550 C. The environmental effect was examined further as a function of strain at 300 and 550 C. S-shaped curves of fatigue life versus pressure obtained at each temperature were generally similar to one another in shape but did show some differentiating features. At all four temperatures there is a transition region in which fatigue lives drop fairly sharply with increases in oxygen pressure until a high pressure plateau is reached at what is termed the maximum transition pressure. This transition pressure is about the same at 300 C as at 20 C but progressively increases with further temperature increases. When these transition pressures are evaluated in terms of a theoretical model of the environmental effect, the agreement is found to be good at low temperatures. However, at high temperatures, the increase in transition pressure is much greater than would be predicted. This shift is attributed to oxidation along crack surfaces reducing the number of oxygen molecules which can reach the advancing crack tip. Supporting evidence is presented in the form of an activation energy calculation. While there was no apparent effect of strain on the maximum transition pressure at either 300 or 550 C, a higher strain decreased the magnitude of the environmental effect at the lower temperature. This behavior probably is related to strain hardening at the lower temperature which is not present at the higher temperature.

KEY WORDS: temperature, fatigue (materials), nickel, environmental effect, oxygen, oxidation, cracks, adsorption, strain, evaluation, tests

In the study of the mechanism of the effect of environment on fatigue, one of the most useful experiments is the observation of the variation in properties as the pressure of a reactive gas is increased. The variation in fatigue life has been demonstrated to be generally S-shaped [*1*].[2] There are plateaus at very low and very high pressures, where an increase in the gas pressure has little or no effect and an intermediate transition range, where the fatigue

[1] Metallurgists, Metallurgy Division, Naval Research Laboratory, Washington, D.C. 20390.

[2] The italic numbers in brackets refer to the list of references appended to this paper.

life drops sharply with increased gas pressure. This decrease has been attributed to gas adsorption at the tip of the propagating crack. Calculations have shown [*2*] that at close to the transition pressure, where the high pressure plateau begins, adsorbed gas should saturate the fatigue crack surfaces as fast as they are being formed, and therefore the environmental effect would be at a maximum. Further pressure increases would not be expected to contribute to the environmental effect.

In order to gain a better understanding of the mechanisms involved it would be desirable to determine the characteristics of these S-shaped curves as a function of temperature. Achter et al [*3*] examined the effect of oxygen on the fatigue of nickel at 300 and 816 C, but the temperature difference was too great to relate the very different curves obtained. Wright and Hordon [*4*] observed a shift in the transition pressure to a higher pressure with a rather slight increase in temperature from 20 to 100 C for aluminum in air but attributed much of this to more rapid crack propagation at the higher temperature.

The present study was undertaken to systematically establish the effect of temperature on the environmental effect of oxygen on nickel over as wide a temperature range as feasible.

Experimental Procedure

The high-temperature, controlled environment fatigue chamber and drive system has been described in detail elsewhere along with specimen geometry and testing procedures [*5*]. Briefly, a sheet metal specimen attached to an extension rod and permanent magnet is vibrated in the environmental chamber by external electromagnets. A constant amplitude of vibration is maintained by electronic feedback loops. The broad resonance peak of the soft nickel of this study did not permit the use of a regenerative technique to maintain the frequency of vibration at resonance; so, frequency was tuned manually with a signal generator. Current to the electromagnets is interrupted, and failure is considered to occur when the power required to maintain a constant amplitude increases to a predetermined value. Experience has shown that crack propagation at this stage is so rapid that the fatigue life is not affected appreciably by the setting of the power level increase for termination.

With this apparatus, specimens can be fatigued at constant amplitude in reversed bending at temperatures up to 800 C and at total pressures ranging from the ultimate vacuum of approximately 10^{-7} to 10^{3} torr of any desired gas. The pressure in the environmental chamber is controlled by means of a wide range variable conductance leak and measured by means of a hot filament ionization gage below 10^{-3} torr and a NRC Model 530 alphatron vacuum gage above 10^{-3} torr.

The ultrahigh-purity oxygen contained the following impurities: 12-ppm argon, 7-ppm nitrogen, 14-ppm krypton, 13-ppm methane, 1-ppm xenon, <1-ppm carbon dioxide, and 11-ppm hydrogen. Analysis of the 99.99 percent nickel showed the following percentages of impurities: 0.006 carbon, <0.001 manganese, 0.0004 iron, 0.001 sulfur, 0.0003 silicon, <0.001 copper, 0.0002 chromium, and 0.0005 cobalt. After machining, the 0.062-in.-thick radiused sheet specimens were vacuum annealed 2 h at 870 C and then electropolished to 0.060 in.

Fatigue life has been determined as a function of oxygen pressure from 10^{-7} to 10^{1} torr at temperatures of 20, 300, 425, and 550 C and at a frequency of 5 Hz. The high-purity nickel used in this study proved too soft to fatigue at higher temperatures. In order to compare directly the effects of oxygen pressure at each temperature, the strain amplitude was adjusted at each temperature to yield a constant fatigue life of about 2×10^{6} cycles at the ultimate vacuum and thus approximately equal crack growth rates. The initial bending strains were measured by means of an especially developed optical technique [*6*]. In order to make comparisons of fatigue life at the various temperatures on the basis of plastic strain, the plastic strain is obtained by deducting the elastic portion from the total strain.

To ensure that strain effects were not contributing to the observations of the effect of temperature, the influence of oxygen pressure was determined at an additional strain at 300 and 550 C.

Results

Fatigue Life Data

The S-shaped curves of fatigue life ratio, N/N_v, versus oxygen pressure at temperatures of 20, 300, 425, and 550 C are shown in Fig. 1, where N/N_v is the ratio of the fatigue life at the chamber pressure to the fatigue life at the ultimate vacuum. The actual fatigue life data are given in Table 1. All four curves are generally similar in shape with some differentiating features. At 20, 300, and 425 C the fatigue lives drop gradually as the oxygen pressure is initially increased, but at 550 C there is an indication of a fairly flat, low pressure plateau. At all four temperatures there is a transition region in which the fatigue lives drop fairly sharply with increases in oxygen pressure until the high pressure plateau is reached at what is termed the maximum transition pressure. At 20 and 300 C this transition pressure is approximately 10^{-3} torr, while at 425 C it is 8×10^{-2} torr, and at 550 C it is 7×10^{-1} torr.

The fatigue life is reduced by a factor of 17 from 10^{-7} to 10^{1} torr at 20 C, while at 300 C this factor is equal to 95. At 425 and 550 C the reduction factor is about 70. At 550 C the high pressure plateau shows an upturn at the

TABLE 1—*Effect of oxygen pressure on fatigue life.*

Temperature, deg C	Plastic Strain, %	Pressure, torr	Fatigue Life, cycles
20.....	0.085	6.0×10^{-8}	2.01×10^{6}
20.....	0.085	1.0×10^{-5}	1.23×10^{6}
20.....	0.085	1.0×10^{-4}	5.79×10^{5}
20.....	0.085	1.0×10^{-3}	1.89×10^{5}
20.....	0.085	1.0×10^{-1}	1.26×10^{5}
20.....	0.085	1.0×10^{1}	1.19×10^{5}
300.....	0.105	1.0×10^{-7}	2.15×10^{6}
300.....	0.105	1.0×10^{-6}	1.17×10^{6}
300.....	0.105	1.0×10^{-6}	1.12×10^{6}
300.....	0.105	1.0×10^{-5}	7.38×10^{5}
300.....	0.105	1.0×10^{-4}	3.18×10^{5}
300.....	0.105	1.0×10^{-4}	2.94×10^{5}
300.....	0.105	3.0×10^{-4}	2.04×10^{5}
300.....	0.105	1.0×10^{-3}	2.92×10^{4}
300.....	0.105	1.0×10^{-1}	2.23×10^{4}
300.....	0.105	1.0×10^{1}	2.40×10^{4}
300.....	0.170	7.0×10^{-8}	3.68×10^{5}
300.....	0.170	1.0×10^{-6}	3.30×10^{5}
300.....	0.170	1.0×10^{-5}	1.85×10^{5}
300.....	0.170	1.0×10^{-4}	1.44×10^{5}
300.....	0.170	1.0×10^{-3}	1.71×10^{4}
300.....	0.170	1.0×10^{-1}	1.56×10^{4}
300.....	0.170	1.0×10^{1}	1.94×10^{4}
425.....	0.088	4.6×10^{-8}	1.60×10^{6}
425.....	0.088	1.0×10^{-5}	1.22×10^{6}
425.....	0.088	1.0×10^{-3}	2.64×10^{5}
425.....	0.088	1.0×10^{-2}	1.63×10^{5}
425.....	0.088	1.0×10^{-1}	2.49×10^{4}
425.....	0.088	1.0×10^{1}	2.56×10^{4}
550.....	0.063	1.0×10^{-7}	2.04×10^{6}
550.....	0.063	1.0×10^{-5}	1.94×10^{6}
550.....	0.063	1.0×10^{-3}	7.67×10^{5}
550.....	0.063	1.0×10^{-2}	4.50×10^{5}
550.....	0.063	1.0×10^{-1}	1.13×10^{5}
550.....	0.063	1.0×10^{0}	2.88×10^{4}
550.....	0.063	1.0×10^{1}	3.96×10^{4}
550.....	0.105	1.0×10^{-7}	7.64×10^{5}
550.....	0.105	1.0×10^{-5}	5.55×10^{5}
550.....	0.105	1.0×10^{-3}	1.86×10^{5}
550.....	0.105	1.0×10^{-2}	1.53×10^{5}
550.....	0.105	1.0×10^{-1}	3.98×10^{4}
550.....	0.105	1.0×10^{0}	1.10×10^{4}
550.....	0.105	1.0×10^{1}	2.15×10^{4}

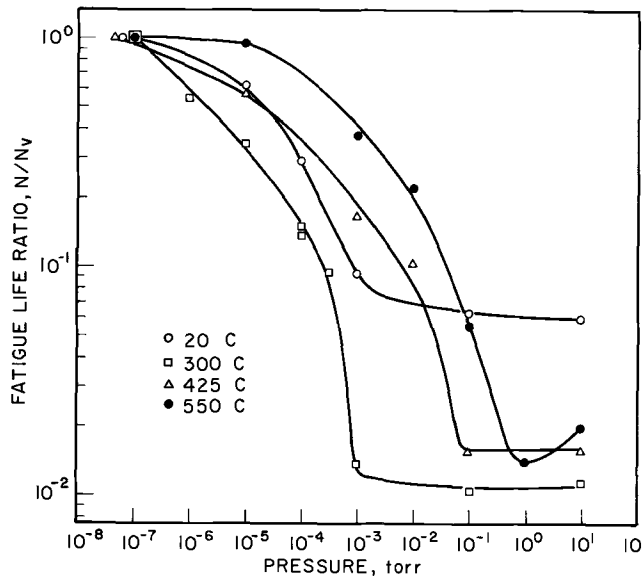

FIG. 1—*Ratio of fatigue life in oxygen to the life at the ultimate vacuum,* N/N_v, *plotted as a function of oxygen pressure at 20, 300, 425, and 550 C.*

highest pressure. This upturn of the pleateau at high oxygen pressures is attributed to oxidation bridging the cracks and providing additional strength [*3*].

The effect of strain on the S-shaped curves is shown in Figs. 2 and 3 for 300 and 550 C, respectively. At 300 C it can be seen that the curves for the two strains are very similar in shape. The major difference is in the magnitude of the reduction of fatigue life by oxygen. While fatigue life is reduced by a factor of 95 at the low strain, the reduction is only 23 at the high strain. The effect of strain on fatigue life is most evident at the ultimate vacuum where the life is six times longer at the lower strain than at the higher strain. On the high pressure plateau, the life at the lower strain is only 1.4 times greater. There is, however, no detectable change in the maximum transition pressure with the change in strain.

At 550 C, Fig. 3, the decrease of fatigue life with increasing oxygen pressure is the same at both strains with the lives 2.7 times longer at the lower strain. The high pressure plateau upturn is demonstrated at both strains, and there is no detectable change in the transition pressure.

Metallographic Observations

Photomicrographs of failed specimen sections show the effect of environment as a function of temperature at the highest and lowest pressures, in

Figs. 4 through 8. There are only moderate differences between the low and high pressure specimens at 20 C (not shown). More deformation occurs at the low pressure, especially at the surface. Although there is more extensive cracking at the high pressure, both specimens exhibit primarily transgranular cracking. The 300 C micrographs show extreme differences at the two pressures. Some of the initial grain structure is retained at the low pressure, Fig. 4, but there is evidence of extensive deformation and fragmentation, both at the surface and near the very broad and rounded cracks that are present. It is not possible to ascertain the mode of cracking. In contrast, the high pressure specimen, Fig. 5, shows the original structure with some surface roughening and deformation. The sharp cracks are primarily intergranular although some cracks started transgranularly. There are many more short cracks present at both pressures at 300 than at 20 C.

At 425 C the structures are changed considerably. It is apparent from the surface roughness that there has been considerable deformation at the low pressure, Fig. 6, but complete recrystallization has occurred. The main cracks are broad and rounded and appear to be largely transgranular with many short surface intergranular cracks. The high pressure specimen, Fig. 7, has recrystallized as well, although there is evidence of prior deformation

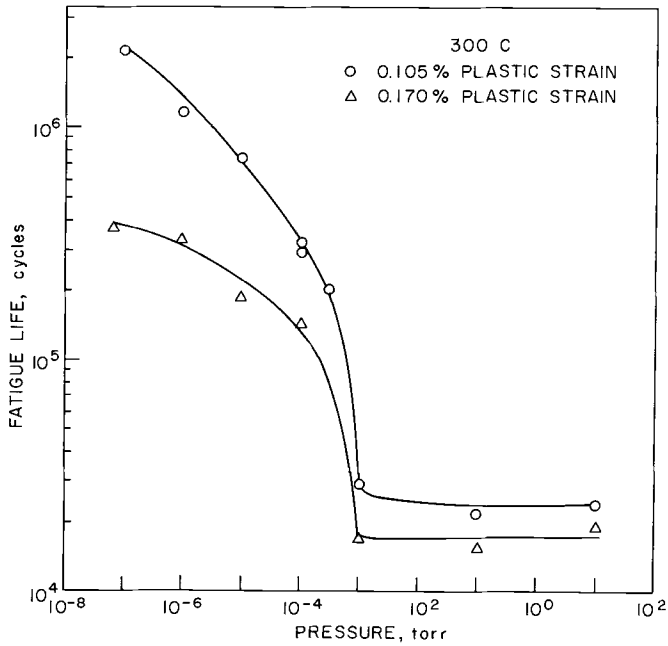

FIG. 2—*Fatigue life plotted as a function of oxygen pressure for plastic strains of 0.105 and 0.170 percent at 300 C.*

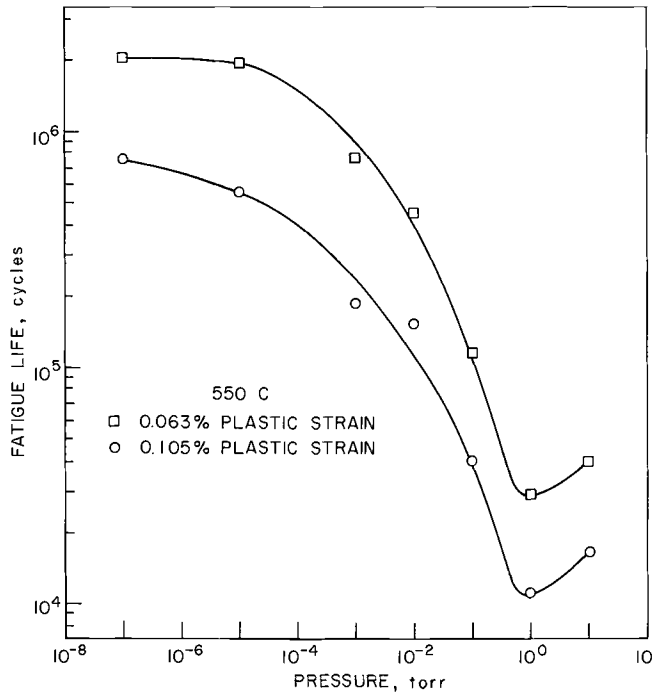

FIG. 3—*Fatigue life plotted as a function of oxygen pressure for plastic strains of 0.063 and 0.105 percent at 550 C.*

since the grain size is larger in the interior than at the surface. Cracking is more extensive and almost exclusively intergranular. Micrographs of etched sections are not shown for 550 C, but the structures obtained are very similar to those at 425 C. The principal difference is that intergranular cracking is shown on the low pressure as well as the high pressure specimen. A significant observation on the high pressure specimen is shown in an unetched section in Fig. 8. The small crack shown is typical of the longer cracks in this specimen, and bulk oxide is present lining the crack surfaces.

The following general observations on the effects of increased oxygen pressure on structure may be made:

1. Much less deformation is associated with crack propagation at high pressures.

2. The change in mode of failure with increasing temperature to intergranular cracking is accelerated significantly by high pressures.

Since the fatigue lives at high pressures are so short, it is only reasonable that there would be less cumulative strain and consequent deformation associated with crack propagation. The tendency to intergranular cracking

FIG. 4—*Longitudinal section of specimen fatigued at 300 C and 10^{-7} torr. Etched with aqua regia saturated with $CuCl_2$ and diluted 10 to 1.* (×100).

FIG. 5—*Longitudinal section of specimen fatigued at 300 C and 10 torr of oxygen. Etchant same as Fig 4.* (×*100*).

FIG. 6—*Longitudinal section of specimen fatigued at 425 C and 10^{-7} torr. Etchant same as Fig. 4.* (×100).

FIG. 7—*Longitudinal section of specimen fatigued at 425 C and 10 torr of oxygen. Etchant same as Fig. 4.* (×100).

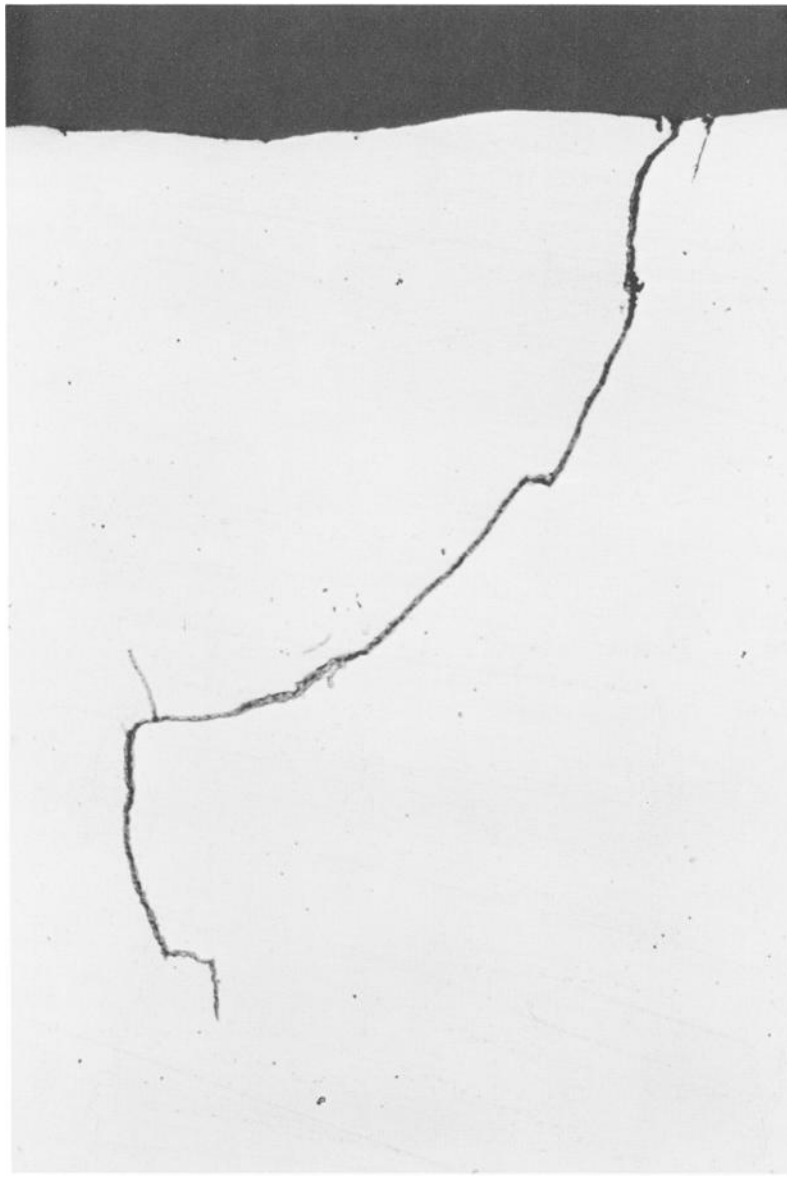

FIG. 8—*Longitudinal section of specimen fatigued at 550 C and 10 torr of oxygen. Unetched.* (×500).

at high pressures has been observed also by Snowden in the fatigue of lead [7]. This tendency may be attributable to the higher reactivity of the grain boundaries and their attendant greater affinity for oxygen which increases the rate of crack propagation.

Discussion

It is possible to evaluate the fatigue life versus oxygen pressure curves of this study in terms of a surface adsorption model of the environmental effect. Smith et al [2] have demonstrated that the maximum transition pressure can be calculated theoretically by equating the time available for coverage of freshly exposed atoms at the crack tip with the gas saturation time as calculated from kinetic theory.

This approach yields the expression:

$$P = \frac{4f(da/dN)D\sqrt{MT}}{7 \times 10^{22}\chi} \quad \ldots\ldots\ldots\ldots\ldots\ldots (1)$$

where:

P = transition pressure, torr,
f = frequency of vibration, Hz,
da/dN = crack growth rate, cm cycle^{-1},
D = planar atomic density, cm^{-2},
M = molecular weight of gas,
T = absolute temperature, deg K, and
χ = interatomic spacing, cm.

Substituting values from the experimental conditions in this investigation of $f = 5$ Hz, $D = 1.85 \times 10^{15}$ cm^{-2}, $M = 32$, and $\chi = 2.5 \times 10^{-8}$ cm, Eq 1 becomes:

$$P = 1.2 \times 10^{2}\,(da/dN)\sqrt{T} \quad \ldots\ldots\ldots\ldots\ldots\ldots (2)$$

Since the high-purity nickel in this study proved too soft to apply the regenerative technique that maintains the specimen at resonance, crack growth rates could not be obtained as with stainless steel [2], but an average value can be calculated. The fatigue lives on the high pressure plateaus at 300, 425, and 550 C are about the same, and it is convenient to calculate an average value of crack growth rate for these temperatures. The average crack length at failure was about half the thickness or 7.5×10^{-2} cm. Dividing this by an average fatigue life of 2.5×10^{4} cycles on the high pressure plateaus yields an average crack growth rate of 3×10^{-6} cm/cycle. The maximum transition pressure, then, at 300 C comes out to 8.6×10^{-3} torr or fairly close to the observed value of 10^{-3} torr.

Although no shift in the transition pressure was detected with a temperature change from 20 to 300 C, a shift of almost 10^3 torr occurred between 300 and 550 C. Achter et al [*3*], in a study of the effect of oxygen on a less pure nickel at 816 C which had a similar fatigue life at high pressures, observed a maximum transition pressure of 1.7×10^1 torr. A total shift of over 10^4 torr is exhibited with an increase of temperature from 300 to 816 C. Based on the effect of a temperature change on the rate of impingement alone a shift by the ratio of the square roots of the temperatures, or less than a factor of 2, would be predicted from 20 to 816 C. Clearly another explanation is required. Either oxygen is not reacting in the same manner at the crack tip, or it is not arriving at the crack tip at the predicted rate.

Sticking probability may either increase or decrease with temperature depending on the nature of the surface reaction and the surface structures formed [*8*]. No experimental evidence has been found to suggest that the sticking probability of oxygen on nickel decreases with temperature, and MacRae [*9*], in his low-energy electron diffraction study, found one of the adsorption structures formed on the (001) surface of nickel to have a strongly temperature dependent sticking probability which varied from 0.04 at room temperature to almost unity in the 150 to 250 C temperature range. Due to the limited temperature range of this study and the crystallographic anisotropy and multiplicity of possible surface structures exhibited by the nickel, the evidence cannot be considered conclusive, but it does not seem likely that the increase in transition pressure can be attributed to a decrease in sticking probability.

The possibility also has been considered that the transition pressure shift is related to the observed change in the mode of failure of nickel of this purity between 300 and 550 C [*10*]. The continuing shift of the transition pressure beyond this temperature range would seem to argue against this, however.

It seems most probable that, as temperature increases, the rate of arrival of oxygen at the tip of the crack is diminished as oxidation increases along the crack surfaces. At higher temperatures a greater number of the oxygen molecules moving down a crack react as they strike crack surfaces and form bulk oxide before reaching the crack tip. In Fig. 9 the logarithm of maximum transition pressure is plotted as a function of reciprocal temperature. It can be seen that a straight line relationship with a negative slope holds on this Arrhenius type plot in the temperature region of transition pressure shift. Although an activation energy can be derived from the plot, it is not possible to compare it directly with activation energies for oxidation for several reasons. The activation energy for oxidation of nickel is determined customarily for the parabolic rate constant rather than actual oxidation rates to which the transition pressure shift would presumably be proportional.

The increase in pressure would in itself cause an increase in oxidation rates, and the required pressure gradient, the variation in oxide film thickness, and surface diffusion along the length of the crack further complicate the model. Fortunately the fatigue lives at the maximum transition pressures are very close to one another so that the times available for oxidation at various crack lengths should be comparable at each temperature. Indeed, this is probably the reason the Arrhenius relationship holds.

Although many aspects of this model are difficult to quantitatively evaluate, it is simple to place our activation energy on a rate constant basis if, as stated above, it is assumed that the transition pressure shift is proportional to oxidation rate. From the parabolic law the square of the oxidation rate is proportional to the rate constant at constant time. The activation energy, then, as derived from Fig. 9, should be doubled for comparison with values based on the rate constant due to the logarithmic nature of the Arrhenius plot. An activation energy of 47.2 kcal/mole then is obtained which is fairly close to the value of 41.2 kcal/mole for the activation energy for the oxidation of high-purity nickel, as determined by Gulbransen and Andrew [*11*]. This model is strengthened further by the observation that an oxide

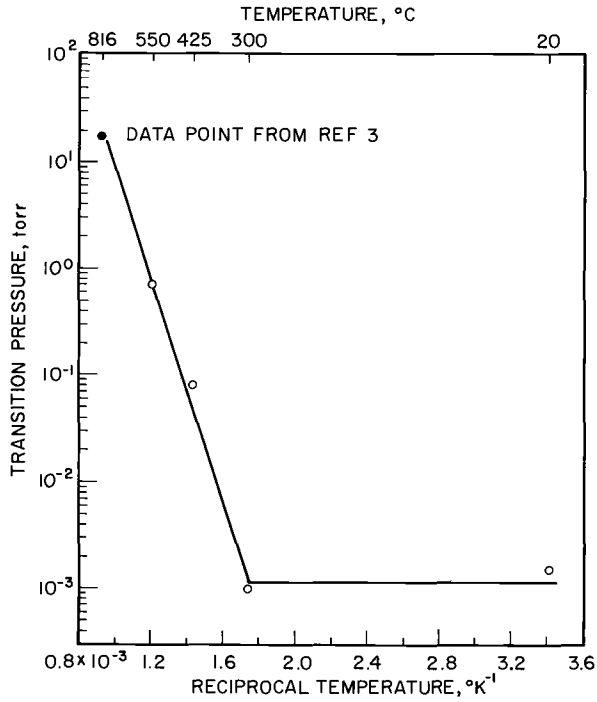

FIG. 9—*Maximum transition pressure plotted as a function of reciprocal temperature.*

film is observed first at the maximum transition pressure at 425 C on the surface of failed specimens. The oxide film at 425 C is too thin to be seen in a sectioned specimen, but oxide was observed in the section at 550 C (Fig. 8).

Theory predicts a shift in the transition pressure with crack growth rate and therefore with strain as well. No such shift was observed at either 300 or 550 C. The predicted magnitudes of the shift would be by factors of only 1.4 and 2.7, respectively, for the two temperatures. This is probably too small an effect to be detected reliably in our results, and much larger changes in strain would be required to evaluate adequately the theory in this particular.

Although the kinetics of the pressure dependence of the environmental effect can be explained on the basis of adsorption theory, the magnitude of the reduction of fatigue life cannot be treated quantitatively at this time. The nature of the interaction of adsorbing oxygen molecules with the atomistic mechanism of fracture at the advancing crack tip should determine the magnitude, and this interaction is not understood well at all.

It is of interest to consider why an increase in strain reduces the environmental effect at 300 C, but no such change is noted at 550 C. There is evidence which indicates that this behavior may be related to strain hardening. In the study of Smith et al [*2*] on stainless steel, the magnitude of the environmental effect on crack growth rate was decreased by an increase in strain[3] at 500 C but not at 800 C. The stainless steel strain hardened appreciably at 500 C but not at 800 C. Furthermore, another lot of stainless steel which did not significantly strain harden at 500 C due to a lower annealing temperature also showed little effect of strain on the environmental effect. Other investigators [*12*, *13*, *14*] have shown an effect of strain at room temperature, where strain hardening would be expected. Since the micrographs of the nickel of our study showed evidence of considerable prior strain at 300 C and a completely recrystallized structure was present at 550 C, the conditions are analogous to those of the investigations cited. Although the detailed mechanism is unknown it seems probable that the temperature dependence of changes in the magnitude of the environmental effect with strain is related to strain hardening at low temperatures, which is not possible at high temperatures due to relaxation.

Acknowledgment

The authors wish to thank T. R. Harrison, Jr., for assistance with the metallography and M. R. Achter for helpful comments and review of the manuscript.

[3] Their constant amplitude fatigue data actually show a reduction in the environmental effect with an increase in crack length which is equivalent to an increase in strain.

References

[1] Achter, M. R., "Effect of Environment on Fatigue Cracks," *Fatigue Crack Propagation, ASTM STP 415*, American Society for Testing and Materials, 1967, p. 181.

[2] Smith, H. H., Shahinian, P., and Achter, M. R., "Fatigue Crack Growth Rates in Type 316 Stainless Steel at Elevated Temperatures as a Function of Oxygen Pressure," *Transactions*, Metallurgical Society, American Institute of Mining, Metallurgical, and Petroleum Engineers, Vol. 245, 1969, p. 947.

[3] Achter, M. R., Danek, G. J., Jr., and Smith, H. H., "Effect on Fatigue of Gaseous Environment under Varying Temperature and Pressure," *Transactions*, Metallurgical Society, American Institute of Mining, Metallurgical, and Petroleum Engineers, Vol. 227, 1963, p. 1296.

[4] Wright, M. A. and Hordon, M. J., "Temperature Dependence of the Fatigue Transition Pressure for Aluminum," *Acta Metallurgica*, Vol. 15, 1967, p. 430.

[5] Achter, M. R. et al, "Flexural Fatigue Machine for High Temperature Operation at Resonance in Vacuum," *The Review of Scientific Instruments*, Vol. 37, 1966, p. 311.

[6] Danek, G. J., Jr., Smith, H. H., and Achter, M. R., "High Temperature Fatigue and Bending Strain Measurements in Controlled Environments," *Proceedings*, American Society for Testing and Materials, Vol. 61, 1961, p. 775.

[7] Snowden, K. U. and Greenwood, J. N., "Surface Deformation Differences Between Lead Fatigued in Air and in Partial Vacuum," *Transactions*, Metallurgical Society, American Institute of Mining, Metallurgical, and Petroleum Engineers, Vol. 212, 1958, p. 626.

[8] Hobson, J. P., "Pumping at Solid Surfaces," *British Journal of Applied Physics*, Vol. 14, 1963, p. 544.

[9] MacRae, A. U., "Adsorption of Oxygen on the {111}, {100}, and {110} Surfaces of Clean Nickel," *Surface Science*, Vol. 1, 1964, p. 319.

[10] Stegman, R. L. and Achter, M. R., "Failure Modes in Nickel Fatigued in Vacuum as a Function of Temperature and Purity," *Transactions*, Metallurgical Society, American Institute of Mining, Metallurgical, and Petroleum Engineers, Vol. 239, 1967, p. 742.

[11] Gulbransen, E. A. and Andrew, K. F., "The Kinetics of Oxidation of High Purity Nickel," *Journal*, Electrochemical Society, Vol. 101, 1954, p. 128.

[12] Snowden, K. U., "The Effect of Atmosphere on the Fatigue of Lead," *Acta Metallurgica*, Vol. 12, 1964, p. 295.

[13] Bradshaw, F. J. and Wheeler, C., "The Effect of Environment on Fatigue Crack Growth in Aluminium and Some Aluminium Alloys," *Applied Materials Research*, Vol. 5, 1966, p. 112.

[14] Hordon, M. J., "Fatigue Behavior of Aluminum in Vacuum," *Acta Metallurgica*, Vol. 14, 1966, p. 1173.

C. H. Wells[1] *and C. P. Sullivan*[1]

Interactions Between Creep and Low-Cycle Fatigue in Udimet 700 at 1400 F

REFERENCE: Wells, C. H. and Sullivan, C. P., **"Interactions Between Creep and Low-Cycle Fatigue in Udimet 700 at 1400 F,"** *Fatigue at High Temperature, ASTM STP 459*, American Society for Testing and Materials, 1969, pp. 59–74.

ABSTRACT: The cumulative damage concept in low-cycle fatigue with intermittent hold times was assessed for Udimet 700 at 1400 F. A 20 or 60 min period of tensile stressing in each strain cycle reduced the cyclic life in conservative agreement with the linear cumulative damage rule. However, the effect of holding compressive strain was more damaging than holding tensile strain. Similarly, the effect of creep prestrain on the subsequent fatigue behavior was more deleterious when applied in compression than in tension. Furthermore, the creep rate in compression was less than half that in tension and continuously decreased with strain.

Observations of the Bauschinger effect indicated that high internal stresses accompanied both creep and plastic deformation; these stresses are attributed to the pileup of dislocations at grain boundaries. It is postulated that the pileup is relaxed by cavitation and that the rate of deformation is governed by the growth of these cavities as they annihilate dislocations. These cavities were observed to be a source of intergranular cracking in creep and low-cycle fatigue. The rate of growth of the cavities, in turn, is affected by the hydrostatic component of stress, accounting for the decelerating creep in compression. In addition the shape of the cavities influences the rate of crack propagation and fracture toughness: round cavities promote toughness, while cavities flattened by compressive creep provide easy propagation paths.

KEY WORDS: fatigue (materials), creep, nickel-base alloy, cyclic loads, cracking, evaluation, tests

In order to predict the service lifetime of materials at elevated temperature, it is necessary to be able to separate time-dependent from cycle-dependent cracking. In this paper various aspects of the interaction between creep and low-cycle fatigue damage are explored for a wrought nickel-base superalloy, Udimet 700, that has found application in gas turbine blades and disks.

The voluminous literature in this area has been reviewed by Meleka [*1*][2] and most recently by Ellison [*2*]. In general it has been found that hold times at

[1] Assistant directors, Advanced Materials Research and Development Laboratory, Pratt & Whitney Aircraft, Middletown, Conn. 06458. Mr. Wells is a personal member ASTM.

[2] The italic numbers in brackets refer to the list of references appended to this paper.

the maximum strain limit significantly reduce the cyclic life and may effect a change of crack initiation mode from transgranular to intergranular [*3*]. Three different viewpoints have been taken in attempts to correlate lifetime under superimposed creep and fatigue conditions. First, the major effect of creep or relaxation in a cycle may be considered to increase the plastic strain range per cycle [*4*], thus reducing the fatigue lifetime according to the Manson-Coffin law. A second hypothesis is that all the damage is in creep, so that the tensile portion of the strain cycle contributes to the creep fracture in the same manner as the stress during the hold period [*5*]. The third possibility is that creep and fatigue mechanisms are mutually independent and that fracture occurs when the sum of the creep and fatigue damage reaches a critical value [*6*]. Consequently, in order to formulate an interaction law it would appear necessary first to identify the mechanisms of time-dependent and cycle-dependent fracture. The danger in extrapolating high-temperature fatigue behavior without such precaution has been emphasized by Edmunds and White [*7*].

The metallographic identification of mechanisms has received much less attention than the mechanical variables, and indeed the separate mechanisms of creep or fatigue are not understood in complex alloys. For this reason the material and test conditions for the present investigation were chosen because a considerable amount of information is available concerning the low-cycle fatigue and creep behavior. The mechanical and metallurgical aspects of low-cycle fatigue of Udimet 700 have been investigated in detail at 1400 F [*8*] and over the temperature range from 70 to 1400 F [*9*] at a frequency of 1 to 2 cpm. The most salient effect of elevated temperature was found to be the onset of intergranular surface crack initiation above 1200 F. The intergranular cracking bypassed the nucleation of slip band cracks, observed at lower temperatures, and drastically reduced the number of cycles required to produce a surface macrocrack. The appearance of the surface cracks could not be distinguished from that under static creep conditions. However, the propagation stage was very much more rapid, with a transition to Stage II transgranular fatigue crack growth occurring at a depth below the surface of about one grain diameter. Ellison and Sullivan [*10*] reported that surface integranular cracking of this material could be detected at 0.8 percent elongation in static creep tests at 1400 F, as contrasted with a greater than 10 percent elongation at rupture. The effect of superimposed low-amplitude stress cycling was not apparent until this level of specimen elongation had been attained; thereupon, the cracks propagated transgranularly across the specimen, significantly curtailing rupture life and elongation by amounts depending upon the frequency and amplitude of the stress. These observations underline a very important consideration in combined creep and fatigue testing, namely, that crack initiation and propagation may involve different modes of fracture, and the

mechanisms of time-dependent and cycle-dependent damage must be determined for each mode. The integranular crack initiation in low-cycle fatigue has been suppressed effectively by a thin (0.002 to 0.003 in.) intermetallic coating [*11*], suggesting a prominent role of oxygen diffusion along grain boundaries. On the other hand, a small but definite amount of intergranular cracking has been observed in the specimen interior, unconnected with the free surface. Intergranular cracking in Udimet 700 often occurs adjacent to the grain boundary in the gamma prime depleted zone adjacent to the carbide or boride particles. In previous work it was suggested [*11*] that intergranular cracking results from the impingement of coarse slip bands upon the grain boundary. The basis for this argument was, first, observations of surface slip traces at 1400 F and, second, the Bauschinger effect in uniaxial strain cycling. It was demonstrated [*12*] that the hysteresis loop size and shape could be predicted by assuming the strain hardening to be entirely attributable to the blockage of slip bands by grain boundaries, with a long-range internal stress resulting from the pileup of dislocations and aiding their motion under a reversal of load. The slip band displacements and the magnitudes of the stress singularities, in turn, were shown to be proportional to the total strain.

Three major types of interaction between creep and low-cycle fatigue are considered in this paper:

1. The effect of creep and relaxation during each cycle on low-cycle fatigue endurance.
2. The effect of creep prestrain on subsequent low-cycle fatigue behavior.
3. The effect of monotonic and cyclic prestrain on subsequent creep behavior.

Experimental Procedure

Most of the tests were conducted on ⅜-in.-diameter, 1-in.-gage length buttonhead specimens prepared from 1-in. HRCG Udimet 700[3] bar stock by grinding, mechanical polishing through 600 grit paper, and finally electropolishing in a solution of 7 parts methanol to 1 part sulfuric acid to remove all traces of cold work. Rough-machined specimens were heat treated in argon according to the following schedule: 2125 F/4 h air cooled; 1975 F/4 h air cooled; 1550 F/4 h air cooled; 1400 F/16 h air cooled. The elongation over the uniform gage length was measured by clamping the halves of a Wiedemann-Baldwin PSH-8MS extensometer to thin ridges ground on the specimen. The buttonhead ends were clamped to rigid loading rods in a Wiedemann Mark G loading frame employing preloaded ball screws and SR 4 load cells. The machine controls were arranged specially for the combined low-cycle fatigue and creep cycle. It was thought that creep damage

[3] Composition: 19.5Co, 15.0Cr, 5.1Mo, 4.4Al, 3.5Ti, 0.06C, 0.03B, 0.19Fe; Si, Mn, Cu all <0.01; Zr <0.05; balance Ni.

could be determined more accurately if the dwell period involved a constant stress rather than constant strain, thus simplifying comparison with the static creep test. In each cycle the specimen was unloaded from the peak tensile strain to the level of creep stress desired during the hold time. To minimize the number of test variables, a single total strain range, 0.016 in./in., and steady stresses of 70 and 80 ksi for 20 and 60 min per cycle were applied. In auxiliary tests the machine was rewired to hold zero strain or 0.016 strain in each cycle within about ± 0.0001 in./in. Strain was controlled by electronic limit switches on the Y-axis of a Moseley 2D-2 recorder. The Y-axis was modified by gearing a slave linear variable differential transformer (LVDT) transducer to the pen drive such that the master LVDT output in the extensometer was balanced continually by that of the slave, thus providing a strain reading at a constant magnification ratio and stability over long test durations. During the strain cycle the load reading was transmitted from the testing machine dial to the X-axis of the recorder. At the start of each hold period this axis was switched from a load base to time base, so that the strain history in each cycle was recorded. At the same instant the machine control was switched from strain cycling to either load hold or strain hold, and a low crosshead speed selected. When the desired time period had elapsed, the machine was switched back to complete the strain cycle at the higher crosshead speed, and the hysteresis loop was completed on the recorder. The chart drive speed during the hold period was selected to index the hysteresis loops by convenient intervals. Pure creep tests also were conducted in the same machine and with the same specimen design. The accuracy with which the stress was maintained was $\pm$ 1 percent, neglecting area change during the test.

Other tests to determine the effect of tensile prestrain upon subsequent tensile creep were conducted in deadweight creep machines on ¼-in.-diameter, 1½-in.-gage length specimens, similarly prepared and instrumented. Two weight elevators were installed in each machine, one to provide the steady creep stress and the other supporting a large weight to allow prestraining the specimen via the manual drawhead drive.

In all tests the specimen temperature was measured at the center and both ends of the gage length by chromel-alumel thermocouples and controlled within $\pm$ 1 F throughout the test. All tests were carried out at 1400 F.

Results

Fracture Behavior

The results of tests combining creep or relaxation in each strain cycle are summarized in Table 1 together with the "pure" low-cycle fatigue and creep data. In addition to fracture lives, an estimate of the number of cycles to

initiation has been made from plots of load range versus number of cycles, wherein initiation was defined to coincide with a break in the strain softening curve [*11*]. These results show that initiation under cyclic conditions may be less rapid than in static creep at the same temperature and stress, but that creep loading significantly reduces the cyclic life. Also it is apparent that compressive relaxation is more deleterious than tensile relaxation. This last point was checked by subjecting other specimens to a one percent tensile or compressive creep prestrain under a static stress of 80 ksi. The results are summarized in Table 2. In this case the rate of cracking was more rapid following compressive prestrain, and actually slightly reduced by tensile prestrain.

TABLE 1—*Results of tests combining creep or relaxation.*

Hold Conditions	Cycles (time) to Initiation	Cycles (time) to Rupture
TESTS AT 1400 F, 0.016 TOTAL STRAIN RANGE WITH HOLD TIME		
None, 2 cpm.....	170 (< 2 h)	197
70 ksi/20 min.....	135 (45 h)	170 (57 h)
70 ksi/60 min.....	105 (105 h)	125 (125 h)
80 ksi/20 min.....	94 (31 h)	128 (43 h)
80 ksi/60 min.....	54 (54 h)	71 (71 h)
0.016 strain/15 min..	...	155 (41 h)
0 strain/15 min.....	...	113 (32 h)
STATIC TENSILE CREEP AT 1400 F [*10*]		
70 ksi.....	(75 h)	(250 h)
80 ksi.....	(25 h)	(55 h)

TABLE 2—*Tests at 1400 F, 0.016 total strain range following creep prestrain.*

Prestrain under 80 ksi	Cycles to Initiation	Cycles to Fracture
0.010 tension (21 h).....	160	224
−0.0094 compression (64 h).	120	154

Effect of State of Stress on Creep

In the course of producing the creep prestrain it was noted that the behavior in compression was quite different from that in tension under the same nominal stress. Figure 1 shows a secondary creep rate in tension, with an

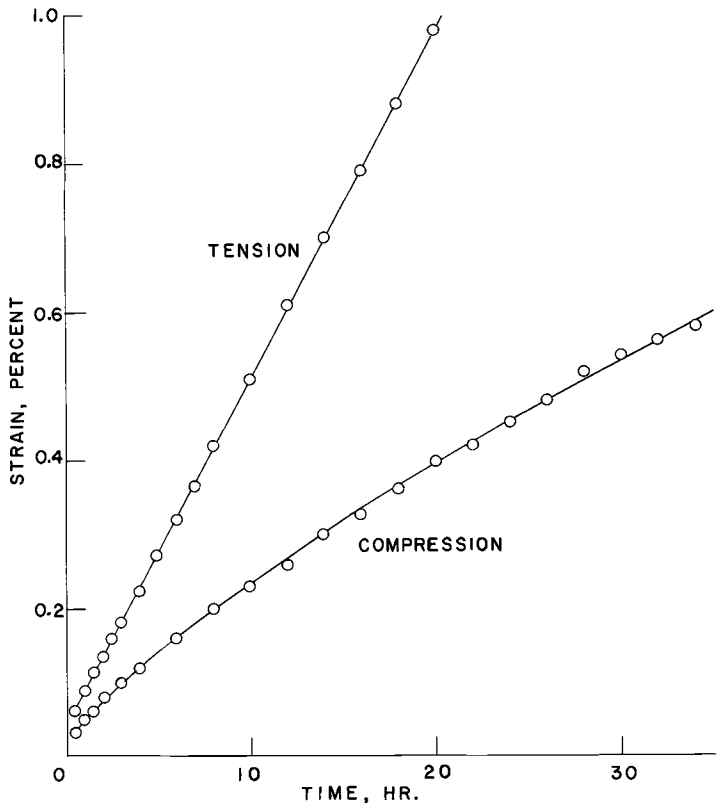

FIG. 1—*Creep curves in tension and compression for Udimet 700 at 1400 F under 80 ksi axial stress.*

elongation of one percent reached in about 20 h. In contrast the creep rate in compression continually decreased, so that the compressive prestrain of 0.94 percent required 64 h. This discrepancy was at first attributed to differences in true stress accompanying diametral strain and to a large stress dependence of creep rate. Expressing the creep rate in terms of the applied load, P, the original area, A_o and the axial strain, ϵ,

$$\dot{\epsilon} = B\left[\frac{P}{A_o(1 \mp \epsilon)}\right]^n$$

where the minus sign signifies tensile creep. Integrating this expression, one obtains

$$\pm 1 \mp (1 \mp \epsilon)^{n-1} = (n + 1)\, B\left(\frac{P}{A_o}\right)^n t$$

with the upper signs applying to tension and the lower to compression. Then

at the same time and for the same initial stress, the differences between the creep strains in tension and compression may be found from the relationship,

$$(1 - \epsilon_t)^{n+1} + (1 + \epsilon_c)^{n+1} = 2$$

For Udimet 700 at 1400 F the stress dependence of creep rate, n, lies between 10 and 12. For a compressive creep strain of one percent, this calculation predicts a corresponding tensile creep strain of between 1.10 and 1.14 percent on the basis of area change alone. Consequently, the creep behavior illustrated in Fig. 1 represents an effect of hydrostatic stress on the mechanism of the creep process.

Bauschinger Effect

As an indication of the relative magnitudes of internal stress developed in static creep and plastic deformation, the Bauschinger effect was compared for the 0.94 percent compressive creep prestrain and a plastic prestrain of 1.0 percent applied at a rate of about 0.01 in./in./min. The subsequent stress-strain curves are seen in Fig. 2 to be essentially identical.

Effect of Prestrain on Creep

Finally, the effect of a one percent plastic tensile or creep prestrain upon the subsequent tensile creep behavior was determined. The results are shown in Figs. 3-5. No effect of a single tensile prestrain was noted at either 80 or 70 ksi. Compressive prestrain resulted in a long period of transient creep, varying as $t^{-1/3}$, and a slight increase in rupture life. The transient creep represents the relaxation of internal stresses, which in this case aid tensile deformation.

The increments of creep strain during each period of constant stress in the interaction tests were added and the total creep strain plotted against elapsed

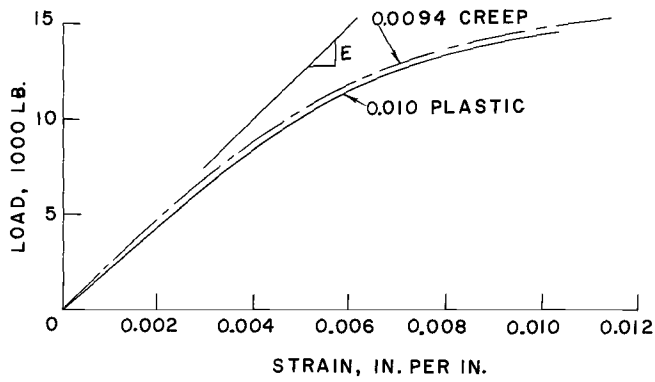

FIG. 2—*Comparison of the Bauschinger effect for compressive prestrain in creep and short-time yielding.*

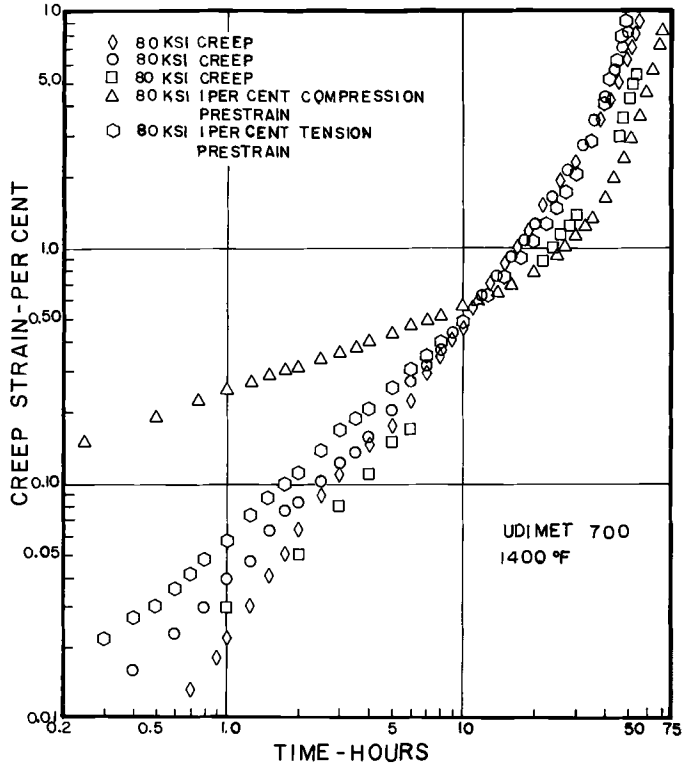

FIG. 3—*Effect of prior plastic prestrain on the creep behavior of Udimet 700 under 80 ksi axial tension.*

time. No difference could be found between this curve and the usual static creep curve for the 80 ksi stress (Fig. 4). At 70 ksi, however, the creep rate in cyclic loading was more rapid than the static rate and was greater at the higher frequency of straining, as shown in Fig. 5.

Metallographic Observations

Longitudinal sections of static creep specimens were etched to reveal slip and cracking behavior. The slip traces were planar and heterogeneous (Fig. 6) in both tensile and compressive creep under 80 ksi axial stress and were similar to those produced by short-time plastic deformation. Thin foil transmission electron microscopy revealed no difference in the distribution, density, or structure of dislocations in pure creep, pure fatigue, or the combined creep and fatigue specimens. These observations support the identity of the Bauschinger effect following plastic and creep prestrain. Surface integranular cracking was evident in the tension creep specimen but not in the compression specimen. Several examples of internal grain boundary cracking were observed in the instance of compressive creep; one such crack is shown in Fig. 7.

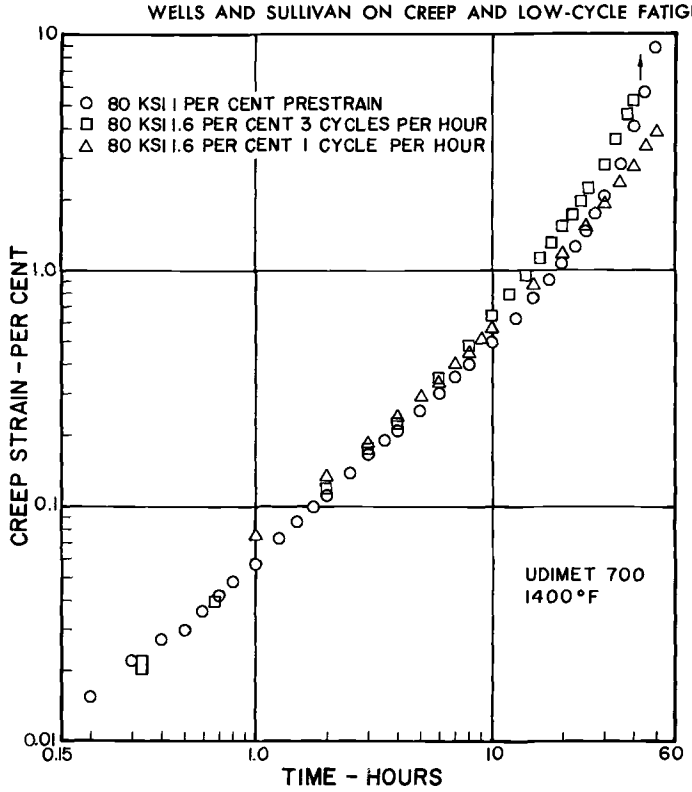

FIG. 4—*Comparison of effects of monotonic and cyclic prestrain on the creep behavior of Udimet 700 under 80 ksi tensile stress.*

Some cracks appeared to be oriented normal to the stress axis in the plane of observation, and some were relatively sharp. In contrast, the internal grain boundary cracks in tensile creep, shown in Fig. 8, often consisted of rows of individual cavities of more circular cross section. It should be pointed out, however, that the shapes of such small cracks depend critically upon specimen preparation techniques.

In the combined creep and fatigue specimens, crack initiation was intergranular and primarily concentrated at the free surface. One effect noticed in specimens subject to superimposed creep was the production of broad, crack containing shear zones along twin and grain boundaries, in addition to the grain boundary cracking normal to the stress axis observed in pure low-cycle fatigue [*8*]. The appearance of typical surface cracks may be seen in Fig. 9. Light polishing below the surface indicated that depletion of grain boundary precipitates was a precursor to intergranular cracking, Fig. 10.

Significant internal intergranular crack growth was observed in all the specimens with hold times at 70 and 80 ksi. There was no definite trend in degree of cracking with either hold time or stress. Twin boundary shear and

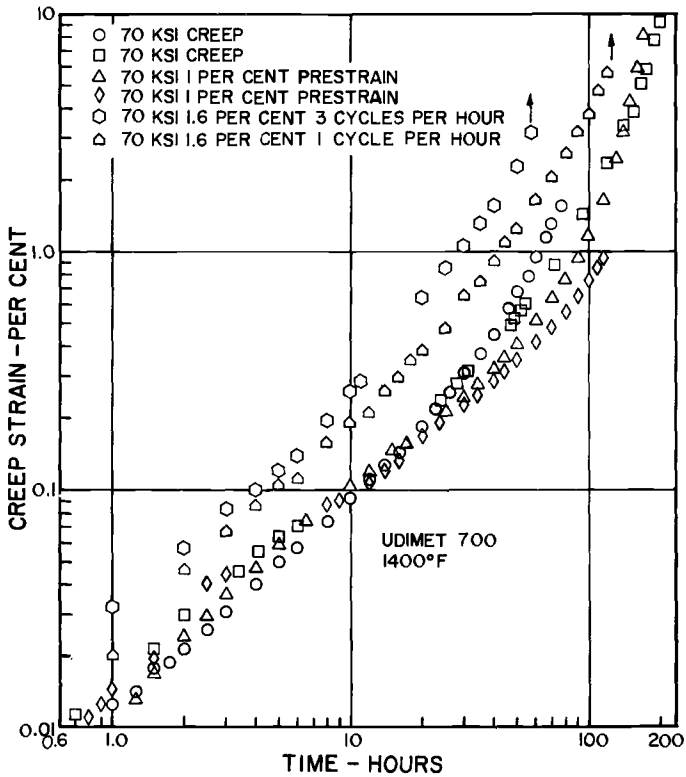

FIG. 5—*Comparison of effects of monotonic and cyclic prestrain on the creep behavior of Udimet 700 under 70 ksi tensile stress.*

cracking were also evident. In other respects, propagation did not differ substantially from that in tests without hold time; patchy areas of brittle fatigue striations were observed on the fracture surfaces. Wedge or triple-point cracking, resulting from grain boundary shear, as not significant in these tests.

Discussion

The mechanism of creep-low cycle fatigue interaction suggested by the results of this investigation contains elements of models proposed by Smith and Barnby [*13*] and by Gittus [*14*]. The former showed how a pileup of edge dislocations at a grain boundary particle could develop a stress concentration sufficiently large to nucleate a cavity, while Gittus proposed a theory of time-dependent cavity growth. The existence of the Bauschinger effect and heterogeneous planar slip in Udimet 700 implies the presence of dislocation pileups and tensile stress concentrations large enough for cavity nucleation

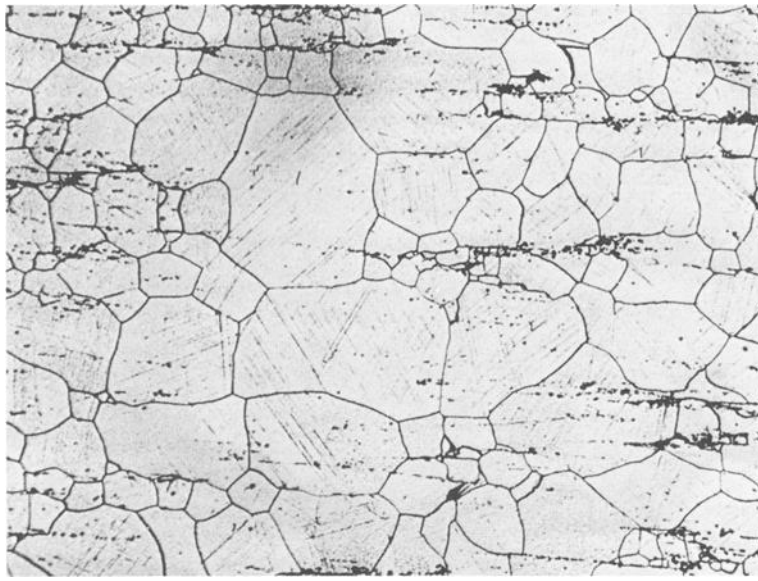

FIG. 6—*Internal deformation revealed by etching in tension creep specimen strained 1.34 percent. Tensile axis horizontal.* (×55).

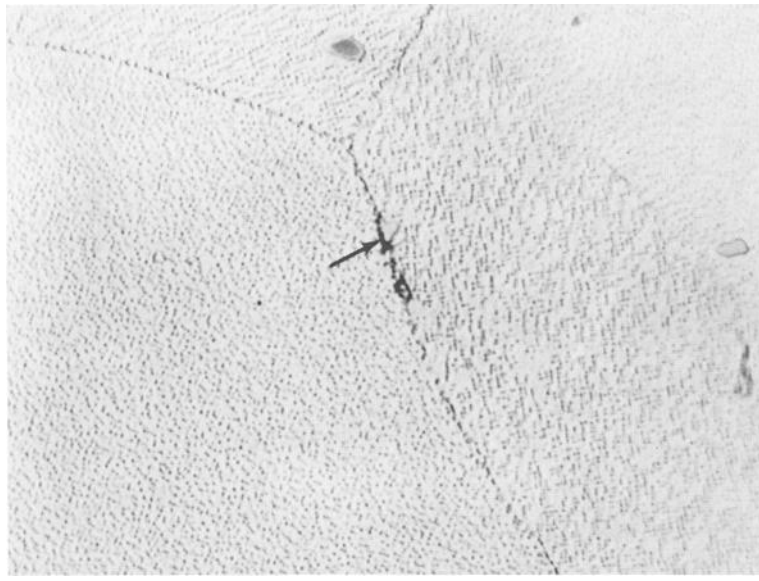

FIG. 7—*Grain boundary crack (arrow) in compression creep specimen strained −1.16 percent. Compression axis horizontal. Etched.* (×1100).

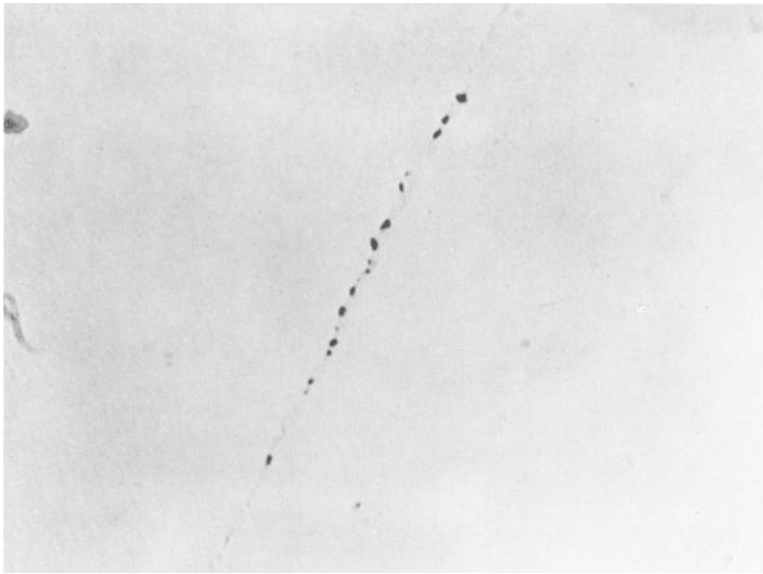

FIG. 8—*Grain boundary cavities in tension creep specimen strained 1.34 percent. Tensile axis horizontal. As-polished.* (×*1100*).

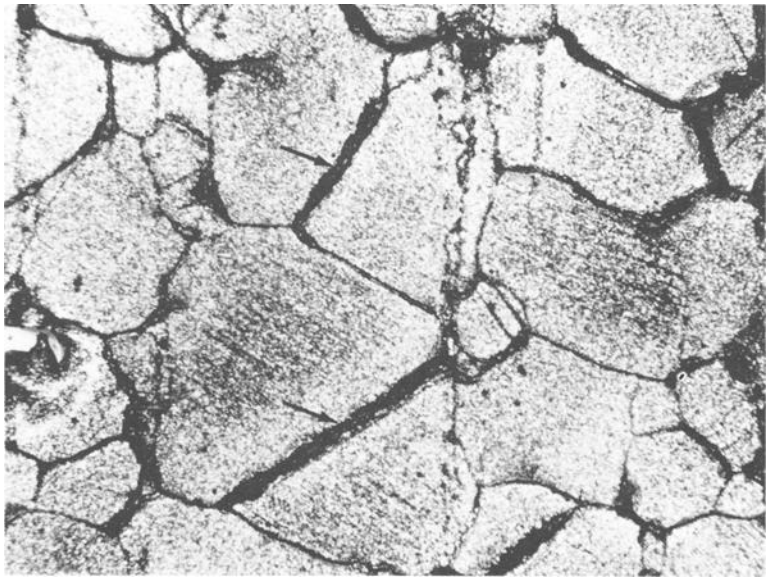

FIG. 9—*Accentuated shear deformation (arrows) along grain boundaries in specimen held at 70 ksi for 60 min each cycle. Stress axis vertical. Electropolished. Metallographic replica. Surface oxidized.* (×*110*).

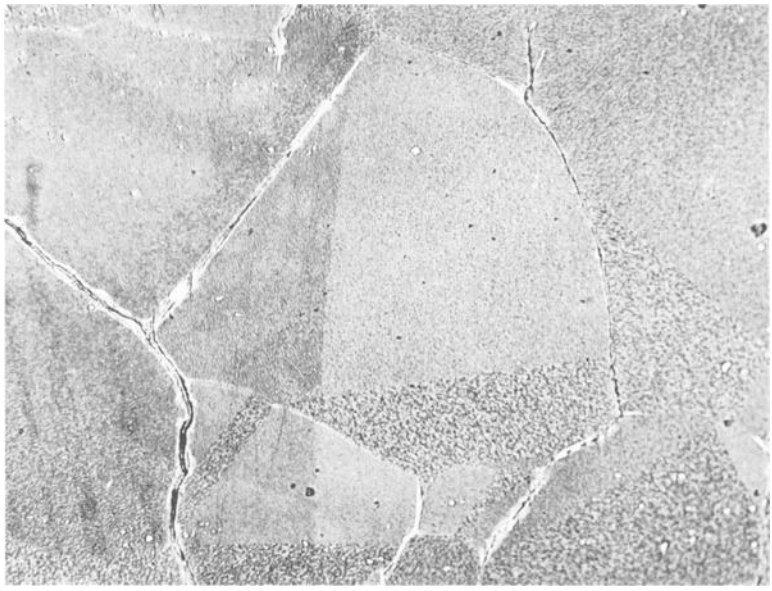

FIG. 10—*Denudation of grain boundaries in specimen held at* $\epsilon_T \simeq 0.0$ *for 15 min each cycle. Stress axis horizontal. Surface oxide removed and surface etched. Metallographic replica.* ($\times 220$).

under either an applied tensile or compressive stress. Thereupon the cavities can grow by vacancy diffusion, and as they grow they allow dislocations to escape from the pileups and annihilate at the cavity boundaries. Eventually these cavities became large enough to grow by plastic deformation, and under cyclic loading they can propagate along the grain boundary in a manner analogous to Stage II fatigue cracks. This mechanism is accelerated at the free surface by diffusion of oxygen along the boundaries, which would prevent sintering of the cavities under reversal of load and possibly fill the cavities with oxide.

Considering the difference in static creep in tension and compression, it appears that a tensile stress promotes the growth of individual cavities, while a compressive stress prevents the cavities from enlarging. It is suggested that aside from the effect on creep rate, the role of the hydrostatic stress is to change the rates of crack propagation along the boundaries in fatigue. In the case of tension the boundaries contain rows of well-rounded holes, while in compression the cavities grow into elongated flat cracks. The work required to fracture a grain boundary is greater in the event the boundary contains round holes, both because the stress concentration of each cavity is smaller and because they may comprise a smaller fraction of the grain boundary

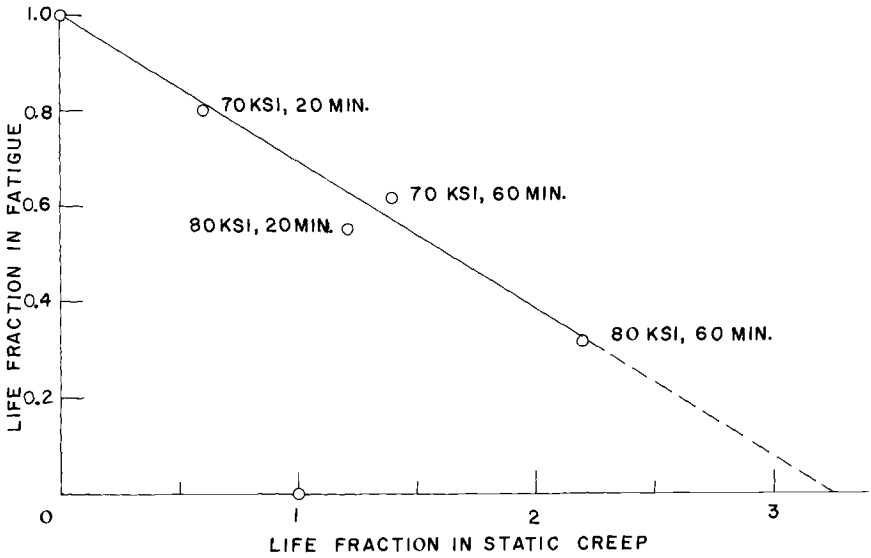

FIG. 11—*Application of linear cumulative damage rule to macrocrack initiation in creep and low-cycle fatigue.*

area than the flat cracks. This is proposed to be the reason for the more damaging effect of compressive creep on cyclic lifetime.

Addressing the problem of cumulative damage, it has been implied that deformation and cavity nucleation are similar in creep and fatigue and governed by the internal stress and time rather than number of cycles; thus, the creep and fatigue mechanisms could be considered identical. The obvious difference, however, is in the rate of cavity growth and coalescence to form a grain boundary microcrack, which may be very different in creep from that in fatigue. We consider the identification of the mechanisms of cavity growth to be the critical problem in this area, and pending the outcome of such investigations, the relevance of the static creep test to crack initiation in creep and fatigue must be questioned. Figure 11 is a plot of the fraction of cyclic life consumed in pure low-cycle fatigue versus the fraction of stress-rupture lifetime in a static tension creep test, based upon the crack initiation data of Table 1. While a linear cumulative damage law can be contrived to express these results, the crack initiation life in static creep required to correlate the results is three times the life at which surface grain boundary cracks have been observed and greater than the time to rupture under constant load.

Conclusions

1. The interaction of low-cycle fatigue with a period of creep in each cycle can be predicted from the standpoint of linear cumulative damage provided a fictitiously large crack initiation lifetime in static creep is assumed.

2. The effect of holding compressive strain is more damaging than holding tensile strain. Similarly, compressive creep prestrain is more deleterious than the same strain applied in tension.

3. The creep rate in compression is less than that in tension and decreases with strain.

4. The Bauschinger effect and metallographic observations indicate that deformation is heterogeneous and planar and accompanied by large stress concentrations where dislocations pile up against grain boundary particles.

5. A mechanism for the interaction of creep and fatigue damage is proposed that is consistent with the results of the interaction tests.

6. The rates of grain boundary cavity growth and coalescence in creep and fatigue are not understood, and the relevance of the static creep test to creep-fatigue interaction is in doubt.

Acknowledgments

The authors would like to thank V. Mata and D. N. Tishler for assistance in the mechanical testing and G. M. Rowe and H. Rand for assistance in microstructural evaluation.

References

[1] Meleka, A. H., "Combined Creep and Fatigue Properties," *Metallurgical Reviews*, Vol. 7, 1962, pp. 43–93.

[2] Ellison, E. G., "The Interaction of Creep and Fatigue—with Special Reference to Thermal Fatigue," University of Bristol, 1968.

[3] Walker, C. D., "Strain-Fatigue Properties of Some Steels at 950 F (510 C) with a Hold Time in the Tension Part of the Cycle," *Joint International Conference on Creep, Proceedings*, Institution of Mechanical Engineers, Vol. 178, 1963–64, pp. 3–49.

[4] Swindeman, R. W. and Douglas, D. A., "The Failure of Structural Metals Subjected to Strain Cycling Conditions," *Transactions*, American Society of Mechanical Engineers, *Journal of Basic Engineering*, Vol. 81, 1959, p. 203.

[5] Taira, S., Ohnami, M., and Kyogoku, T., "Thermal Fatigue under Pulsating Thermal Stress Cycling," *Bulletin*, Japan Society of Mechanical Engineers, Vol. 6, 1963, p.22.

[6] Tilly, G. P., "Influence of Static and Cyclic Loads on the Deformation Behavior of an Alloy Steel at 600 C," *Thermal and High-Strain Fatigue*, The Metals and Metallurgy Trust, London, 1967, pp. 198–210.

[7] Edmunds, H. G. and White, D. J., "Observations of the Effect of Creep Relaxation on High-Strain Fatigue," *Journal of Mechanical Engineering Science*, Vol. 8, 1966, pp. 310–321.

[8] Wells, C. H. and Sullivan, C. P., "Low-Cycle Fatigue Damage of Udimet 700 at 1400 F," *Transactions Quarterly*, American Society for Metals, Vol. 58, 1965, pp. 391–402.

[9] Wells, C. H. and Sullivan, C. P., "The Effect of Temperature on the Low-Cycle Fatigue Behavior of Udimet 700," *Transactions Quarterly*, American Society for Metals, Vol. 60, 1967, pp 217–222.

[10] Ellison, E. G. and Sullivan, C. P., "The Effect of Superimposed Fatigue on the Creep Behavior of the Nickel-Base Alloy Udimet 700," *Transactions Quarterly*, American Society for Metals, Vol. 60, 1967, pp. 88–98.

[11] Wells, C. H. and Sullivan, C. P., "Low-Cycle Fatigue of Udimet 700 at 1700 F," *Transactions Quarterly*, American Society for Metals, Vol. 61, 1968, pp. 149–155.

[*12*] Wells, C. H., "An Analysis of the Bauschinger Effect in Some Engineering Alloys," *Transactions*, American Society of Mechanical Engineers, *Journal of Basic Engineering*, Vol. 89, 1967, pp. 893–896.

[*13*] Smith, E. and Barnby, J. T., "Nucleation of Grain-Boundary Cavities during High-Temperature Creep," *Metal Science Journal*, Vol. 1, 1967, pp. 1–4.

[*14*] Gittus, John, "Theory of Fatigue Failure by Cavity Formation," *Thermal and High-Strain Fatigue*, The Metals and Metallurgy Trust, London, 1967, pp. 142–153.

E. Krempl[1] *and C. D. Walker*[2]

Effect of Creep-Rupture Ductility and Hold Time on the 1000 F Strain-Fatigue Behavior of a 1Cr-1Mo-0.25V Steel

REFERENCE: Krempl, E. and Walker, C. D., **"Effect of Creep-Rupture Ductility and Hold Time on the 1000 F Strain-Fatigue Behavior of a 1Cr-1Mo-0.25V Steel,"** *Fatigue at High Temperature, ASTM STP 459*, American Society for Testing and Materials, 1969, pp. 75–99.

ABSTRACT: A single heat of wrought 1Cr-1Mo-0.25V steel was heat treated to a very low and to a higher level of creep-rupture ductility. Completely reversed, uniaxial strain-fatigue tests were run on the two materials at 1000 F with hold times of 1, 10, or 60 min used at the maximum tensile strain point of the cycle. The total strain range in the tests was either 0.5 or 1.0 percent. The cycles to failure decreased significantly as the hold time increased. The hold-time effect was more pronounced in the low than in the high creep-rupture ductility material, and was greater in the 0.5 percent than in the 1.0 percent total strain range tests. Log-log plots of cycles to failure versus hold time formed curves which tended to bend downward, showing an increased hold-time effect at the longer hold times. The fatigue cracks in both the low and the high creep-rupture ductility material tended to shift from transgranular to intergranular as the hold time increased, which indicates that creep-rupture damage occurred during the hold periods.

KEY WORDS: fatigue (materials), strain measurement, testing, creep-rupture ductility, metals, steel, heat treatment, creep relaxation, evaluation, tests

Rapid steam turbine startups and load changes can create high thermal stresses in localized regions of steam turbine rotors and shells. The thermal stresses can cause plastic deformation to occur during the startup or load change, and, as a result, residual stresses may exist when a relatively steady-state operating condition is reached. The residual stresses may be tensile or compressive depending on the nature of the preceding plastic deformation. Any residual stresses which are present will decrease by a creep relaxation

[1] Associate professor, Department of Mechanics, Rensselaer Polytechnic Institute, Troy, N.Y., formerly with Materials and Processes Laboratory, General Electric Co., Schenectady, N.Y. 12305.

[2] Developmental metallurgist, Structural Metallurgy Unit, Materials and Processes Laboratory, General Electric Co., Schenectady, N.Y. 12305.

process while the turbine is operating. This sequence of events can be repeated many times as the turbine is stopped and restarted, or when additional rapid load changes are made. An elevated temperature strain-fatigue test, with a hold at the maximum tensile strain point of the cycle, has been used widely to obtain information on the resistance of materials to this type of service [*1-6*].[3] This type of test was used in the work discussed in this paper.

The objectives of this study were to determine how creep-rupture ductility and hold time affect the 1000 F strain-fatigue behavior of a 1Cr-1Mo-0.25V steel at low strain ranges. The fatigue tests were of a uniaxial type rather than in bending, and, therefore, it was possible to directly measure the stresses during cycling and the stress relaxation during the holds. The nature of the cracks in the failed fatigue specimen were documented with microstructural studies. Hardness changes which occurred in the test section of the fatigue bars during test also were determined.

A considerable amount of strain-fatigue testing with hold time has been done on chromium-molybdenum (Cr-Mo) and chromium-molybdenum-vanadium (Cr-Mo-V) steels in recent years [*1-6*]. Much of it has been in bending rather than uniaxial so that the stress history could not be measured directly, and little work has been done on the effect of creep-rupture ductility on strain-fatigue characteristics.

Test Material

The test material came from a disk which was parted from a steam turbine rotor. All of the specimens tested in this work had a tangential orientation in the disk.

The average chemical composition of the test material is given in Table 1.

TABLE 1—*Chemical composition, weight percent.*

C	Cr	Mo	V	Mn	Si	Ni	P	S
0.28	1.03	1.10	0.24	0.88	0.30	0.40	0.009	0.006

The steel was heat treated to a relatively high and to a very low level of creep-rupture ductility. The high creep-rupture ductility material was produced by applying a heat treatment patterned after those normally used for this type of rotor steel. The low creep-rupture ductility material received a special heat treatment which was designed specifically to develop a very low level of creep-rupture ductility. The austenitizing temperature was higher than conventionally used, and the tempering temperature was lower. The final heat treatments received by the two sets of test material are given in Table 2.

[3] The italic numbers in brackets refer to the list of references appended to this paper.

TABLE 2—*Final heat treatments.*

Material Condition	Normalize	Temper
HD, high creep-rupture ductility	1775 F/6 h/AC[a]	1270 F/12 h/FC[c]
LD, low creep-rupture ductility	1870 F/24 h/CC[b]	1200 F/34 h/FC

[a] AC = air cool.
[b] CC = control cool at about the same rate as for material above.
[c] FC = furnace cool.

The designations HD and LD which appear in Table 2 will be used throughout the rest of this paper to refer to the two test materials.

The tensile properties of the two materials were determined at room temperature (RT) and at 1000 F. The results are given in Table 3.

TABLE 3—*Tensile properties.*

Material	Temperature, deg F	Tensile Strength, psi	Yield Strength, psi, for Offset of		True Fracture Strength, psi	Elongation in 2 in., %	Reduction of Area, %
			0.02%	0.2%			
HD	RT	110 000	87 500	90 000	...	21.0	56.8
	1000[c]	70 600	52 000	65 000	114 000	...[a]	77.6
LD	RT	135 000	113 000	125 000	...	13.0	35.8
	1000[c]	93 000	71 800	86 900	107 000	17.8[b]	53.5

[a] Bar failed outside of the gage length.
[b] Elongation in 1.4 in.
[c] Strain rate was 0.01 in./in./min.

The 1000 F creep-rupture properties were determined and are plotted in Fig. 1. The two materials had a wide spread in creep-rupture ductility level, as was intended. The LD material had a considerably higher creep-rupture strength.

Fatigue Test Program

Fatigue Tests and Test Cycle

The fatigue tests were run at 1000 F with a hold for a specific length of time at the maximum tensile strain point of the strain-fatigue cycle. The imposed strain-time cycle and the resulting stress-time pattern are shown schematically in Fig. 2. The decrease in stress during the hold periods is due to the conversion of elastic to plastic strain by a creep relaxation process.

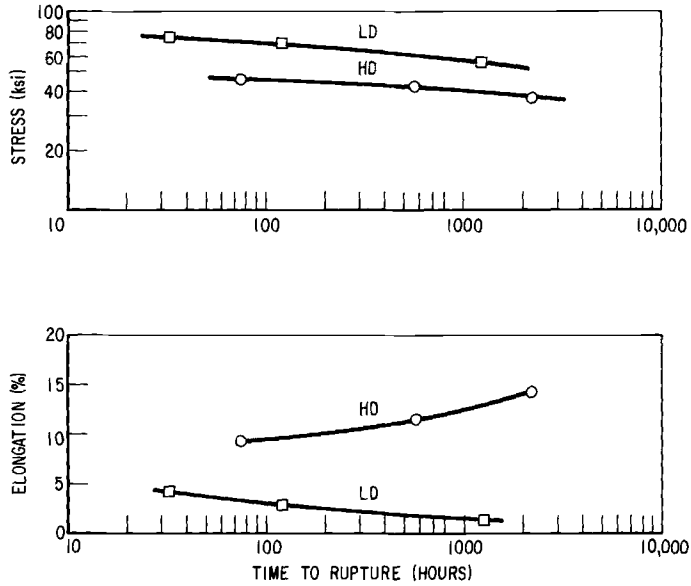

FIG. 1—*Creep-rupture strength and ductility at 1000 F.*

The fatigue test conditions (hold time, strain range) for the two test materials are listed in Table 4. All of the tests were conducted at zero mean strain.

TABLE 4—*Fatigue test conditions.*

Total Strain Range, %	Hold Time, min
0.5	1, 10, 60
1.0	1, 10, 60

The rate of cycling would have been about 2/min if no holds had been used in the cycle. A specimen was considered to have failed when the nominal stress during the tension hold dropped to below 1000 psi.

The cycle shown in Fig. 2 was intended to simulate the strain history that can occur in turbine rotors or shells during a cold start; that is, when the temperature of the equipment is initially close to room temperature. Rotors and shells also are exposed to hot starts and to rapid load changes, and the strain history for these can be significantly different than for a cold start. Therefore, detailed analysis of actual operating conditions is necessary to realistically factor fatigue data into the design and operation of components [7].

Test Specimen

The test specimen is shown in Fig. 3. True displacement control was achieved by clamping split plates to the ridges located at each end of the gage length. Relative motion between the two plates was carried outside of the heating furnace by quartz rods to an extensometer where the motion was measured and controlled.

Placement of the ridges on the gage length represents a compromise. It ensures reliable displacement control and minimizes elastic follow-up, but may cause premature fatigue cracking due to stress concentration. The influence of the ridges on fatigue life will be discussed later.

Fatigue Test Equipment

The tests were performed in two modified universal testing machines. One of them was screw driven, the other one was operated hydraulically. To accomplish the strain cycle depicted in Fig. 2, special controls were added to the machines. They consisted of an on-off type scanning and controlling

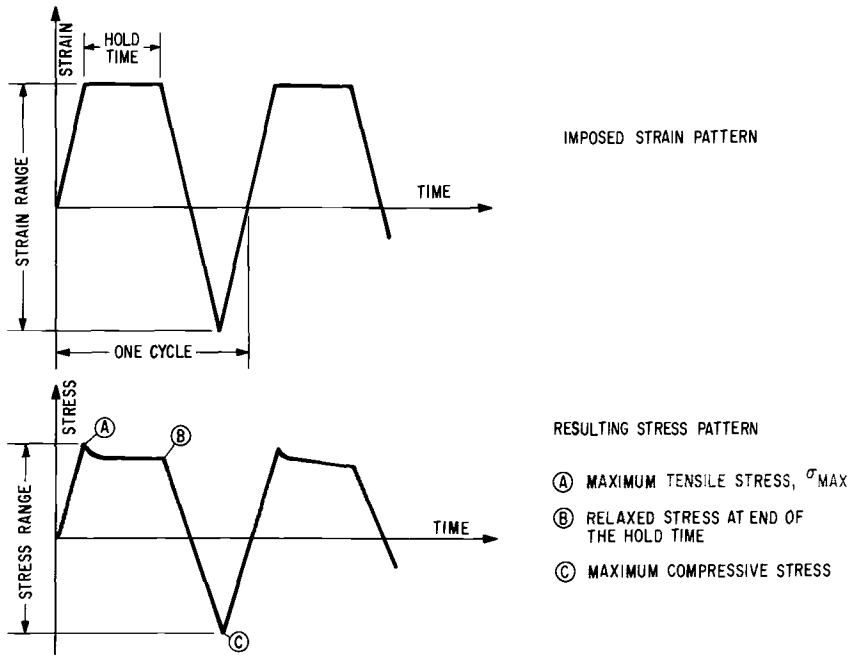

FIG. 2—*Schematic showing strain pattern imposed on the specimen and resulting stress pattern. Note: The peak stresses and the relaxation curve vary throughout the life of the specimen.*

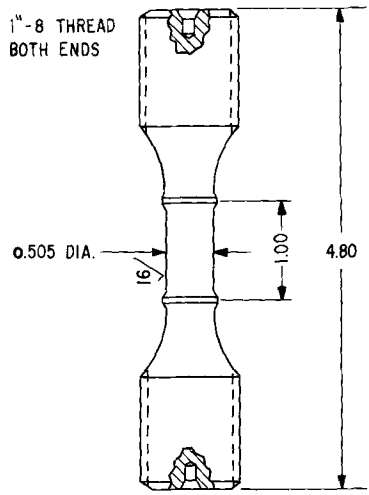

FIG. 3—*Test specimen.*

device to maintain the desired displacement range throughout the test and to keep the displacement constant during the hold time. The hold time was adjusted with suitable timers.

The specimens were maintained at temperature with large resistance wound furnace 2 ft long in one case and 4 ft long in the second, coupled to a suitable controller. The temperature over the gage length of the specimen was maintained at 1000 ± 2 F.

A continuous load record was obtained during the tests so that changes in the peak loads and in the relaxation curve were documented.

Results

Fatigue Test Data

The results of these extremely long low-cycle fatigue tests (up to 2200 h) are plotted in Fig. 4 for the HD and LD materials. The following observations about the life reducing hold-time effect can be made:

The hold-time effect is more pronounced for the LD material than for the HD material. Within one given material, the effect is strain range dependent and is greater at the low than at the high strain range. As the hold time is increased, the effect seems to become more severe, as indicated by a slight downward bending of the curves. An attempt was made to run two tests at each hold time for the 0.5 percent strain range to get an estimate of the

possible scatter of the low-cycle fatigue tests. The observed scatter in Fig. 4 indicates that duplicate tests at each condition are desirable.

In addition to the above described difference in the fatigue life of the HD and LD materials, the behavior during cycling is also different. The LD material strain softens much less than the HD material, or, to put it another way, the decrease in stress range with cycles is greater for the HD material than for the LD material, Figs. 5 and 6. The change in stress range is approximately linear on a log cycle versus stress range plot and, therefore, can be represented by:

$$\sigma/\sigma_1 = -k_\sigma \log n + 1 \quad \ldots\ldots\ldots\ldots\ldots\ldots\ldots\ldots (1)$$

where:

σ = stress range at cycle n, psi,
σ_1 = stress range at the first cycle, psi,
k_σ = coefficient, and
n = cycle number.

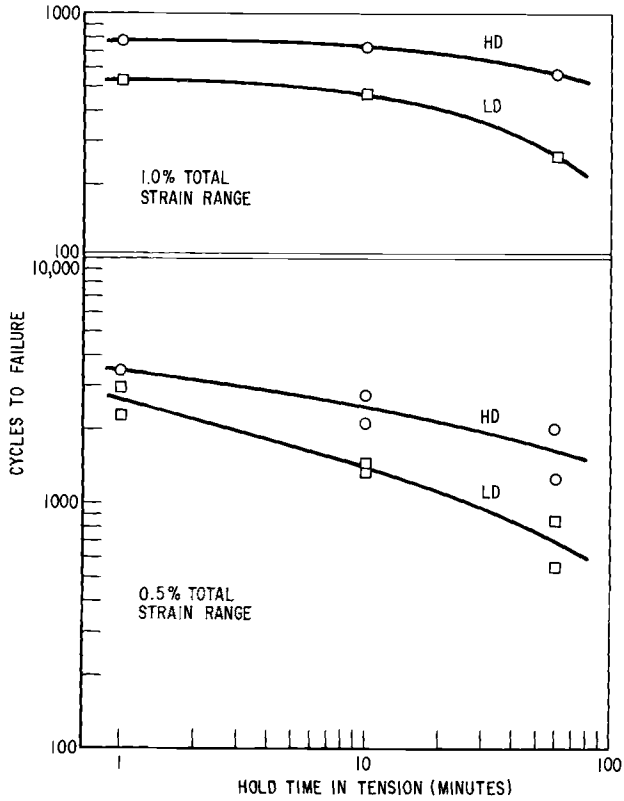

FIG. 4—*Effect of hold time in tension on cycles to failure.*

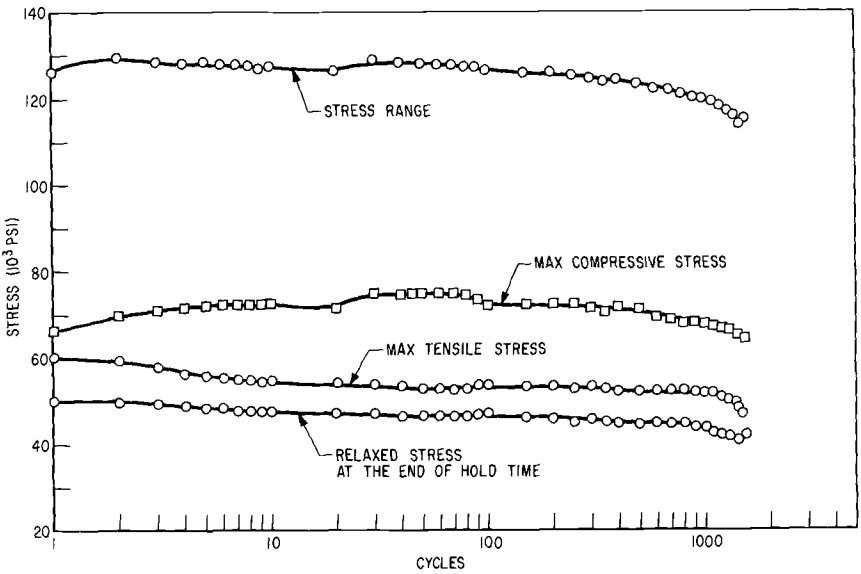

FIG. 5—*Variation of the peak stresses and of the relaxed stress at the end of the hold time during cycling. Test condition 0.5 percent total strain range, hold time 10 min, LD material.*

This equation will represent only the variation of the stress range approximately up to about 75 percent of the fatigue life of the material. The coefficient k_σ depends on the material and on the strain range. Typical values of the coefficient k_σ are listed in Table 6. It is evident that the k_σ values are higher for the HD material at both strain ranges than for the LD material.

The form of Eq 1 can be used to describe the variation with cycles of the maximum tensile and compressive stress as well as the relaxed stress at the end of the hold time which are plotted in Figs. 5 and 6. The coefficients k_σ, however, will be different for each stress.

The form of the relaxation curve changes together with the peak stresses during cycling, and its shape was obtained from a load versus time record. Examples of the variation of the relaxation curves during the fatigue life are given in Fig. 7 (LD material) and in Fig. 8 (HD material). The two figures are for a total strain range of 0.5 percent and contain the curves of 1, 10, and 60 min. The dimensionless stress σ/σ_{max} is plotted versus hold time at the indicated life fractions of the specimens. The symbol σ_{max} denotes the average maximum tensile stress at the respective life fraction of each specimen, and its value is listed on the diagram for each hold time. The symbol σ stands for the instantaneous stress during hold time.

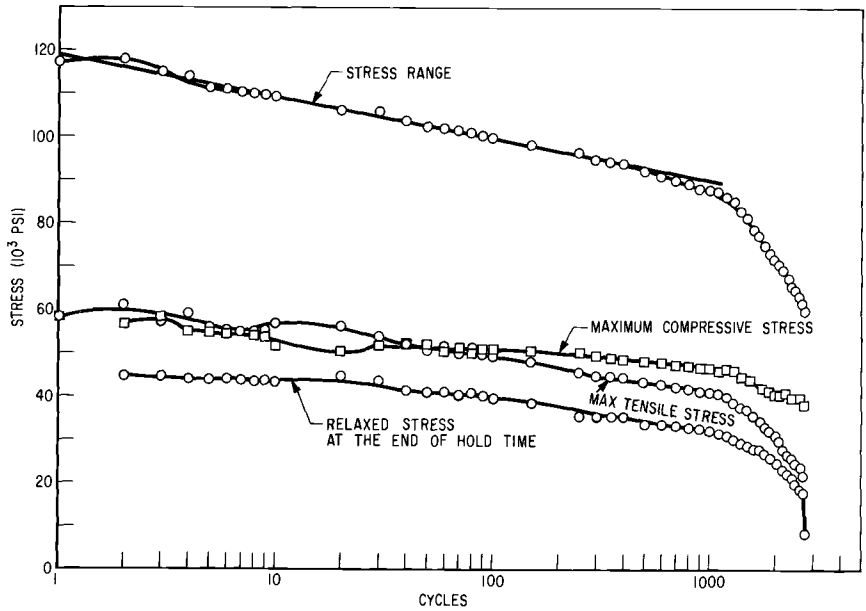

FIG. 6—*Variation of the peak stresses and of the relaxed stress at the end of the hold time during cycling. Test condition 0.5 percent total strain range, hold time 10 min, HD material.*

It can be seen that the curves for the three different hold times plot on top of each other after an initial adjustment period. This then would indicate that the length of hold time during a cyclic test will not alter the shape of the relaxation curve. In addition, the stress ratio σ/σ_{max} at the end of the hold time stays relatively constant throughout the life of the specimens. This is true despite the fact that the maximum tensile stress is decreasing constantly throughout the test. Precise measurements with high load resolution should check on this finding in later tests.

The dimensionless stresses σ/σ_{max} are always higher for the LD material than for the HD material, Figs. 7 and 8. This is in addition to the high absolute values of the maximum tensile stress σ_{max} of the LD material. The high relaxation resistance of the LD material is apparent.

The shape of the dimensionless relaxation curves plotted in Figs. 7 and 8 is affected by the strain range imposed on the specimen. The dimensionless relaxation curves for 1.0 percent total strain range are not shown, but they drop to different σ/σ_{max} values than the curves for 0.5 percent strain range.

After Test Microstructure of Fatigue Specimens

A longitudinal cross section of each of the failed fatigue specimens was examined metallographically to determine the nature of the cracks. The

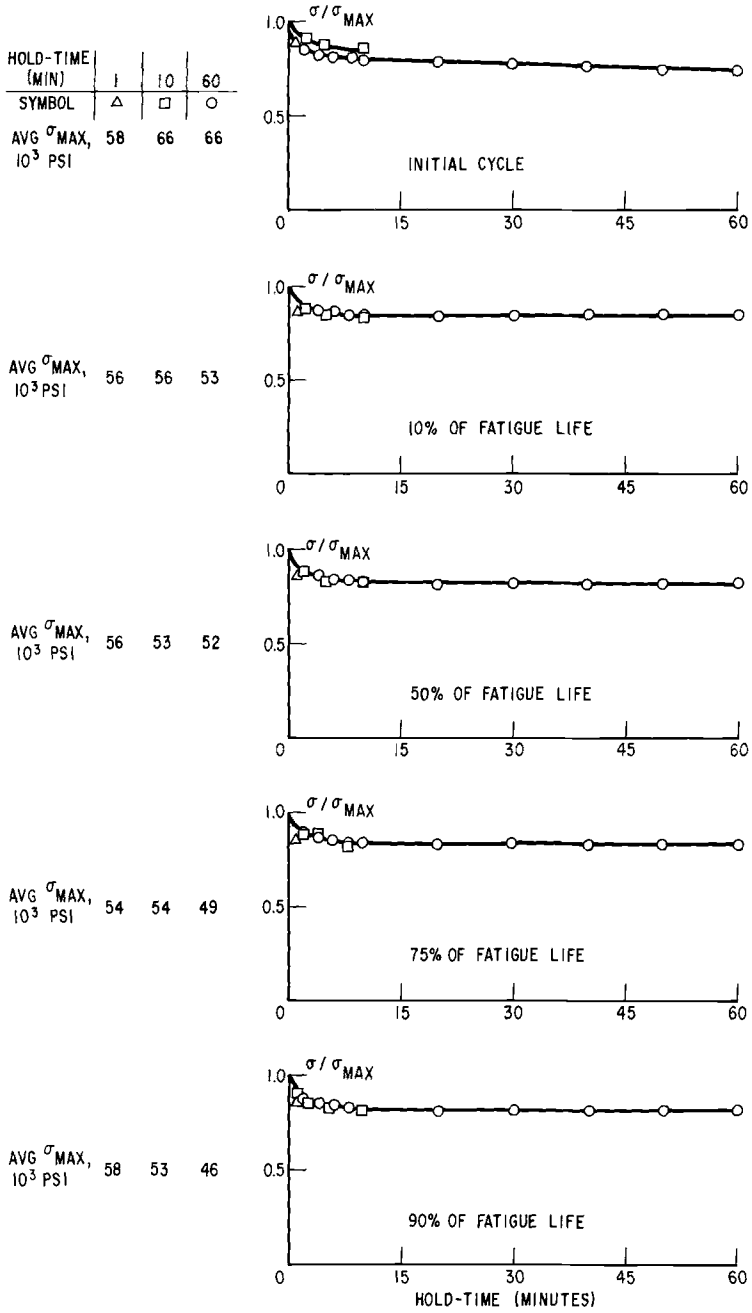

FIG. 7—*Variation of the relaxation curve with cycling. LD material for 1, 10, and 60-min hold time.* σ = *instantaneous stress during hold time,* σ_{max} = *maximum tensile stress at the respective life fraction, absolute value is listed at each diagram.*

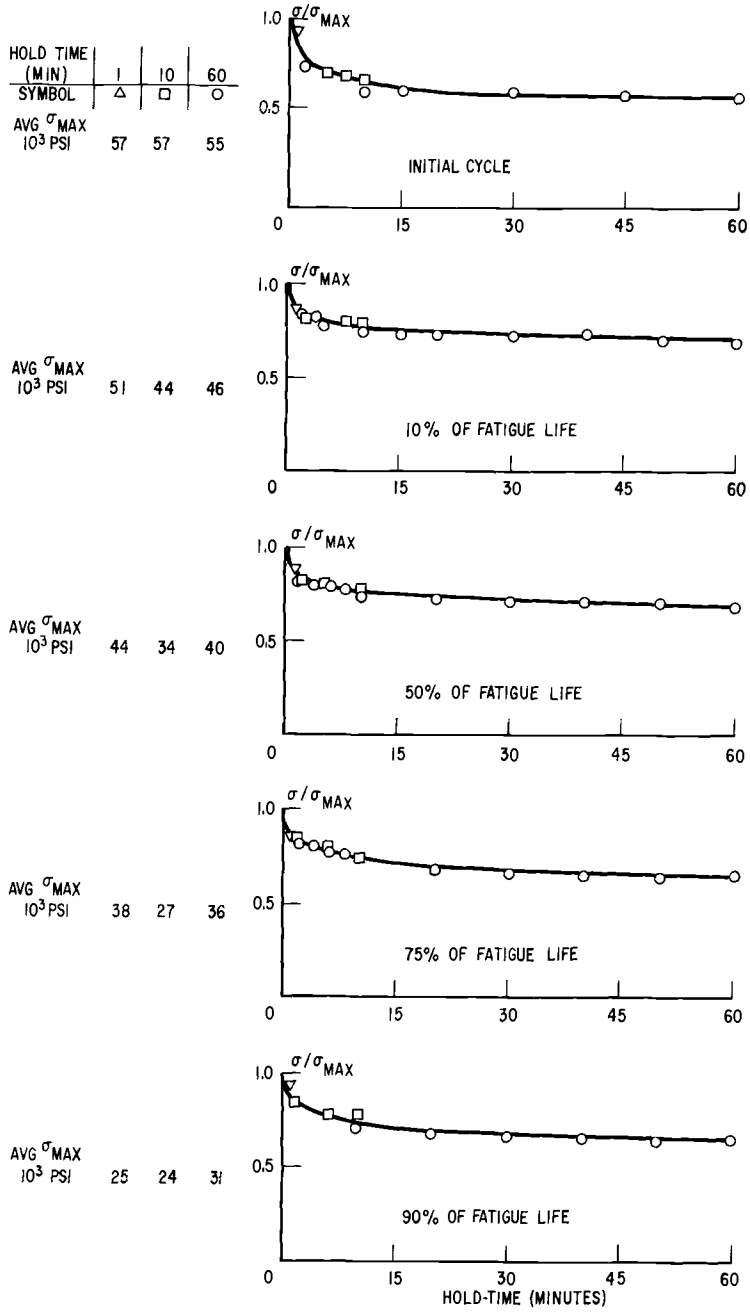

FIG. 8—*Variation of the relaxation curve with cycling. HD material for 1, 10, and 60-min hold time.* σ = *instantaneous stress during hold time,* σ_{max} = *maximum tensile stress at the respective life fraction, absolute value is listed at each diagram.*

specimens always contained one or two long cracks which were the primary cause of failure. These main cracks generally were located close to one of the ridges which were machined at the ends of the test section. In addition, shorter secondary cracks always were present at the surface of the test specimens and also in completely internal locations for some test conditions. The nature of the cracks are described for the HD and then for the LD fatigue specimens in the paragraphs which follow.

The main cracks in the HD specimens were completely transgranular. In other words, they propagated across the grains, as is illustrated by Fig. 9.

The short secondary cracks in the HD material were all transgranular except in the 60-min hold tests at 0.5 percent total strain. The surface secondary cracks in these tests were transgranular, but short intergranular cracks also were present in internal locations. The intergranular cracks were generally less than 0.010 in. long and were found both close to the main crack and some distance away. A $\times 500$ view of an internal crack which is mostly intergranular is shown in Fig. 10. The location in Fig. 10 is about 0.25 in. from a main crack and close to the center line of the fatigue bar. The intergranular cracks often initiated at small inclusions, as Fig. 10 illustrates.

The main cracks in the LD fatigue specimens propagated by a combination of transgranular and intergranular cracking. The cracks were almost always transgranular at the outer surface. However, at a depth of 0.010 to 0.080 in., the mode of crack propagation changed to either a combination of transgranular-intergranular or to a completely intergranular mode. The mixed mode was present in the 1 and 10-min hold tests, while almost completely intergranular cracking occurred in the 60-min hold tests. The tip of a main crack which propagated by a transgranular-intergranular mode is shown in Fig. 11.

The shorter secondary cracks which were located at the surface of the LD material behaved like the main cracks. They propagated from the surface by a transgranular mode and then shifted to a mixed or to a completely intergranular mode after propagating inward 0.010 to 0.080 in. Completely internal cracks were present also in LD specimens. These internal cracks were short and predominately intergranular. They were located alongside of and ahead of the main cracks in all cases, and in the 10 and 60-min hold tests at the 0.5 percent total strain range tests were present also throughout the test section.

The lack of intergranular cracks at the surface of the specimens is in contradiction to the model of high-temperature fatigue cracking discussed by Manson [*8*], and it appears that the model is not completely applicable to low-alloy steels of the Cr-Mo and Cr-Mo-V type. It is unusual in these steels to develop intergranular creep-rupture type cracks right at the surface of *smooth* test specimens, both in creep-rupture and in high-temperature

fatigue tests. Significant restraint generally is required to produce intergranular cracks. Therefore, intergranular creep-rupture type cracks tend to develop in these materials in internal locations, or will develop at the surface if a notched test specimen is used. The cracking behavior found for the HD and LD materials coincides with the observations of Hill [5] during reverse bending, strain-fatigue tests at 1022 F on a wrought 1 percent Cr-Mo-V steel.

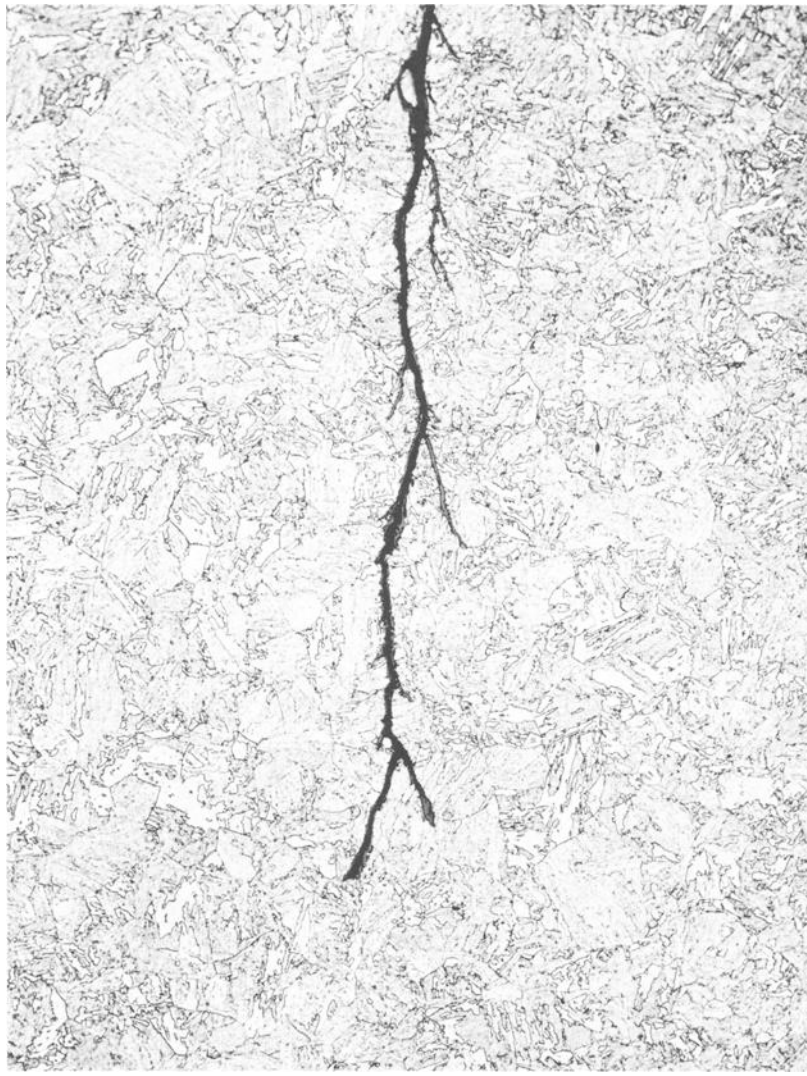

FIG. 9—*Transgranular main crack in HD specimen* ($\times 100$).

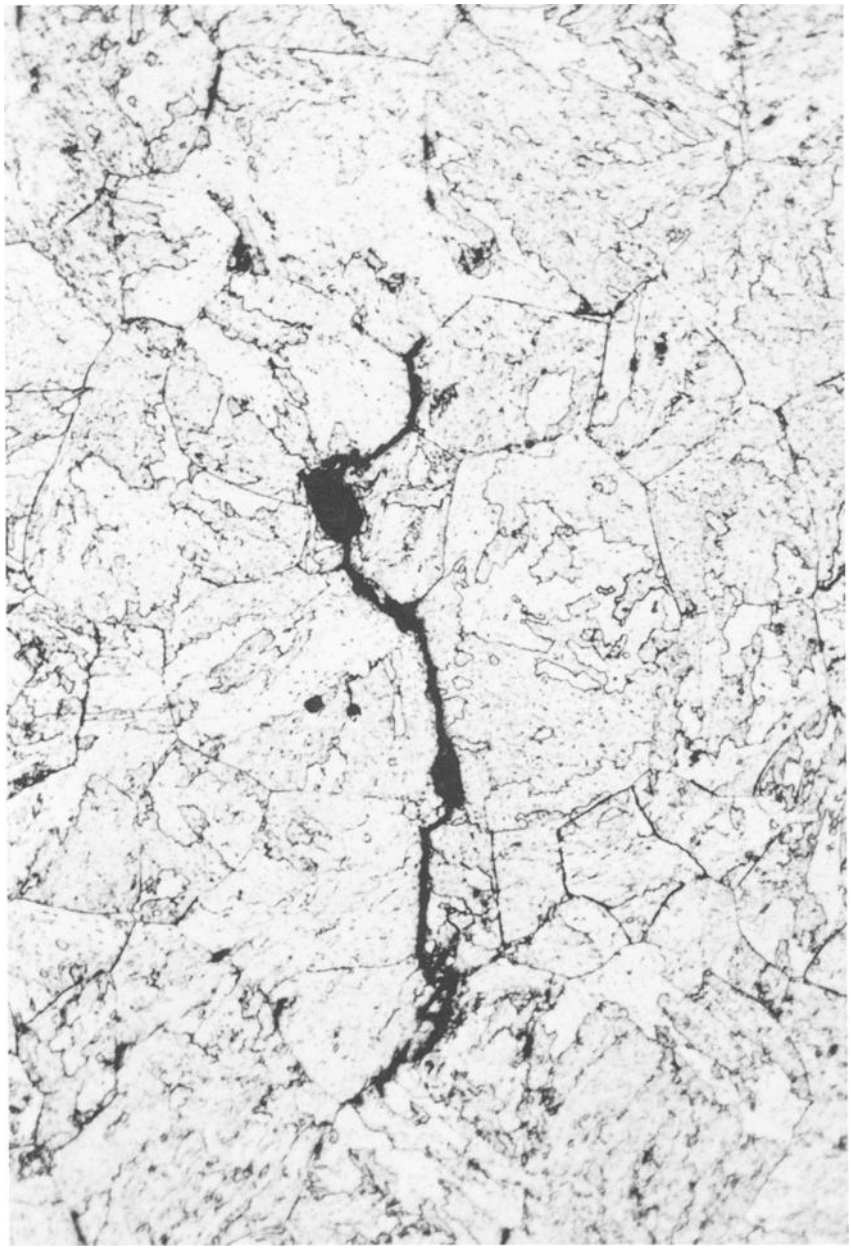

FIG. 10—*Internal, mostly intergranular crack in HD specimen tested at 0.5 percent total strain range with 60-min hold time* (×*500*).

FIG. 11—*Transgranular-intergranular main crack in LD specimen* ($\times 100$).

The relative number of cracks which formed at the surface of the various specimens was determined to establish what factors influenced surface crack initiation. This was done by counting the number of cracks which ran from the surface of each specimen while viewing a polished longitudinal cross section at about $\times 20$. Only those cracks lying between the two raised ridges were counted. Almost all of the cracks in this work were transgranular close to the surface, so the results would refer to initiation of transgranular cracks at, or very close to, the surface of the specimens. The crack counts were rounded off to the nearest five and are given in Table 5.

TABLE 5—*Number of surface cracks in fatigue specimens.*

Material	Total Strain Range, %	Hold Time, min	Number of Cracks[a]
HD.....	0.5	1	5
		10	10, 10[b]
		60	5, 10
	1.0	1	110
		10	90
		60	20
LD.....	0.5	1	5, 10
		10	...
		60	5, 5
	1.0	1	70
		10	80
		60	10

[a] Crack count on a single, longitudinal cross section.
[b] Two values are given because two specimens were tested.

The total strain range had a major effect on the number of cracks developed, the number being consistently higher in the 1.0 percent than in the 0.5 percent total strain range tests. There were no major differences in the number of cracks in the HD versus the LD materials for the same test conditions. The effect of hold time on the number of cracks was not consistent. In the 0.5 percent total strain range tests, the number of cracks stayed about the same as the hold time was increased from 1 to 60 min. However, in the tests at 1.0 percent total strain range, there were significantly fewer cracks in the 60-min hold tests than in the 1 and 10-min tests.

After Test Hardness of Fatigue Specimens

The strain softening of the specimens during fatigue testing was apparent not only from the decrease in stress range as the test progressed, but also from the before and after hardness in the test section of the fatigue bars. The average decrease in test section Vickers hardness for the various groups of bars is given in Table 6.

TABLE 6—*Hardness drop in test section and* k_σ *values for Eq 1.*

Material	Total Strain Range, %	Average Decrease in Vickers Hardness	Range of k_σ
HD.....	1.0	40	0.14 to 0.35
	0.5	21	0.14 to 0.27
LD.....	1.0	32	0.18 to 0.27
	0.5	9	0.02 to 0.11

The size of the hardness change increased as the strain range increased and was greater in the high than in the low ductility material. A correlation between k_σ and the hardness decrease is apparent. Variations in hold time did not affect the size of the hardness change. The hardness in the shoulder areas of the fatigue specimens did not change during testing, which shows that the hardness decreases are not conventional tempering effects.

Hardness decrease data for this Cr-Mo-V alloy have been produced in other programs which employed the same fatigue test procedures and test temperature as this, but which encompassed a broader range of testing. Those data and the data from this work form a reasonably smooth curve when the test section hardness drop is plotted versus the total strain range, as shown in Fig. 12. Strain softening probably is related more closely to plastic strain than to total strain, and, therefore, there might be less scatter if the necessary data were available to plot hardness versus plastic strain range rather than total strain range.

Discussion

Causes of the Hold-Time Effect

The causes of the hold-time effect will be discussed from two viewpoints. The first will be to consider just the bulk response of the material in terms of strains and stresses. This approach will then be supplemented by microstructural observations.

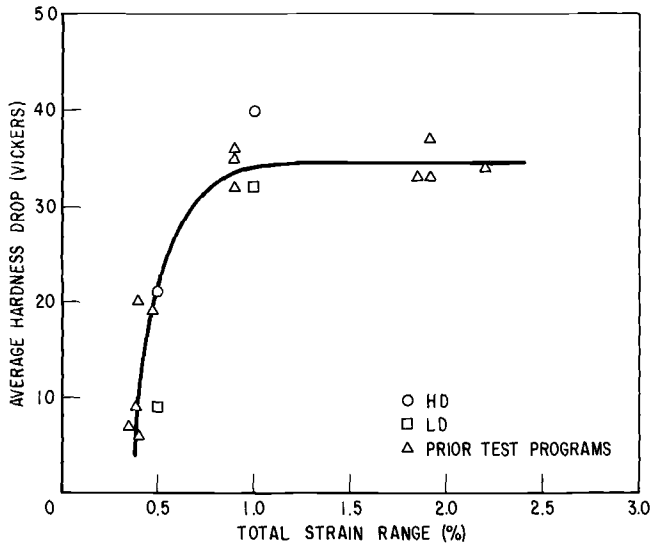

FIG. 12—*Hardness drop in fatigue bar test section versus total strain range.*

It generally is recognized that the plastic strain is a good measure of fatigue life especially at low endurances. The effect of hold time in a strain-controlled test on the plastic strain range per cycle can be deduced from Fig. 13. The maximum increase in the plastic strain range due to hold time, FG, can be computed from the amount of stress relaxation, BC, and the modulus of elasticity. This increase in the plastic strain range is offset partially by the greater compressive stress (*D*) for the cycle with hold time than the compressive stress (*A*) without hold time, but the total increase is still of significant magnitude.

This increase in plastic strain accounts for part, but not all, of the observed hold-time effect. The relaxation curves in Figs. 7 and 8 show that a large part of the total drop in stress occurs in the first 10 min. Very little decrease in stress occurs thereafter, and, as a result, there is very little further increase in plastic strain. The results in Fig. 4, however, show that the life reduction becomes more severe as the hold time increases from 10 to 60 min. To account for this life reduction it is assumed that creep-rupture damage is introduced during hold time so that a certain life fraction of creep-rupture life is expending during each time increment of the hold time. If a further assumption is made that this creep damage and the low-cycle fatigue damage are additive, the hold-time effect can be explained qualitatively. Also, the difference in the

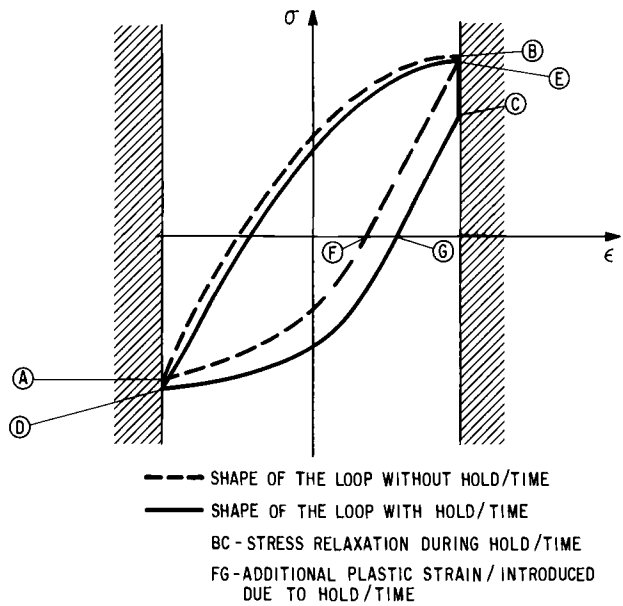

FIG. 13—*Schematic showing the influence of hold time on the shape of the hysteresis loop.*

effect of hold time on the LD and HD materials can be explained by the assumption that creep-rupture damage occurs during the hold time.

To illustrate this point, the relaxation data at 50 percent of the life, shown in Figs. 7 and 8, are used. The relaxed stress for the LD material is about 40,000 psi for most of the hold time compared to about 24,000 psi for the HD material. These stresses will lead to creep-rupture failure is roughly 10,000 and 40,000 h, respectively. It is clear that the percentage of rupture life expended during a unit of hold time (creep-rupture life) is higher for the LD material than for the HD material. Since creep-rupture and cyclic damage add up to determine failure, less cyclic life is available for the LD material than for the HD material.

In summary, it appears that the increase in plastic strain range per cycle and the introduction of creep-rupture damage make important contributions to the hold-time effect.

The microstructural studies support the viewpoint that creep-rupture damage is introduced during hold periods. This statement is based on the observation of increased amounts of intergranular cracking as the hold time was increased. There are several mechanisms by which the introduction of creep-rupture damage could decrease the cycles to failure. A number of the specimens developed internal, intergranular cracks throughout the test section, such as the one shown in Fig. 10. The linkup of a main crack with these internal cracks should increase the rate of propagation of the main crack and therefore cause a decrease in cycles to failure. The linkup of a main transgranular crack with internal, intergranular cracks could cause a transgranular-intergranular cracking mode, such as appears in Fig. 11. It is not so easy to visualize the mechanism of the creep-rupture damage in those cases where the main crack was completely transgranular. One can speculate that a main transgranular crack might propagate not only while the test specimen is being pulled to the maximum tensile strain position of the fatigue cycle, but also may continue to propagate during the hold period. The stress level at the tip of a large main crack would appear to be high enough to make this a possibility. As previously mentioned the nominal relaxed stress in the HD specimens tested at 0.5 percent total strain range was about 24,000 psi. However, the local stress at the tip of the main crack would be much higher than this because of the decreased test specimen cross section and, more important, the stress concentrating effect of the crack. It does not take much multiplication of the 24,000 psi figure to raise the local stress to a range which coincides with a relatively short-time, creep-rupture failure, as shown by Fig. 1.

Oxidation speeds up the crack initiation process by helping to create rumples and other local stress concentrations on the surface of fatigue specimens. Oxidation also may affect the rate of crack propagation. The

introduction of a hold period could change the magnitude of the oxidation effects on a per cycle basis. Special fatigue test procedures which include tests in vacuum or an inert atmosphere will be required to clarify the role of oxidation in causing the hold-time effect.

Cycles-to-Failure Versus Hold-Time Plot

The plots of number of cycles to failure versus hold time in Fig. 4 indicate that the hold-time effect becomes more severe as the hold time increases beyond 1 h; that is, that the curves bend downward. The effect seems to be especially pronounced in the 0.5 percent total strain range tests. To check this observation, the results of this paper are compared with previously published data [*2*, *3*, *5*] in Fig. 14. All of the curves in Fig. 14 bend downward. The bend in the curves makes extrapolations to longer hold times than tested very uncertain.

The curves in Fig. 14 indicate the possibility of cracking in very few cycles if the ductility is very low and the hold time long. Cracking, in fact, can occur during a single stress-relaxation cycle when heavy sections of Cr-Mo-V steel are welded and then stress relieved. Intergranular creep-rupture type cracks can develop in the coarse grained regions of the heat-affected zones during the heatup and hold at the stress relieving temperatures [*9*]. The creep-rupture ductility tends to be low in the course gained regions of a weld heat-affected zone because the hardness is high, especially during the heatup to the stress relieving temperature. The time involved in the heatup and hold period of a stress relief for Cr-Mo-V steels is typically over 6 h and, therefore, would constitute a long hold period during which creep relaxation could occur.

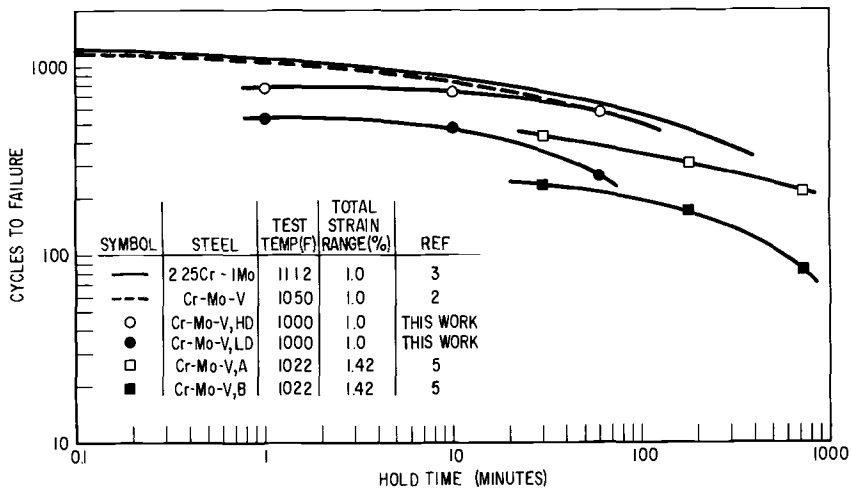

FIG. 14—*Hold time versus cycles to failure for this study and for others in the literature.*

Effect of the Test Specimen Ridges on Cracking

The ridges to which the extensometer grips were attached were located directly on the test section of the fatigue bar, as shown in Fig. 3. They were put there to achieve more accurate displacement control and minimize elastic follow-up during the hold periods. It was realized that they would cause some stress concentrating effect, and, therefore, their contours were designed carefully to keep the effect to a minimum. Evaluations indicated that the stress concentration factor of the ridges was about 1.1.

The main cracks in the fatigue specimens generally were located close to a ridge, and, therefore, it is apparent that the ridges caused enough of a stress concentrating effect to bias the location of the main crack. However, it is believed for several reasons that the ridges did not have a major effect on cycles to failure. Prior to adopting the ridge on the test section design, 1000 F no-hold tests were run at 0.4 percent total strain range using specimens with the ridges on the shoulders and others with ridges on the test section. The cycles to failure for the two types of bars were not significantly different, even in those cases where specimens failed adjacent to the ridges. Secondly, as described in the microstructure section, there were always other cracks in the failed fatigue bars besides those at the ridges. These secondary cracks were often of very major size, particularly in the 1.0 percent total strain range tests.

Interrelation of Material Properties

The tension, creep, low-cycle fatigue, relaxation, and hardness tests reported for the two conditions of heat treatment strongly suggest that there is a consistent interrelation between the properties measured in the different tests, for example, the HD material was characterized by high, hot-tensile ductility, high creep-rupture ductility, good low-cycle fatigue life, and unfortunately low creep-rupture strength, and comparatively low-deformation resistance during cycling (high degree of cyclic strain softening). On the other hand, the LD material showed low, hot-tensile ductility, low creep-rupture ductility, low low-cycle fatigue strength, as well as high creep-rupture strength, and high deformation resistance during cycling (low degree of cyclic strain softening).

In addition to the interrelationships described above, the change in hardness of the fatigue specimens during test correlates with the k_σ factor (Eq 1) for the stress-range change during cycling, as shown in Table 6. A small hardness change for the LD material corresponds with the low k_σ value. The HD showed high hardness change and a high k_σ value.

The above observations strongly suggest that an attempt should be made to obtain the total picture of the time-dependent-deformation behavior by considering creep, relaxation, and fatigue deformation behavior together.

It is no longer appropriate to consider relaxation, creep, and fatigue as separate items of investigations. These phenomena are just the response of a material to different conditions of straining. It would be desirable to find a deformation law that could describe the observed behaviors in different tests.

Prediction Methods

The severity of the observed life reducing hold-time effect makes it desirable to look for a method of predicting this effect. Due to the complexity of the problem and due to its recent nature, attempts are presently few and conceptual in nature.

Edmunds and White [*3*] made an attempt to predict the hold-time effect at low-strain ranges where creep effects are most significant. They assumed in essence time (cycle) independent material properties and proposed various methods with fair to bad success of prediction.

Cycle dependent relaxation and creep-rupture properties were obtained in this paper, and, therefore, the prediction method in Table 3 of Ref *3* was re-evaluated. The ductility depletion concept (fracture in a low-cycle fatigue test with hold time occurs when the accumulated plastic strain due to hold-time stress relaxation, *FG* in Fig. 13, equals the elongation at fracture in a creep-rupture test of the same duration) will predict a much shorter fatigue life than observed. The result is in complete agreement with the findings of Edmunds and White [*3*].

Manson and Halford [*10*] developed a special prediction method for low-cycle fatigue life without hold time at elevated temperature. An attempt was made to check to what extent their prediction might be used for low-cycle fatigue tests with hold time, especially since they were proposing a rather generous 10 percent rule which may cover the hold-time effect.

The results of their 10 percent rule prediction are shown in Fig. 15 for both ductility versions of the Cr-Mo-V steel. The 10 percent rule predicts a longer fatigue life than observed.

An attempt also was made to account for the creep-rupture effect by using Eq 2 of Ref *10*. Owing to the flat creep-rupture curve of the HD material, the exponent $(m + 0.12)/m$ in Eq 2 will become negative for this material. The exponent for the LD material is positive. At the same frequency Eq 2 then will predict a longer life for the HD material than for the LD material. This trend corresponds to the observed behavior.

In the process of determination of the low-cycle fatigue life with the Manson method [*10*, *11*], it was found that the true fracture stress determined from Fig. 19 of Ref *11* was much higher than the one actually measured, Table 3. The observed discrepancy is rather large. The difference between the predicted and the observed true fracture stress may be due to the reduced strain-hardening capacity of the material at 1000 F. The empirical

relationship, Fig. 19, was based on evidence obtained at room temperature where strain-hardening rates are high.

The results of the high-strain fatigue tests of the HD material agree rather well with the curves published in Fig. 9 of Ref 7, see Fig. 15. Only one point for the HD material falls short for the curve indicating the life for 1-h hold. The results for the LD material exhibit shorter lives than indicated by Fig. 9 of Ref 7. However, the LD material is a special case since it was heat treated to produce an abnormally low level of creep-rupture ductility.

New Work

In future tests, the total time-dependent deformation behavior should be obtained with accurate and fast responding servo-controlled machines. Tension, creep, relaxation, and fatigue deformation behavior should be documented accurately. Information of this type will help to develop a constitutive law to describe time-dependent material behavior at elevated temperature. The life reduction for hold times in the range 6 to 24 h needs to be investigated because of the uncertainty of extrapolating curves like those in Figs. 4 and 14 to these long hold times. Emphasis should be placed in future work on the determination of cycles to crack and cycles to failure so

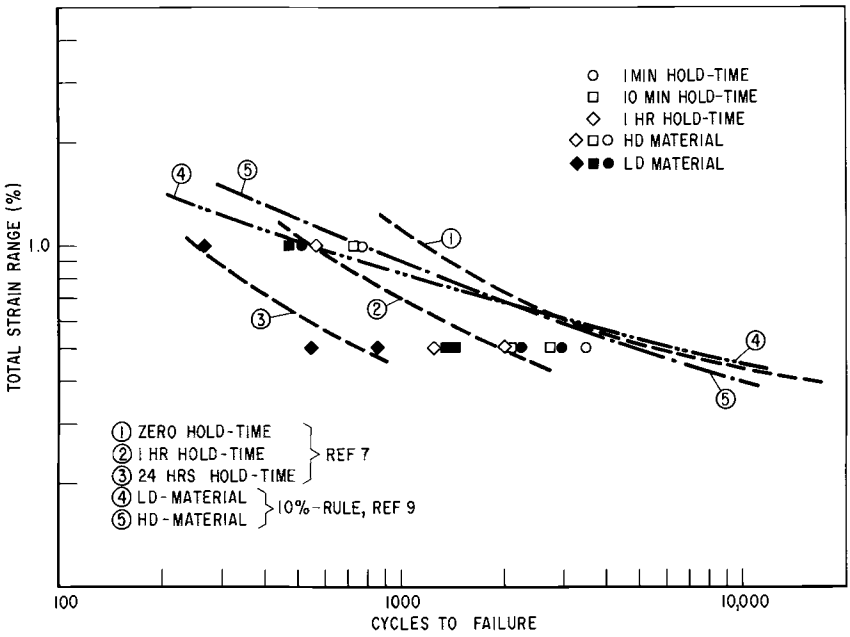

FIG. 15—*Comparison of the results of this investigation with previously published prediction methods.*

that the initiation and propagation phase of the fatigue mechanism can be determined and appropriate analysis tools be developed. Finally, the cycles to crack and cycles to failure for stress-controlled fatigue tests with hold time needs further attention.

Summary and Conclusions

A single heat of 1 Cr-1Mo-0.25V steel was heat treated to a low and to a high level of creep-rupture ductility. Completely reversed, uniaxial strain-fatigue tests were run on the two materials at 1000 F with hold times of 1, 10, or 60 min used at the maximum tensile strain point of the cycle. The total strain range in the tests was either 0.5 or 1.0 percent.

1. The cycles to failure dropped significantly as the hold time was increased with the percentage drop being greater in the 0.5 percent than in the 1.0 percent total strain-range tests.

2. The hold-time effect was much more pronounced in the low than in the higher creep-rupture ductility material. For example, in the 0.5 percent total strain-range tests, the cycles to failure for the high ductility material decreased by about 2:1 as the hold time was increased from 1 to 60 min, while the ratio for the low ductility material was almost 4:1.

3. Log-log plots of cycles to failure versus hold time formed curves whose slopes tended to increase as the hold time increased.

4. The nature of the cracks tended to shift from transgranular to intergranular as the hold time was increased which indicates that a creep-rupture type of damage occurred during the hold periods. The shift was more complete in the 0.5 percent than in the 1.0 percent total strain range tests, and also occurred to a much greater extent in the low than in the high creep-rupture ductility material.

5. Both materials strain softened during cycling as indicated by a continuous decrease in the total stress range. The degree of strain softening was much greater in the high than in the low ductility material.

6. There was a strong interrelation between the material properties measured in the various tests of this investigation which indicates that relaxation, creep, and cyclic-strain softening (hardening) are not separate but are interrelated properties. One aim of further investigations should be to find a unique material law which can represent the observed behavior.

Acknowledgments

The fatigue tests which are reported in this work were performed by R. J. Schaaff, J. J. LaCagnina, and J. J. O'Malley.

References

[1] Walker, C. D., "Strain-Fatigue Properties of Some Steels at 950 F with a Hold Time in the Tension Part of the Cycle," *Joint International Conference on Creep*, The Institution of Mechanical Engineers, 1963, Paper 24, Session 3-49.

[2] Coles, A. D. and Skinner, D., "Assessment of Thermal-Fatigue Resistance of High Temperature Alloys," *Journal of the Royal Aeronautical Society*, Vol. 69, Jan. 1965, pp. 53–55.

[3] Edmunds, H. G. and White, D. J., "Observations of the Effect of Creep Relaxation on High-Strain Fatigue," *Journal of Mechanical Engineering Science*, Vol. 8, No. 3, 1966, pp. 310–321.

[4] Coles, A. et al, "The High-Strain Fatigue Properties of Low-Alloy Creep-Resisting Steels," *International Conference on Thermal and High-Strain Fatigue*, London, The Institute of Metals, 1967, pp. 270–294.

[5] Hill, G. J., "The Failure of Wrought 1% Cr-Mo-V Steels in Reverse-Bending High-Strain Fatigue at 550 C," *International Conference on Thermal and High-Strain Fatigue*, London, The Institute of Metals, 1967, pp. 312–327.

[6] Coles, A. and Chitty, A., "Ductility and Reverse-Bend Fatigue Behavior of C-Mo and Cr-Mo-V Steel," *International Conference on Thermal and High-Strain Fatigue*, London, The Institute of Metals, 1967, pp. 328–345.

[7] Timo, D. P. and Sarney, G. W., "The Operation of Large Steam Turbines to Limit Cyclic Thermal Cracking," Paper 67-WA/PWR-4, American Society of Mechanical Engineers, Nov. 1967.

[8] Manson, S. S., "Interfaces Between Fatigue, Creep, and Fracture," *International Journal of Fracture Mechanics*, Vol. 2, No. 1, March 1966, pp. 327–363.

[9] Bentley, K. P., "Precipitation During Stress Relief of Welds in Cr-Mo-V Steels," *British Welding Journal*, Oct. 1964, pp. 507–515.

[10] Manson, S S. and Halford, G., "Application of a Method of Estimating High-Temperature Low-Cycle Fatigue Behavior of Materials," *Transactions Quarterly*, American Society for Metals, Vol. 61, No. 1, March 1968, pp. 94–102.

[11] Manson, S. S., "Fatigue: A Complex Subject—Some Simple Approximations," *Experimental Mechanics*, May 1965, pp. 193–226.

Masaki Kitagawa,[1] *C. E. Jaske,*[2] *and JoDean Morrow*[1]

Influence of Temperature on Reversed Creep

REFERENCE: Kitagawa, Masaki, Jaske, C. E., and Morrow, JoDean, "**Influence of Temperature on Reversed Creep,**" *Fatigue at High Temperature, ASTM STP 459*, American Society for Testing and Materials, 1969, pp. 100–110.

ABSTRACT: Torsional reversed creep data are presented for tubular specimens of commercially pure aluminum to illustrate the influence of test temperature on creep deformation resistance under repeated stress reversals. Test temperatures range between 300 and 510 K. These data plus results on other metals show that multiple stress reversals cause a deceleration of creep deformation at test temperatures below about 0.4 of the absolute melting temperature. A significant acceleration of creep may occur at higher temperatures. An optimum temperature for maximum acceleration of creep occurs at a temperature of approximately half of the melting temperature.

The engineering significance of the decrease in creep deformation resistance at high temperatures due to multiple stress reversals is discussed. Creep rupture time and the failure life in high-temperature fatigue or thermal fatigue with large hold times may be reduced significantly by an acceleration of creep at high temperatures.

KEY WORDS: creep, reversed creep, accelerated creep, torsional creep, high-temperature fatigue, thermal fatigue, metals, aluminum, evaluation, tests

In 1954, an ASTM symposium was held on the effects of cyclic heating and stressing on the mechanical behavior of metals at elevated temperatures. Most of the work to that date on cyclic stressing during creep was reviewed. Frey [*1*][3] in his summary of the symposium, pointed out that the reported research indicated either no influence of changing the stress during a creep test or a slightly deleterious effect. In every case cited the stress was increased, reduced, or brought to zero periodically during the creep test. However, there is no mention of the effect of *reversing* the stress.

[1] Research assistant and professor, respectively, Department of Theoretical and Applied Mechanics, University of Illinois, Urbana, Ill. 61801. Mr. Morrow is a personal member ASTM.

[2] Battelle Memorial Institute, Columbus, Ohio, formerly research assistant, University of Illinois, Urbana, Ill. 61801.

[3] The italic numbers in brackets refer to the list of references appended to this paper.

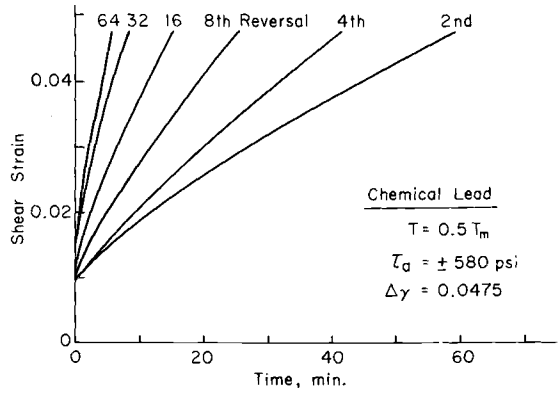

FIG. 1—*Creep curves showing acceleration due to multiple stress reversals.*

Background

In 1963, Morrow and Halford [*2*] reported that the creep deformation resistance of chemical lead at room temperature [0.5 T_m][4] is reduced greatly by repeatedly reversing the creep stress. Figure 1 is an example of their creep curves after various number of stress reversals. During about 60 stress reversals, the average creep rate increased about ten times, compared to the creep rate of a virgin specimen.

Since 1963, the structural changes induced in metals by stress reversals which may cause an increase in creep rate have been studied. To clarify whether the structural changes are persistent after multiple stress reversals, Freund [*3*] performed unidirectional creep tests on the same chemical lead after several stress reversals. In Fig. 2, a typical result is compared with a static creep curve under the same stress. It is seen that the creep rate after cycling remains larger than that of virgin lead. Thus, stress reversals cause persistent structural alterations which permanently reduce the creep deformation resistance of lead at room temperature.

Review

A summary of published results on reversed creep of metals is given in Table 1. The earliest study of this sort appears to be that of Andrade and Jolliffe [*4*] in 1952. They investigated the effect of only one or two stress reversals on the creep deformation resistance of lead and cadmium at room temperature [0.5 T_m]. No acceleration of creep was noted for the cadmium. For the lead, the creep rate increased after both the first and second stress reversals. They attributed this difference in the reversed creep behavior of

[4] The test temperature is shown in brackets as a fraction of the absolute melting temperature of a particular metal, T_m.

TABLE 1—*Summary of published work on reversed creep.*

Metal and Ref	Temperature, T_m	No. of Stress Reversals	Type and No. of Tests		Remarks
Chemical Pb [2]	0.5	100	torsion of tube	13	acceleration—creep rate about ten times as much as creep rate of virgin specimens was observed after 60 to 100 stress reversals
Chemical Pb [3]	0.5	20	torsion of tube	8	acceleration—the steady state creep rate after stress reversals was much larger than that of virgin lead
Commercial Cd [4]	0.5	1 or 2	shear of disk	5	deceleration
Commercial Pb [4]	0.5	1 or 2	shear of disk	5	acceleration
Spectroscopically pure Pb [4]	0.5	1 or 2	shear of disk	7	acceleration
Magnesium [5]	0.32	10	shear, constant period of 10 min per reversals	1	deceleration
20Cr-25Ni-Cb steel [6]	0.55	83	axial, constant period of 10 h per reversals	1	acceleration—after each compressive creep test, strain was brought back to zero by tensile force.
20Cr-25Ni-Cb steel [6]	0.55	63	axial, constant period of 10 h per reversals	1	acceleration—both tensile and compressive creep curves were examined.
Ni-Pd 0.1 at % [7]	0.47	2	axial	1	deceleration—stress was reversed at tertiary creep stage.
Cu-15Al alloy [7]	0.52	2	axial	1	deceleration—stress was reversed at tertiary creep stage.
1100-F Al [8]	0.32 to 0.55	60	torsion of tube	15	acceleration at high temperature; deceleration at low temperature.
Chemical Pb [9]	0.5 to 0.7	60	torsion of tube	4	acceleration—observed less acceleration at the higher temperature.

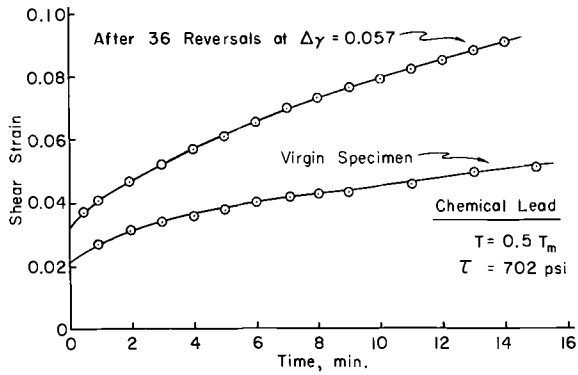

FIG. 2—*Effect of multiple reversals on static creep curve.*

the two metals to the difference between the glide system for face-centered-cubic (fcc) and hexagonal-closed-packed (hcp) metals.

A more recent example of the reversed creep behavior of an hcp metal is Conrad's study [5] of magnesium crystals at room temperature [0.3 T_m]. He found that the total creep deformation in a 10-min interval decreases appreciably for the first and second reversals but changes only slightly for subsequent reversals.

Hughes [6] has reported an acceleration of creep for a 20Cr-25Ni-Cb steel under reversed tensile-compressive loading at a temperature of 1025 K [0.55 T_m]. The experimental results of Davies and Wilshire [7] on a nickel-palladium (Ni-Pd) alloy and Cu-15Al alloy showed a deceleration of creep after one reversal of stress at test temperatures of 773 K [0.47 T_m] and 673 K [0.52 T_m], respectively.

Purpose

To our knowledge there has not yet been a systematic study of the influence of temperature on reversed creep. The purpose of this paper is to show the manner in which the reversed creep behavior depends upon the test temperature.

Experimental Program

Reversed creep tests were performed on commercially pure aluminum over a range of temperatures. Table 2 lists the test conditions and summarizes the results. The test procedure and apparatus are reported in Ref *8* and are briefly described below.

TABLE 2—*Summary of reversed creep data on 1100-F aluminum.*

Temperature, T_m	Shear Strain Range, $\Delta\gamma$	Shear Stress Amplitude, τ_a psi	Number of Stress Reversals						$\bar{\dot{\gamma}}_r/\bar{\dot{\gamma}}_o$
			1	5	9	17	33	65	
			$\bar{\dot{\gamma}}$, Average Creep Rate, min^{-1}						
0.32	0.050	±6060	0.0010	0.00046	0.00025	0.00022	...	...	0.22
0.40	0.100	±4470	0.00026	0.00030	0.00030	..	...	...	1.15
	0.050	±4740	0.00094	0.00144	0.00108	0.00072	...	...	0.66
0.43 to 0.44	0.100	±4120	0.0023	0.0025	0.0038	0.0042	0.0040	...	1.74
	0.100	±4640	0.011	0.015	0.016	0.016	0.019	0.020	1.82
	0.050	±4640	0.013	0.014	0.012	0.010	0.010	...	0.77
0.49 to 0.50	0.100	±3160	0.00043	0.00073	0.00068	...	...	...	1.58
	0.100	±3300	0.0011	0.0014	0.0014	0.0015	0.0020	...	1.82
	0.100	±4230	0.10	0.12	0.13	0.14	0.19	0.20	2.00
	0.050	±3300	0.0085	0.0079	0.0089	0.014	0.015	0.015	1.77
0.52 to 0.53	0.100	±3400	0.0063	0.0091	0.0097	0.015	0.022	0.021	3.33
0.53	0.100	±3710	0.0090	0.016	0.021	0.025	0.034	0.036	4.00
0.55	0.100	±3160	0.008	0.014	0.015	0.014	...	..	1.88
	0.100	±3310	0.026	0.035	0.036	0.041	0.043	0.045	1.73
	0.100	±3560	0.041	0.10	0.090	0.083	0.080	...	1.95

Material and Specimen

Tubular specimens with an outside diameter of 0.500 in., a wall thickness of 0.0625 in., and a reduced section of 3.25 in. were machined from ¾-in. rods of 1100-F (99+ percent purity) aluminum alloy. After machining, they were annealed in vacuum of 10^{-2} torr at 620 K for 30 min and furnace cooled.

Test Apparatus

Tests were performed on a hydraulic closed-loop servo-controlled torsion system. Torque was measured by a strain gaged cell in series with the specimen. Angle of twist was measured using two concentric probes fastened inside the specimen over a 1.50-in. gage length. The ends of the probes were attached to the case and the shaft of a rotary variable differential transformer (RVDT).

Temperature was held constant by a closed-loop controller operating a three-zone radiant heater. Two chromel-alumel thermocouples placed on the specimen surface at the ends of the gage length were used to provide a feedback signal to the temperature controller.

Clamping of the Specimen

The lower end of a specimen was secured by threading it into a split collet which seats in a conical hole on the torsional actuator. The upper end was connected to the load frame through a liquid-solid grip and a splined shaft in series. The splined shaft allowed freedom of axial movement during changes in specimen length and the liquid-solid grip assured proper alignment without clamping distortion.

Control Condition

In each test the shear stress was maintained constant (as in an ordinary static creep test) until a preset shear strain limit was reached. The signal from the RVDT was used to trigger a flip-flop circuit which reversed the direction of the torque, allowing the specimen to creep in the opposite direction under the same magnitude of stress. When the strain reached zero the stress was reversed again until the maximum strain was reached. The test was continued in this manner, as is shown in Fig. 3, until the creep rate was essentially constant from cycle to cycle.

Experimental Results

Fifteen aluminum specimens were tested at six different temperatures between 300 K [0.32 T_m] and 510 K [0.55 T_m] at shear strain ranges of 0.050 and 0.100. The average creep rate per reversal, $\bar{\dot{\gamma}}$, was calculated by dividing the creep strain by the period of one reversal, as defined in Fig. 3. Because there

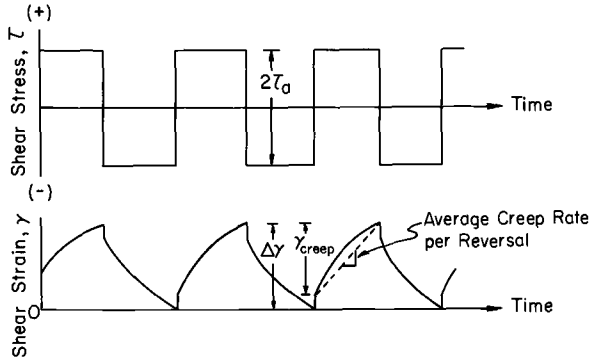

FIG. 3—*Schematic stress-time and strain-time curves.*

was sometimes a small difference in the creep curves in the clockwise and counterclockwise directions, the reported average creep rates are those for a whole cycle (that is, average for two reversals).

Changes in the average creep rate with the number of stress reversals are tabulated in Table 2, and typical results are plotted in Fig. 4. At low temperature [0.32 T_m], creep is decelerated by stress reversals. At high temperatures [>0.5 T_m], average creep rate increases with the number of stress reversals. In the intermediate temperature range [0.40 to 0.44 T_m], acceleration of creep was observed for a strain range of 0.100, and deceleration occurred for a strain range of 0.050. However, at about 0.5 T_m, acceleration of creep took place regardless of strain range.

In all tests reported here, the average creep rate changes greatly during the first several cycles. After the rapid initial change, the alteration of the average creep rate with additional stress reversals is less. Eventually the average creep rate is nearly constant from cycle to cycle. The ratio of this nearly constant

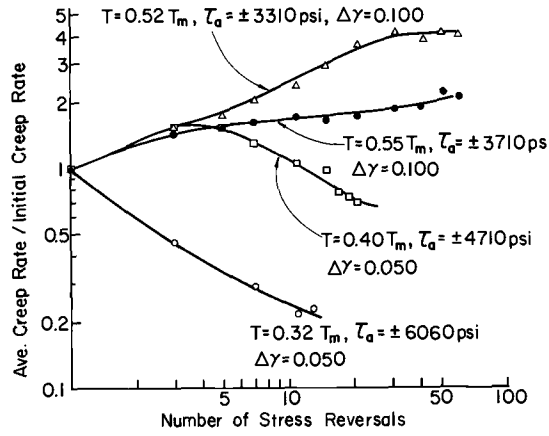

FIG. 4—*Change in average creep rate with the number of stress reversals.*

average creep rate to the average creep rate of the first cycle, $\bar{\dot{\gamma}}_r/\bar{\dot{\gamma}}_o$, is listed in Table 2. A ratio larger than one indicates an acceleration of creep due to reversed stressing, and a ratio smaller than one indicates a deceleration of creep.

At the test temperature of 0.52 T_m, the largest acceleration of creep was observed. The degree of acceleration becomes less when the test temperature is increased from 0.52 to 0.55 T_m. A recent investigation on lead [9] also shows that less acceleration occurs when the test temperature is increased from 0.5 to 0.70 T_m. These experimental data indicate that there exists an optimum temperature for maximum acceleration of creep around 0.5 T_m.

Discussion

The experimental results show that there exists a transition temperature above which creep deformation resistance will be decreased by stress reversals. For commercially pure aluminum the transition temperature appears to be approximately 0.4 T_m. This transition temperature seems to be slightly dependent upon the strain range (Table 2).

In order to compare the results with similar data for other metals, the ratio of the final average creep rate to the initial rate are plotted in Fig. 5 along with similar results for other metals involving multiple stress reversals. The

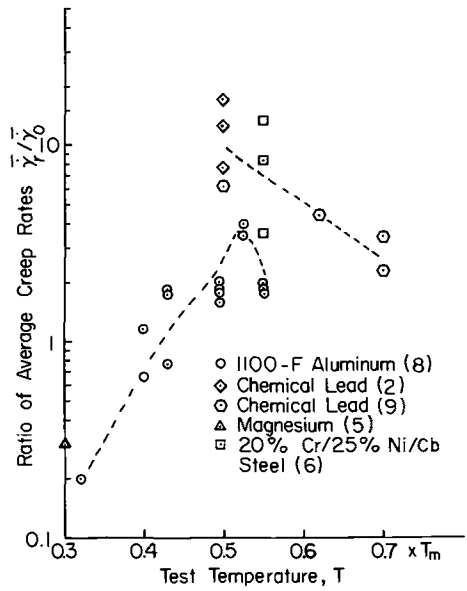

FIG. 5—*Change in average creep rate after multiple stress reversals as a function of temperature.*

test temperature is shown as a fraction of the absolute melting temperature for each metal plotted. The present estimate of the transition temperature is seen to be consistent with the plotted data for other metals. In the earlier investigation of lead [*2*] and in Hughes' results on 20Cr-25 Ni-Cb steel [*6*], acceleration of creep was observed at 0.5 and 0.55 T_m, respectively, which are well above the above mentioned transition temperature. At 0.32 T_m, the creep of magnesium was decelerated due to stress reversals [*5*].

The strain range in reversed creep tests of Refs *2* and *6* varied from about 0.01 to 0.500. Acceleration of creep was reported regardless of such a wide range of strain. Therefore, the effect of strain range on the transition temperatures is believed to be small.

The above comparison was made in terms of the test temperature compared to the melting temperature. For the following reasons, data from Refs *4* and *7* are not included in the comparison. There is some doubt about the effect of crystalline structure, which is implied by the experiments on cadmium [*4*]. These experiments on cadmium and those in Ref *7*, where deceleration was observed at about half of the melting point, involved only two reversals. Furthermore, in Ref *7* the creep stress was reversed in the tertiary creep stage.

Practical Significance

The creep deformation resistance under static and reversed loading are represented schematically in Fig. 6 as a function of temperature. At low temperatures relative to the melting point, reversed stressing increases the creep deformation resistance of metals. At high temperatures stress reversals significantly reduce the creep deformation resistance. The loss of creep deformation resistance, which is of a persistent nature [*3*], may be detrimental for structural members. Such permanent decreases of creep deformation resistance may affect the life of metals at high temperatures.

Creep deformation resistance generally is considered to be an indicator of creep rupture resistance of metals. Empirically, it has been shown for a variety of metals [*10*, *11*] that the creep rupture time, t_r, is related to the minimum creep rate, *mcr*, as follows:

$$\log t_r + m \log (mcr) = \text{constant}$$

The constant m has a value of roughly one. This empirical relationship implies that a metal specimen after being subjected to stress reversals at high temperatures would have a significantly shorter creep rupture life than virgin specimens because of the persistent increase in creep rate caused by reversed creep.

Furthermore, a decrease in the creep deformation resistance would affect adversely the shape of hysteresis loops in high-temperature fatigue and under thermal fatigue conditions. At high temperatures, creep deformation would

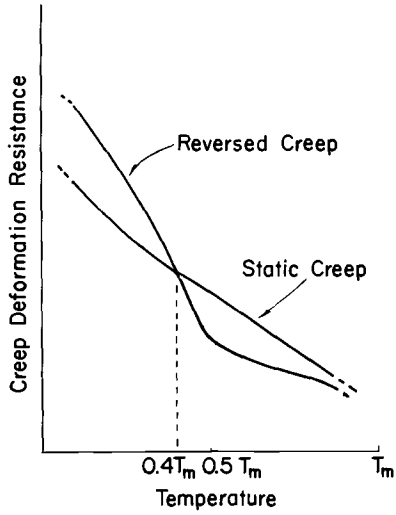

FIG. 6—*Schematic representation of creep deformation resistance as a function of temperature.*

increase the plastic strain range when the total strain range is controlled during the fatigue tests. Plastic strain range would be increased greatly by the loss of creep deformation resistance due to the reversed stressing. That is, the plastic strain range would increase with the number of stress reversals. Since fatigue damage is related intimately to the amount of plastic strain range, this may cause an unexpectedly short fatigue life. The effect would be particularly significant if the temperature is around 0.5 T_m, and if large "hold times" were involved.

Summary

Experimental results show that for 1100-F aluminum, acceleration of creep occurs with repeated stress reversals at high temperatures, and deceleration occurs at low temperatures. The transition temperature above which creep will accelerate due to stress reversals appears to be about 0.4 T_m. Changes in the creep deformation resistance during reversed stressing of other metals as a function of temperature also suggest an acceleration of creep above about 0.4 T_m. The maximum acceleration of creep appears to occur at about 0.5 T_m.

The possible decrease in fracture life resulting from the acceleration of creep due to reversed stressing at high temperature was discussed in relation to creep rupture, high-temperature fatigue, and thermal fatigue. A temperature of about 0.4 T_m is believed to be the temperature above which the creep deformation under stress reversals may have deterimental effect on these fracture properties when metals are subjected to repeated stress reversals.

Acknowledgments

This work was conducted in the H. F. Moore Fracture Research Laboratory of the Department of Theoretical and Applied Mechanics at the University of Illinois. Financial support was provided by the National Aeronautics and Space Administration under Research Grant NGR-14-005-025. The reversed creep experiments on 1100-F aluminum were performed by C. E. Jaske as a part of his M.S. thesis research [*8*].

References

[*1*] Frey, D. N., "Summary of the Symposium," *Effect of Cyclic Heating and Stressing on Metals at Elevated Temperatures, ASTM STP 165*, American Society for Testing and Materials, 1954, pp. 173–175.

[*2*] Morrow, JoDean and Halford, G. R., "Creep under Repeated Stress Reversals," *Joint International Conference on Creep*, Institute of Mechanical Engineers, London, 1963, pp. 3-42 to 3-47.

[*3*] Freund, L. B., "Effect of Repeated Stress Reversals on the Creep of Lead," *Fourth Student Symposium on Engineering Mechanics*, T&AM Report No. 262, Department of Theoretical and Applied Mechanics, University of Illinois, Urbana, Ill., 1964.

[*4*] Andrade, E. N. da C. and Jolliffe, K. H., "The Flow of Polycrystalline Metals under Simple Shears," *Proceedings of the Royal Society of London*, Vol. 213A, 1952, pp. 3–26.

[*5*] Conrad, H., "Effect of Changes in Slip Direction on the Creep of Magnesium Crystals," *Transaction of Metallurgical Society*, American Institute of Mining, Metallurgical, and Petroleum Engineers, Vol. 215, 1959, pp. 58–63.

[*6*] Hughes, A. N., "Creep of a 20% Cr/25% Ni/Nb Steel under Reversed Creep Conditions," TRG Report 1018(6), United Kingdom Atomic Energy Authority, 1965.

[*7*] Davies, P. W. and Wilshire, B., "Void Growth During Secondary Creep," *Philosophical Magazine*, Vol. 11, 1965, pp. 189–190.

[*8*] Jaske, C. E., "The Influence of Temperature on Reversed Creep," M.S. thesis, Department of Theoretical and Applied Mechanics, University of Illinois, Urbana, Ill., 1967, see also T&AM Report No. 674.

[*9*] Kitagawa, Masaki, "Enhanced Grain Boundary Sliding During Reversed Creep of Lead," M.S. thesis, Department of Theoretical and Applied Mechanics, University of Illinois, Urbana, Ill., 1968, see also T&AM Report No. 319.

[*10*] Garofalo, F., *Fundamentals of Creep and Creep-Rupture in Metals*, MacMillan, New York, 1965, pp. 202–208.

[*11*] Monkman, F. C. and Grant, N. J., "An Empirical Relationship between Rupture Time and Minimum Creep Rate in Creep-Rupture Tests," *Proceedings*, American Society for Testing and Materials, Vol. 56, 1956, pp. 593–620.

A. E. Carden[1] *and T. B. Slade*[2]

High-Temperature Low-Cycle Fatigue Experiments on Hastelloy X

REFERENCE: Carden, A. E. and Slade, T. B., **"High-Temperature Low-Cycle Fatigue Experiments on Hastelloy X,"** *Fatigue at High Temperature, ASTM STP 459*, American Society for Testing and Materials, 1969, pp. 111–129.

ABSTRACT: Low-cycle fatigue behavior of Hastelloy X at elevated temperature is presented. We studied the effects of test temperature, cycle frequency, and stress temperature arrangement with special attention given to the minimum ductility (short-time tension test) at or near 1300 F. Isothermal fatigue data at 800, 1300, 1500, and 1800 F are presented along with strain controlled thermal fatigue data for temperature ranges of 600 to 1800, 800 to 1300, and 1800 to 1300 F. The method of universal slopes can be used to describe the fatigue behavior under elevated isothermal and cyclic thermal fatigue conditions. The thermal fatigue behavior determined from controlled strain tests can be applied to the thermal cycle behavior of bundles of thin tubes joined to a rigid plate.

KEY WORDS: fatigue (materials), elevated temperature, cyclic loads, nickel-base alloys, method of universal slopes, evaluation, tests

In a recent paper the low-cycle thermal fatigue characteristics of Hastelloy X thin-walled tube bundles were described [*1*].[3] The tubes were joined to a massive base plate which was maintained at a low temperature, while the tube crowns were cycled thermally utilizing a radiant heat source. The base plate prevented the free thermal expansion of the tubes so that a cyclic mechanical deformation was imposed on the tube crowns leading to circumferential cracking after 18 to 80 cycles. The specimen configuration and testing procedure were intended to approximate the behavior of rocket nozzle coolant tubes. Since Hastelloy X was a candidate material for the nozzle, low-cycle thermal fatigue data of the material were desired. The previous study evaluated the effect of the structural geometry and temperature field; the study reported herein was initiated to examine the behavior of the material

[1] Associate professor, Department of Mechanical Systems Engineering, University of Alabama, University, Ala. 35486. Personal member ASTM.

[2] Graduate student, Aerospace Engineering, University of Alabama, University, Ala. 35486.

[3] The italic numbers in brackets refer to the list of references appended to this paper.

under conditions where the temperature and strain could be programmed and measured.

Because of the rather limited amount of low-cycle high-temperature fatigue data available for this alloy [*2*], a complete analysis of low-cycle fatigue of the nozzle under cyclic temperature conditions was not possible. Methods for the thermal fatigue analysis of rocket nozzle configurations were treated by Avery et al [*3*], but their discussion did not relate the component behavior to the thermal fatigue behavior of the materials used. Because the rocket nozzle tubes are under a large compressive stress at the maximum temperature they tend to "ripple" or buckle. Avery et al describe a simple relationship that would predict tube buckling under cyclic thermal fields. The parameters used in that analysis do not include time at temperature for the thermal cycle nor considerations of ductility or strength. Other investigators have shown interest in thermal fatigue [*4*] and thermal buckling [*5*] of rocket nozzle tubes. We performed a limited fatigue test program to provide some additional information on the thermal fatigue behavior of Hastelloy X.

The low-cycle fatigue behavior of a component is quite often strain limited and therefore closely related to the ductility of the material. It is necessary to perform the fatigue tests under conditions of strain rate and temperature that are similar to that experienced in service. As most nickel-base high-temperature alloys show a minimum in ductility in the temperature range of 1100 to 1500 F, the cyclic temperature tests must evaluate the most adverse conditions of cycling to and through these temperatures. Coffin [*6*], in fact, has discussed some of these factors affecting our understanding of "fatigue ductility."

The tensile ductility of Hastelloy X, as indicated by elongation, is strain rate dependent at elevated temperatures and passes through a minimum at or about 1300 F. Several fatigue tests of this program were conducted at and near this temperature. Furthermore, tension tests at several strain rates and temperatures were performed so that reduction of area data could be obtained as a function of the two variables. Moreover, the study of the failed sections of the Hastelloy X tube bundles showed that "the coolant tubes failed by an intergranular mode of fracture that was propagated under tensile stress during the cooling portion of the thermal cycle" [*7*]. The arrangement of the stress and temperature in some of the fatigue tests was programmed to evaluate the effect of large tensile stresses on the cooling portion of the cycle. From the earlier work [*1*] it was known that time at temperature did influence both the onset of buckling and cyclic life. It seemed necessary that hold time (or frequency) must be considered in the fatigue test program. While it is true that the thermal fatigue failure of the tube bundles was influenced greatly by buckling (the radius-to-thickness ratio (r/t) of the tubes was about 20), the specimen geometry for the thermal fatigue tests was chosen

to be more resistant to instability under high-cyclic strains (an r/t of about 5). Once a ripple (local instability) forms in the tube bundles the maximum strain range of the cycle rapidly increases.

The purpose of the test program described in this report was to determine the effects of several parameters on the elevated temperature low-cycle fatigue of Hastelloy X in the life region of 10 to 1000 cycles. These parameters were: (1) the minimum tensile ductility temperature regime, (2) the test temperature (for isothermal) and maximum temperature (for cyclic thermal), (3) the stress-temperature arrangement for thermal fatigue, (4) frequency, and (5) hold time.

Experimental Procedure

Both tension tests and fatigue tests were performed for this investigation. Since the primary purpose of this report is to discuss the fatigue data, only brief summary statements will be made concerning the experimental procedure and the results of the tension tests.

The material used in this investigation was Hastelloy X whose composition and properties can be found in Ref *8*. The fatigue specimens were cut from 1-in.-thick plate in the longitudinal direction (heat 260-5-271). The tension specimens were machined from ⅜-in.-diameter rod (heat X4-4453).

About 30 tension tests were performed in an Instron testing machine to determine the tensile properties as a function of strain rate and temperature. The specimens had a uniform cross section of 1.5 in. length and a nominal outside diameter of 0.188 in. Crosshead speeds were programmed for 0.002, 0.02, 0.2, and 2.0 in./min. Tests were conducted in air at several temperatures from 70 to 1700 F. Because no extensometer was used to measure strains, only the reduction of area and ultimate tensile strength are reported herein.

Fatigue tests were performed in an Instron testing machine. Resistance heating was used to maintain the specimen temperature. Thirty-two gage chromel-alumel thermocouples welded to the specimen at midlength were used to measure the specimen temperature. Threaded tubular specimens were used with a gage section of 1 in., 0.390 in. outside diameter, and a 0.035-in.-thick wall. The specimen dimensions are shown in Fig. 1.

The temperature was controlled by a separate system that was synchronized with the motion of the Instron crosshead. For the isothermal fatigue tests the specimen was maintained at constant temperature, plus or minus 10 F. Better control of the temperature was obtained on the longer life tests where was little heat released in the specimen as a result of the large deformations. The self heating tended to perturb the temperature control slightly. For the thermal cycle tests the heating and cooling rates were linear. This test system has been described more completely elsewhere [*9*]. All but four

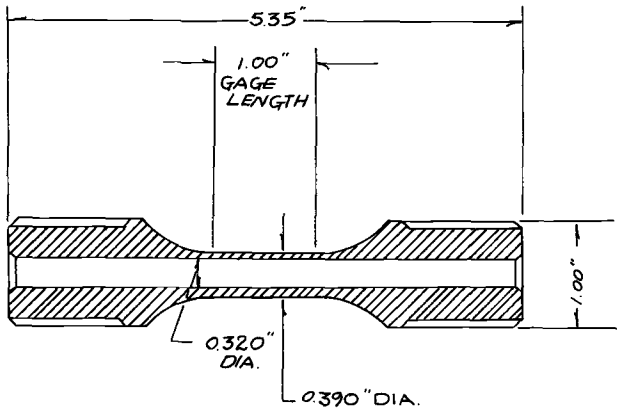

FIG. 1—*Fatigue test specimen.*

of the fatigue tests were performed in flowing argon at 36 cycles per hour, were extension controlled, and had no hold time at either extreme of extension. In addition, four isothermal fatigue tests were performed in air at 1500 F; two at higher frequencies (one at 360 and one at 420 cycles per hour) and two at 36 cycles per hour but with 30-s hold time at constant load at each cycle extreme. The creep strain that occurred during this hold time was approximately three times the magnitude of the plastic strain that was present at the initiation of the hold period. Because the fatigue program was limited to 22 specimens the cyclic life was restricted to the regime of 10 to about 1000 cycles. Boundary conditions were selected so that trends could be observed, and two or more specimens were used for each fatigue test condition.

The fatigue testing program included several stress-temperature arrangements. Isothermal tests at 800, 1300, 1500, and 1800 F were conducted as well as thermal cycle tests at 800 to 1300, 600 to 1800, and 1800 to 1300 F. The stress-temperature arrangements are shown schematically in Fig. 2. The symbols used in this figure are used in all of the succeeding figures to identify the stress-temperature arrangement. The cyclic temperature conditions were selected so that a tensile stress existed at or near 1300 F.

The Instron crosshead extension limits were used to control the specimen strain range value. For a cyclic temperature test the specimen was cycled thermally before clamping the lower specimen grip to the crosshead. The free thermal expansion of the specimen was recorded. The Instron extension limits were selected to yield a cyclic life in the range of 10 to 1000 cycles. The diagram of the Instron displacement and specimen thermal displacement is shown in Fig. 3. The mechanical deformation applied to the specimen is

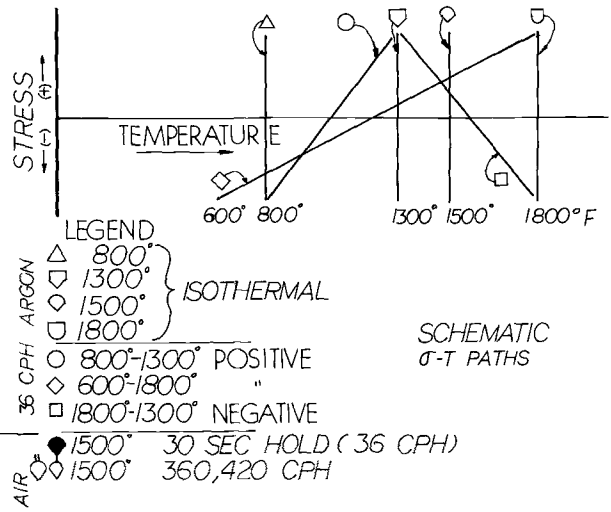

FIG. 2—*Stress temperature arrangement for fatigue tests. A symbol is shown with each test condition. These symbols are used in the remainder of the figures to identify the data.*

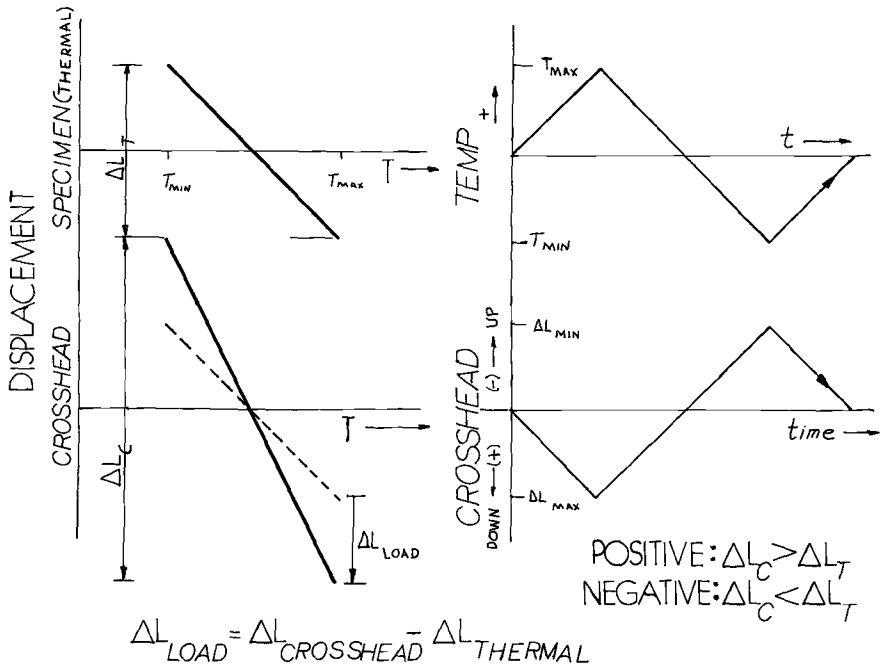

FIG. 3—*Schematic of crosshead and specimen—thermal displacement for thermal cycle tests.*

the difference of the crosshead displacement and the specimen thermal displacement. The sign convention requires a positive crosshead displacement to be greater than the specimen thermal displacement. A negative stress-temperature loop is one having a decreasing stress while heating. For those isothermal tests having a constant load hold, the load limits were used to program the cycle.

Strain measurement was accomplished by the use of two strain transducers: one for diameter change and the other for change of length of a ½ in. gage length. The temperature profile over the central ½ in. length is not perfectly flat, but the calculations of the strain ranges using data from each transducer lead to essentially equal values of strain. Portions of the two transducers are shown in the photograph of Fig. 4. Using such transducers with idential calibration constants, the difference of the two outputs is independent of the thermal component of strain. A plot of load versus the difference-of-transducer output is then essentially a stress versus mechanical component of strain diagram. The internal width of this loop is a measure of the plastic-strain range; the external width is a measure of the total (elastic plus plastic) strain range, and the area inside the loop is a measure of the plastic-strain-energy dissipated per cycle. The strain output of the x-y record must be divided by a function of one-plus-Poisson's ratio to determine the longitudinal elastic plus plastic components of strain. Reference *9* gives a more detailed explanation of the analysis of the hysteresis loop.

Test Results

Tensile data are often used as a basis for predicting low-cycle fatigue behavior. The tensile data of Hastelloy X are summarized in Figs. 5 and 6. The elongation data (Fig. 5) were obtained from sheet specimens and reported by the manufacturer [*8*]. The modulus of elasticity data (Fig. 6) were obtained from Oak Ridge National Laboratory.[4] The tensile strength and true strain at fracture data are the averages of results of four crosshead speed test conditions. Although the strain rate was not constant after necking began, the results do not show a large effect of crosshead rate (0.002 to 2.0 in./min) on the two properties. The predominate effect on true strain at fracture seems to be one of temperature. Furthermore, the minimum ductility as determined from reduction of area data occurs near 1000 F. The tensile strength decreases with increasing temperature. The ratio of ultimate tensile strength to yield strength (at 0.002 offset) is about 2.2 from 70 to 1200 F and decreases to about 1.3 at 1800 F. The strain hardening exponent for this material varies from about 0.35 to 0.18 for monotonic tensile loading from 70 to 1200 F. It then drops to a value of from 0.04 to 0.02 from 1400 to 2000 F.

[4] Harman, D. G., private communication, 1966.

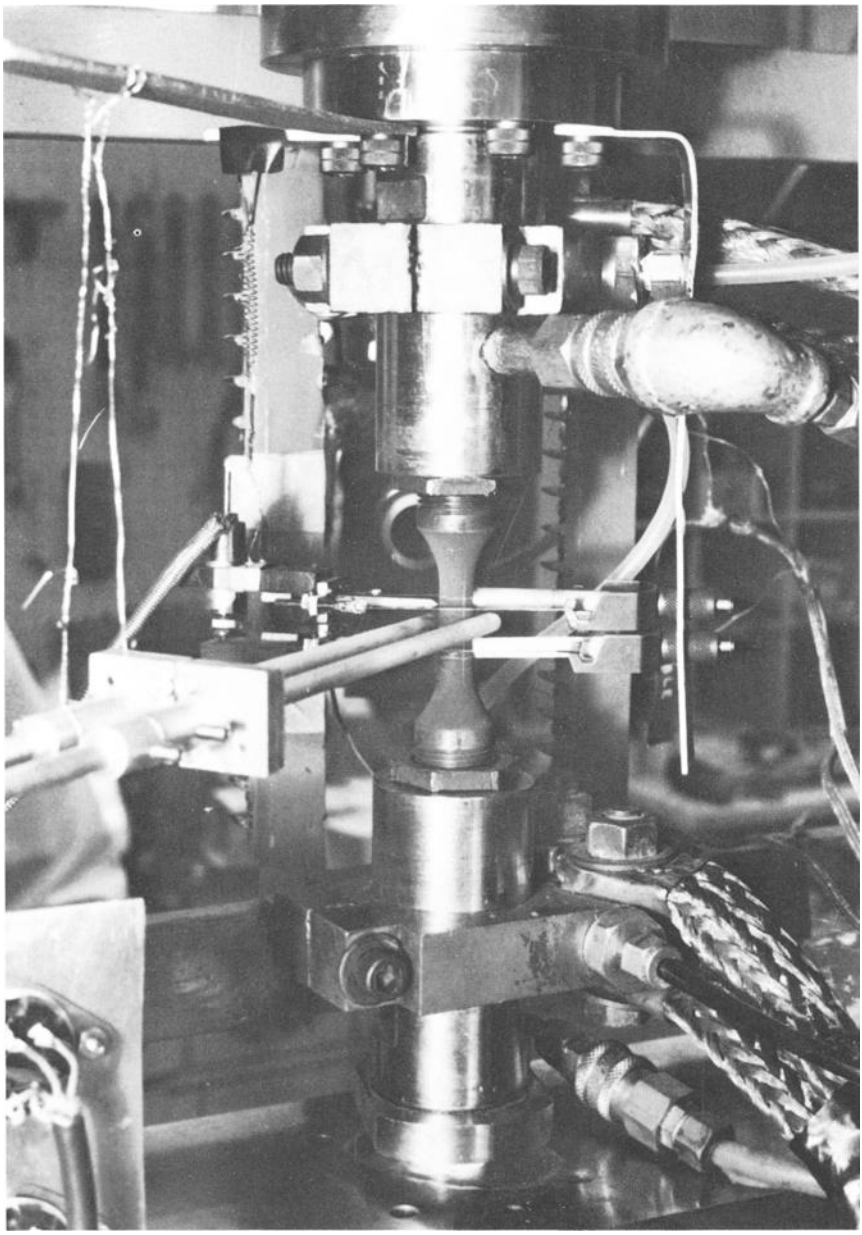

FIG. 4—*Photograph of fatigue specimen, grips, and strain transducers. The diametral transducer is shown partly in foreground, the longitudinal one is shown in the left background.*

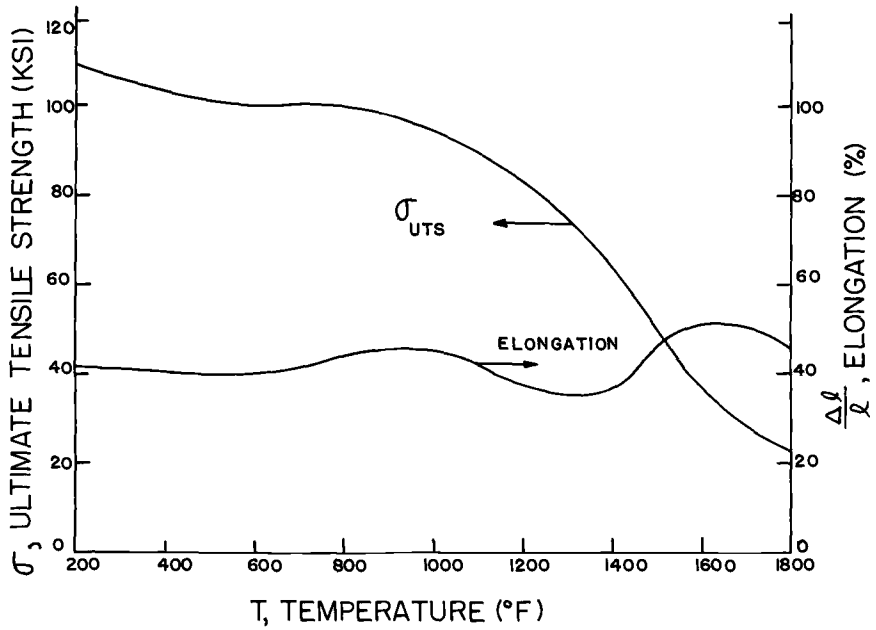

FIG. 5—*Tensile properties of Hastelloy X. Ultimate tensile strength and elongation.*

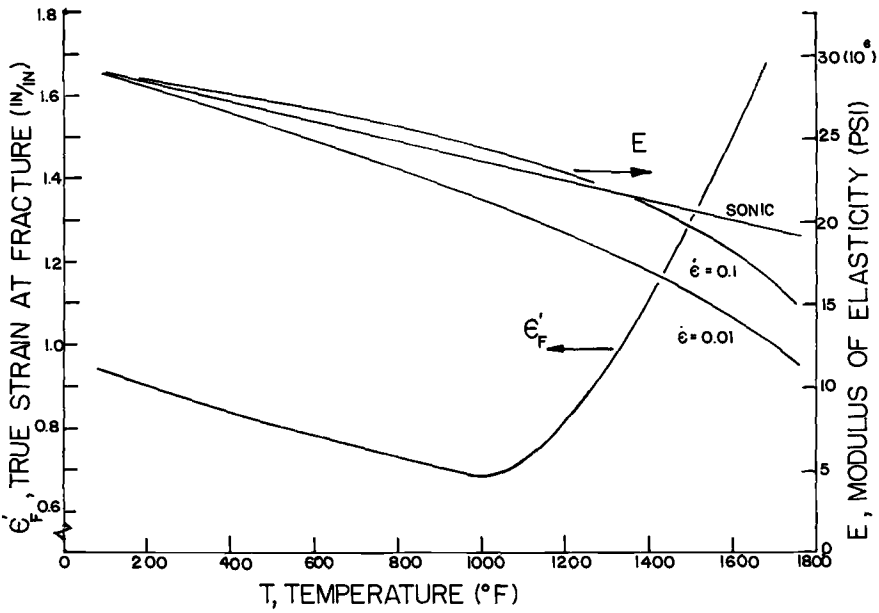

FIG. 6—*Tensile properties of Hastelloy X. Modulus of elasticity and true strain at fracture.*

Fatigue Results

Because the Instron extension limits were fixed and because the material exhibited hardening, the stress range and plastic-strain range values changed during the period of the test. The values of the various quantities plotted in this report are the values determined at 63 percent of life.

At the very low life region some of the specimens experienced rather severe distortion. The most noticeable occasion of such instability was in the 1300 to 1800 F thermal cycle data. Only two other specimens showed any marked distortion, and these were 800 F isothermal tests. Both of the 800 F test specimens failed in the region near the fillet; all of the other specimens failed within 0.2 in. of the center.

Failure is defined as the value of cyclic life for a specimen that contains a crack that is equal to or greater than one half of the circumference of the specimen. Specimens experiencing high-strain ranges showed significant banding (surface roughening) over the full 1 in. gage length. The surfaces showed a number of small fissures oriented at 45 deg to the principal axes. The main fracture surface showed the linking of many of these small cracks. In general, the main crack propagated in a radial plane perpendicular to the specimen axis.

The stress range versus life relationships are shown in Fig. 7. A line representing an equation of the form

$$\Delta\sigma N_f^{0.12} = K; \qquad \frac{K}{E} = D$$

was used to represent the data. A universal slope method allows a simple comparison of the data. Except for the 800 F data, the slope of minus 0.12 fits the data well. The value of K decreases with increasing temperature. The use of the ultimate tensile strength, doubled, as an approximation of $\Delta\sigma$ at $N_f = \frac{1}{4}$ is conservative. The thermal fatigue data lie in between the two isothermal curves that describe the behavior at each of the temperature extremes. The results of those tests having a hold condition under constant load (1500 F) show a slightly inferior stress range to life comparison when compared to other 1500 F data. The results of the two higher frequency tests (360 and 420 cycles per hour at 1500 F) correlate well with the 36 cycles per hour data.

For the thermal cycle tests the stress amplitudes at each extreme of temperature are unequal, and there is therefore a "mean stress." Because of the temperature dependency of the strength of the material, unequal stresses are required for equal and opposite plastic strains. The mean stress does not imply a mean strain. There can be a cyclic instability, but this is not a consequence of the imbalance of the tensile and compressive stresses [*10*].

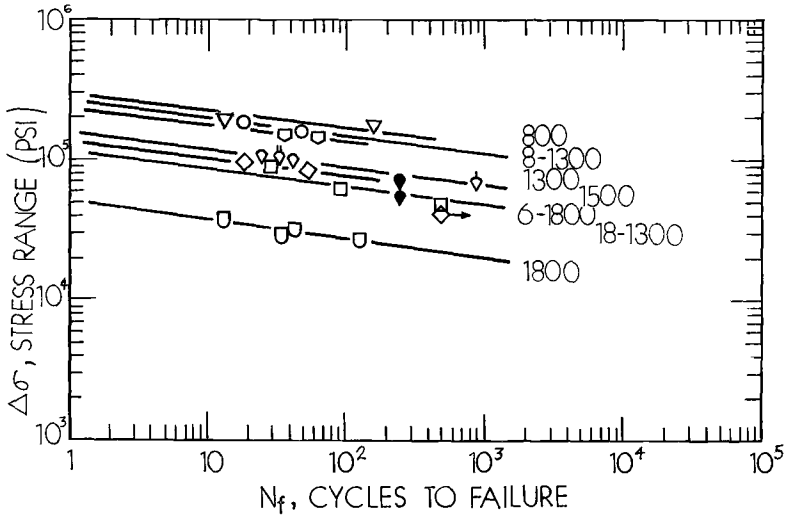

FIG. 7—*Stress-range fatigue data.*

If both sides of the stress range equation are divided by the modulus of elasticity, an elastic-strain range equation is obtained. The values of K/E will be plotted as a function of temperature and discussed later.

The plastic-strain range versus life values are shown in Fig. 8. A relationship of the type

$$\Delta\epsilon_p(N_f)^{0.6} = C$$

was used to represent the data. Except for the 800 and 1800 F isothermal data, most of the data show a slope of about minus 0.8. We will not attempt to settle the question of which slope should be used. If the empirically determined value of slope is used, recommended methods of relating the constant C to the ductility do not work as well. As a compromise we elected to use a universal slope of minus 0.6. The use of a universal slope through the data allows a more direct comparison of the results of several test conditions. In general, increasing the maximum temperature decreases the constant C. The 800, 1300, and 1500 F isothermal data are grouped having values of C of 0.22, 0.23, and 0.29, respectively. The isothermal 1800 F tests and the cyclic thermal tests of 1800 to 1300 and 600 to 1800 F temperature also are grouped and show C values of 0.12, 0.11, and 0.10, respectively. The C value for the 800 to 1300 F tests was 0.15. If the minimum and maximum tensile ductilities, as determined from reduction of area data, are used to predict a value of C, the values of C range from 0.05 to 0.12. In other words, the band predicted from tensile data would be a reasonable prediction and slightly conservative for the cyclic temperature fatigue behavior. The cyclic temperature fatigue

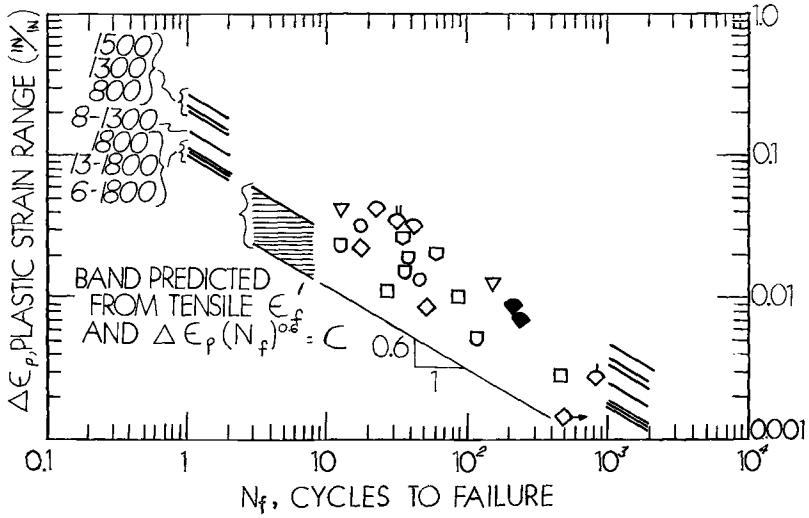

FIG. 8—*Plastic strain-range fatigue data.*

data show, in two cases, approximately the same results as the maximum temperature isothermal fatigue data. In the other case (800 to 1300) the cyclic temperature data are inferior to the isothermal data (800 and 1300 F). In this latter comparison there is approximately a 40 percent reduction in life. Except for this case, no special reduction of fatigue life can be shown for those tests having 1300 F as a part of the thermal regime for fatigue deformamation.

Moreover, the addition of time dependent strain (30-s hold time at constant load) or the increase in frequency did not affect greatly the fatigue behavior at 1500 F.

The total strain range versus life curve is shown in Fig. 9. One of the plastic strain and elastic strain curves shown in Figs. 7 and 8 are combined and shown on Fig. 9. In general, the method of universal slopes works well as a basis for describing the total strain range versus life relationship. If isothermal tensile data had been used to predict the behavior a slightly conservative prediction results. For the cyclic temperature, minimum properties over the range of the thermal cycle should be used. In general, the fatigue life decreases with increasing maximum temperature for a given strain range.

There does not seem to be a gross inferiority of the low-cycle fatigue characteristics at or near the temperature where the minimum ductility occurs. Because the elastic strain range is only a small fraction of the total strain range, there does not seem to be a drastic alteration of the total strain range versus life relationship for the tests that had appreciable creep strains. That this is true is an indication that the material senses only the plastic

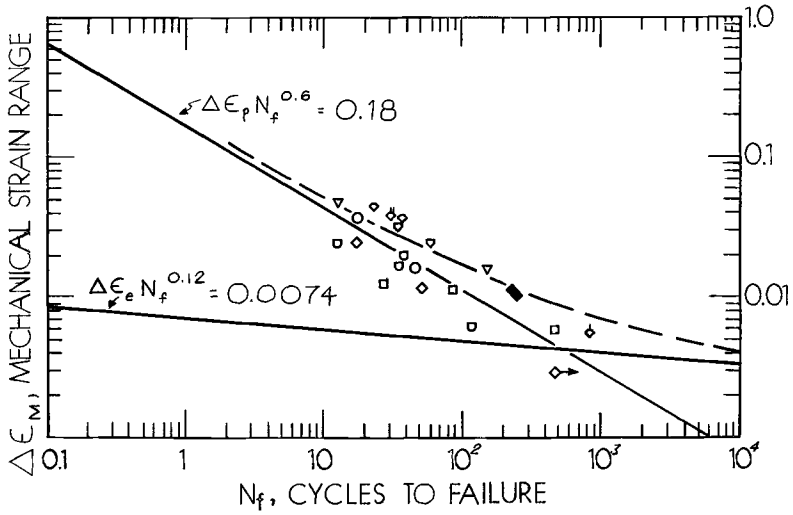

FIG. 9—*Total strain-range fatigue data.*

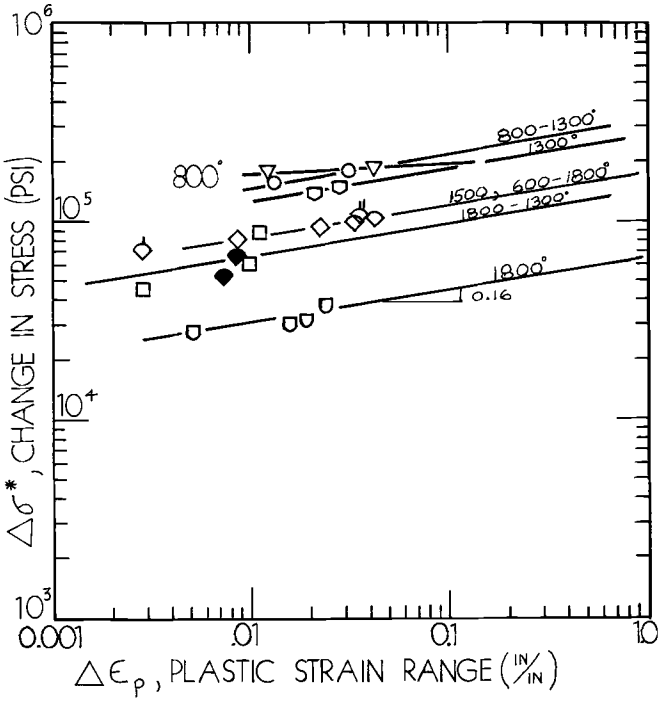

FIG. 10—*Stress range—plastic strain-range relationship (cyclic stress-strain data).*

strain magnitude and does not differentiate between yield-type strains and time-dependent strains. Admittedly, there are too few data to make conclusive statements, but the indication is that this is true.

The cyclic strain hardening exponent has been suggested as a basis for predicting fatigue behavior [*11*]. The stress range versus plastic-strain range values are plotted in Fig. 10. An equation of the form

$$\Delta\sigma = S'(\Delta\epsilon_p)^{n'}$$

describes the behavior. These data show a decreasing intercept value (that is, the stress range value at a strain of unity, or S' in the equation). A slope of 0.16 fits the data well except for the 800 F points. The cyclic temperature fatigue behavior lies in the region between the relationships describing the isothermal behavior at the two thermal extremes. The monotonic hardening exponent is between 0.35 and 0.04 over the temperature range 800 to 1800 F.

The values of C, D, and S' from the equations describing plastic strain range, elastic strain range, and cyclic stress-strain behavior are plotted as functions of temperature in Fig. 11. The values for cyclic thermal data are identified on each curve. Obviously, the cyclic thermal values tend to be

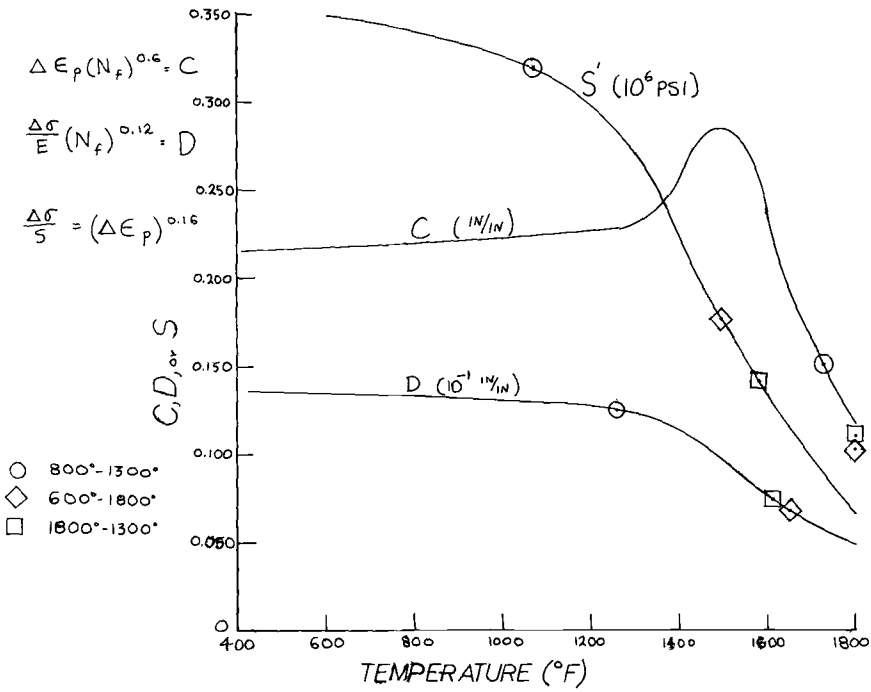

FIG. 11—*Constants* D, C, *and* S' *from stress-fatigue, plastic strain fatigue, and cyclic stress-strain data.*

located toward the maximum temperature of the cycle. If tensile or cyclic stress-strain data or both are used to obtain or predict the values of C, D, and S' as functions of temperature, slightly conservative predictions are obtained for the elevated temperature fatigue behavior. For the cyclic thermal fatigue case we recommend using the minimum value of C, D, or S' determined over the range of the thermal cycle. It appears that the method of universal slopes coupled with the techniques suggested by Manson [*12*] or Feltner [*13*] are adequate for predicting the thermal fatigue behavior of Hastelloy X in the region of 20 to 800 cycles.

If the fatigue life is related to the stress-strain behavior of the material then a plot of plastic strain energy versus life should be meaningful. Such a plot is shown in Fig. 12. Two curves with slopes of minus one are drawn through the data. The lower curve is an average for the 1800, 600 to 1800, and 1800 to 1300 F test data; the other curve is an average for the remainder of the data. The 1800 F data consistently show a lower strain energy value than those from the lower temperature tests. A slope of minus one infers that a constant total-plastic-work criterion is valid for the fatigue of Hastelloy X at elevated temperature.

It has been suggested by a number of authors that elevated temperature fatigue data can be analyzed by a time-under-stress criterion of failure [*14*, *15*]. Based on these suggestions a plot of integrated time-under-stress versus life is shown in Fig. 13. The ordinate values are obtained in the following manner. A typical stress-time record is obtained, and the total time for one cycle is

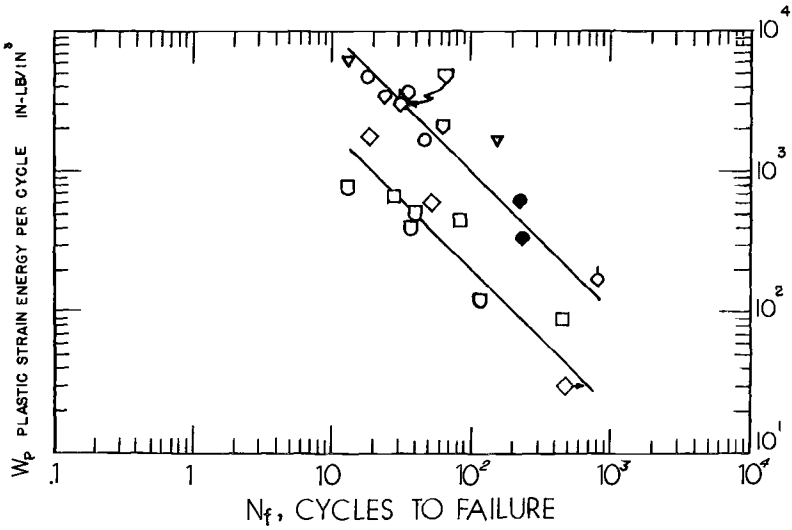

FIG. 12—*Plastic strain-energy (per cycle) fatigue data.*

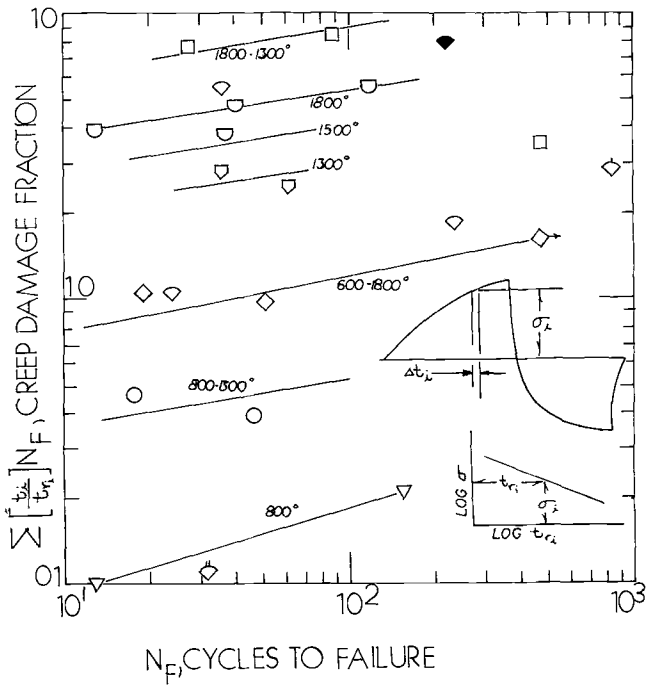

FIG. 13—*Integrated time-under-stress relationship.*

divided into a number of equal increments (in this case about 30). The average values of stress and temperature for each increment of time is determined. Each time increment is then divided by the time to rupture based on creep rupture data for the specified value of average stress and temperature. All time increments of the cycle are weighted equally. Tensile and compressive stresses, elevated- and low-temperature conditions were evaluated in the same manner. These ratios then are summed, and the total is multiplied by the number of cycles to failure. There are several problems in reaching a proper assessment of the method. The uniaxial creep test has a mean strain and an increasing value of stress during the test. The increasing stress leads to third stage creep and lowers the time to rupture when considering the true stress behavior. Furthermore, in reversed loading the primary creep generally reappears on each reversal of loading. In the reversed loading there is some cycle dependent effect that accelerates the crack propagation. Moreover, the evaluation of the typical fatigue cycle for the summation of the creep damages is not truly typical because of the power relation of creep rupture to stress. That is, the stress values for each fatigue cycle change during the fatigue test, especially at the first. Nevertheless, the data do show interesting

effects. The data are scattered over two decades of the ordinate about the value of unity. If the fatigue damage ratio is unity it implies that the damage done in the fatigue test in terms of time under stress is equal to the time under stress for the creep rupture test. Note the following trends in the data presented. The 800 F data are at the bottom of Fig. 13. The 1800 F isothermal are near the top of the graph. The 1300 to 1800 F are above the 1800 F data, but all of these tests showed a tendency to geometric instability. The general trend is for the relationship to shift upward as the temperature increases. If there is a cyclic temperature condition, then the data, in general, lie somewhere between the two isothermal lines. Too, the relationships seem to slope upward. Perhaps the slope is caused by the fact that these tests were in the very low-cycle fatigue range. At longer lives the relationship may level off to some steady value. The presentation of the data here are meant to be more suggestive than conclusive.

Perhaps a simpler relationship of time-under-stress is more meaningful. A plot of peak stress (at the maximum temperature) versus total time for the cycle period at that temperature are plotted in Fig. 14. For the isothermal data the total cycle period is multiplied by the cycles to failure. For the cyclic thermal case, only the half-cycle period was multiplied by cycles to failure. For the 1800 to 1300 F data, the peak stresses are compressive. For the isothermal case both time under tensile and compressive stresses were summed. The data show a fair correlation to uniaxial monotonic isothermal creep data for Hastelloy X bar stock [*8*]. The relationships shown in Fig. 14 are considerably easier to obtain than those plotted in Fig. 13. The agree-

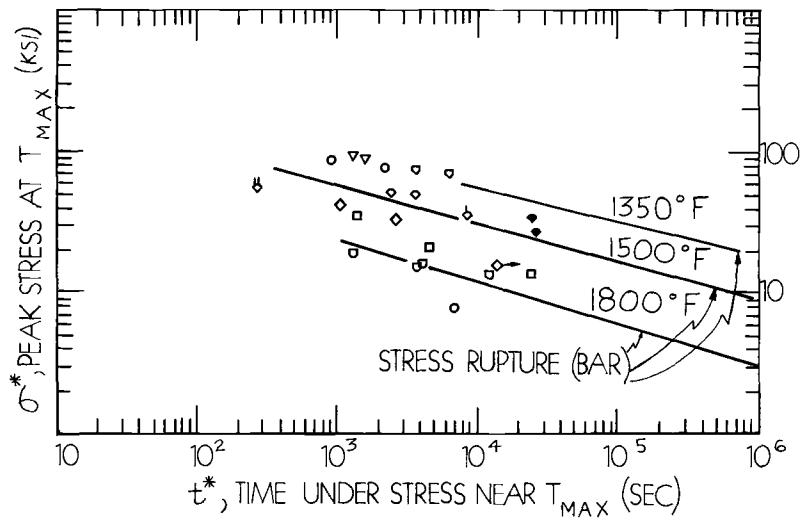

FIG. 14—*Peak stress versus time-under-stress relationship.*

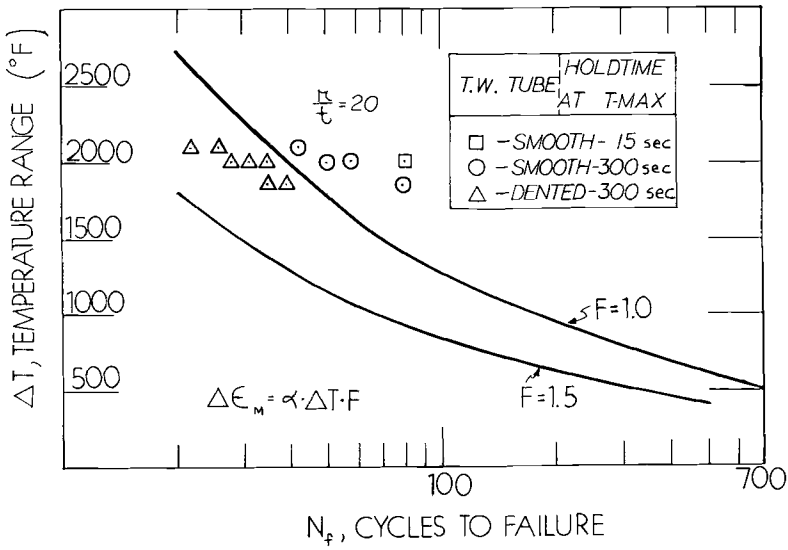

FIG. 15—*Thermal cycle fatigue data for Hastelloy X tube bundles. Curves derived from Fig. 9.*

ment between time under stress for the cyclic case may be fortuitous, but it does seem worthy of recognition and further study. Furthermore, the fact that the data from the two isothermal hold-time tests, and the two higher frequency tests, show good agreement to the 36 cycles per hour data indicate that the effect of longer hold times could be predicted from these data.

Finally, the total strain range curve plotted in Fig. 9 is used to derive a thermal cycle relationship for the nozzle tube bundle. From the controlled strain fatigue data the total strain ranges are recorded for a number of cyclic lives. These strain ranges were divided by the mean coefficient of thermal expansion for 70 to 1800 F. The resulting temperature range values are then plotted versus the corresponding cycles to failure. This technique assumes that the total strain range in the thermal cycle case is some constant times the thermal strain; or,

$$\Delta\epsilon_m = \alpha\Delta TF$$

The derived temperature range versus life curves for F values of 1.0 and 1.5 are shown in Fig. 15. The data shown on the figure are the results of thermal cycling tests of Hastelloy X tube bundles cycling from −200 F to a maximum temperature. Some of the tests had a 300-s hold time at the maximum temperature, and some had controlled defects placed in the tubes at the beginning of the test. The defects tend to initiate the formation of a local instability. The smooth tubes thermally cycled with the short hold at the peak temperature show a correlation to the derived curves but with a constraint factor of

less than unity. Hold time tends to increase the factor F, as does predenting. The derived thermal cycle curves with an appropriate F value can be used to fit the empirical thermal cycle data. Furthermore, those factors which affect the controlled strain fatigue results would be expected to affect the thermal cycle behavior of the tube bundles. Avery et al [*3*] showed that corrugated tubes allowed some strain relief (lowered F in our analysis) provided that the corrugations were deep enough. He showed that the tendency to buckling was analyzed primarily by the geometry of the tube (r/t) and the thermal strain of the cycle. Harman [*7*] showed that the strain range on the top or bottom of a ripple or both, once it had formed, is greater than that for a straight tube. The depth of the ripples was not great enough to provide strain relief. The effect of the hold time is not understood as being related to creep strains *per se*, but rather in compounding the tendency toward rippling and the attendant strain concentration in the vicinity of the crest or trough of the ripple. The hold time reduces the life of the thermally cycled tube bundles because it aids in the development of the local instabilities.

Conclusions

Although an insufficient number of tests were performed to establish any firm design parameters, the following conclusions based on data trends are valid over the range of variables investigated.

1. The effect of increasing the test temperature (for isothermal) or the maximum temperature (for cyclic thermal) is to lower the strain range fatigue relationship.
2. The only impairment of fatigue properties resulting from the stress-temperature arrangement of the cyclic thermal tests was the greater tendency to buckle for the negative type loop tests.
3. The cyclic-thermal fatigue test results show reasonable agreement to the isothermal temperature when the isothermal temperature is comparable to the maximum temperature of the thermal fatigue test.
4. Over the range of 36 to 420 cycles per hour no significant effect of frequency was detected. Results from tests having relatively large creep strains show reasonable agreement to the sawtooth extension cycle data.
5. Tensile data and the method of universal slopes are adequate to predict the fatigue behavior at elevated temperature. If the cyclic temperature behavior are desired minimum properties over the temperature range should be used.
6. Thermal fatigue behavior of Hastelloy X tube bundles can be related to the low-cycle high-temperature fatigue behavior of the material. Conditions leading to progressive instability in the thermal cycling of the tube bundles are understood as conditions that allow local strain concentrations to develop.

7. The ductility of this alloy, as a function of temperature, is not low enough at the minimum to cause gross impairment of the elevated temperature fatigue behavior.

Acknowledgment

This work was sponsored by the Oak Ridge National Laboratory[5] at the University of Alabama. Grateful appreciation is given to Waymon Humphries, Winton Kelly, Clio Rowell, and Robert Puckett for performing the experiments.

References

[1] Carden, A. E., Harman, D. G., and Franco-Ferreira, E. A., "Thermal-Fatigue Analysis of a Cryogenically Cooled Rocket Nozzle," Paper No. 102, American Astronautical Society, Southeastern Symposium, Huntsville, Ala., Dec. 1966.

[2] Reynolds, M. B., "Strain-Cycle Phenomena in Thin-wall Tubing," General Electric Atomic Products, APED San Jose, Calif., Report No. GEAP 4462, AEC Research and Development Report, 30 Jan. 1964.

[3] Avery, L. R., Carayanis, G. S., and Michky, G. L., "Thermal-Fatigue Tests of Restrained Combustor-Cooling Tubes," *Experimental Mechanics*, Vol. 7, No. 6, June 1967, pp. 256–264.

[4] Kuyper, D. J. and Burge, H. L., "Simplified Thermal Fatigue Analysis for Liquid Rocket Combustion Chambers," *Journal of Spacecraft and Rockets*, Vol. 4, No. 1, Jan. 1967, pp. 126–128.

[5] Heinz, T. A., "Thermal Tube Buckling Design Considerations for Nuclear Rocket Nozzles," AIAA Paper No. 66-583, *Second Joint Propulsion Specialist Conference*, Colorado Springs, American Institute of Aeronautics and Astronautics, 1966.

[6] Coffin, L. F., Jr., "Introduction to High Temperature Low Cycle Fatigue," *Experimental Mechanics*, Vol. 8, No. 5, May 1968, pp. 218–224.

[7] Harman, D. G., "Thermal Fatigue of Rocket Nozzle Cooling Tubes," ORNL-TM-2089, Oak Ridge National Laboratory, Feb. 1969.

[8] Union Carbide Corp., *Hastelloy Alloy X*, Bulletin of Stellite Division, Kokomo, Ind., Oct. 1964.

[9] Carden, A. E., Kyzer, R. D., and Vogel, W. H., "Low-Cycle Fatigue of Three Superalloys under Cyclic-Extension and Cyclic-Temperature Conditions," ASME Preprint 67 MET 19, American Society of Mechanical Engineers, April 1967.

[10] McClintock, F. A. and Argon, A. S., *Mechanical Behavior of Materials*, Addison Wesley, Reading, Mass., 1966.

[11] Morrow, J., "Cyclic Plastic Strain Energy and Fatigue of Metals," *Internal Friction, Damping, and Cyclic Plasticity*, *ASTM STP 378*, American Society for Testing and Materials, 1965, pp. 45–87.

[12] Manson, S. S., "A Simple Procedure for Estimating High-Temperature Low-Cycle Fatigue," *Experimental Mechanics*, Vol. 8, No. 8, Aug. 1968, pp. 349–355.

[13] Feltner, C. E. and Landgraf, R. W., "Selecting Materials to Resist Low Cycle Fatigue," to be presented at ASME Design Engineering Conference, American Society of Mechanical Engineers, 5–8 May 1969.

[14] Spera, D. A., *A Linear Creep Damage Theory for Thermal Fatigue of Materials*, Ph.D. dissertation, University of Wisconsin, Madison, 1968.

[15] Taira, S., "Lifetime of Structures Subjected to Varying Load and Temperature," *Creep in Structures*, Hoff, N. J., ed., Academic, New York, 1962, pp. 96–126.

[5] Operated by the Union Carbide Corporation for the U.S. Atomic Energy Commission.

R. A. DePaul[1] *and A. W. Pense*[2]

Some Microstructural and Alloying Effects Upon Low-Cycle Fatigue Life of Pressure Vessel Steels

REFERENCE: DePaul, R. A. and Pense, A. W., **"Some Microstructural and Alloying Effects Upon Low-Cycle Fatigue Life of Pressure Vessel Steels,"** *Fatigue at High Temperature, ASTM STP 459*, American Society for Testing and Materials, 1969, pp. 130–143.

ABSTRACT: Loading by constant deflection reversed bending was applied to Lehigh cantilever fatigue specimens of a plain carbon steel, A-516, and three low-alloy steels, A-302, A-387B, and HY-80. Fatigue life over the 5000 to 100,000 cycle range was investigated at a loading frequency of 200 cpm. The effect of microstructure was observed by comparing the fatigue resistance of specimens of equal tensile strength but different heat treatment histories. Normalized structures proved to be superior to the corresponding spray quenched and tempered conditions when using total strain range as the test parameter. Where similar structures were compared, the 100,000 cycle fatigue life was found to be related to tensile strength. The fatigue resistance of the low-alloy steels was influenced markedly by heat treatment while the plain carbon steel essentially was unaffected. Increased alloy content altered the slope of the fatigue curve such that the plain carbon steel tends to be superior in the 5000 cycle range, while the low-alloy steels excel above the 20,000 cycle region. This results in a grouping of the curves as to steel composition.

KEY WORDS: microstructure, fatigue (materials), alloy steels, steels, carbon steels, pressure vessels, heat treatment, normalizing, quenching and tempering, evaluation, tests

Fatigue, as one of several basic modes of failure, is of primary consideration in the case of pressure vessel service. Since pressure vessels exhibit an average service life of up to 100,000 cycles, the low-cycle (5000 to 100,000 cycles) fatigue life of pressure vessel type steels, as affected by microstructural changes and alloy content, is of interest to material suppliers and fabricators. The strains involved in the 5000 to 100,000 cycle range differ from those normally considered in fatigue work dealing with endurance limits in that

[1] Research metallurgist, Paul D. Merica Research Laboratory, The International Nickel Co., Inc., Sterling Forest, Suffern, N.Y. 10901. Personal member ASTM.

[2] Associate professor, Department of Metallurgical Engineering and Materials Science, Lehigh University, Bethlehem, Pa. 18015.

they are larger and generally involve some plastic deformation of the material. The behavior of steel as governed by microstructure under these higher strains can differ quite markedly from that when considering the more than 1,000,000 cycle life.

Among the few studies of the effects of microstructure on fatigue resistance that have been undertaken, Cazaud [*1*][3] reports that a quenched and tempered structure was found to be desirable for good fatigue resistance. While the quenched and tempered structure was the most promising from an endurance standpoint, a tempering temperature of 650 to 850 F provided a fatigue limit of maximum value but also resulted in minimum impact strength. Such a microstructure cannot be used in many applications and especially pressure vessel service which requires a more favorable balance of these two properties. This leads to higher tempering temperatures in an attempt to bring the impact and fatigue properties into a better balance.

Dolan and Yen [*2*], and Sinclair and Dolan [*3*] found that quenched and tempered martensite had higher long-time fatigue strength than a pearlite-ferrite structure with the same hardness. Kooistra [*4*] reports that composition, microstructure, and previous mechanical work influence fatigue resistance in the same manner as they affect tensile strength when relatively small strains are considered. Little work has been reported which compares low-cycle fatigue resistance with the alloy content of the steel. Stout and Pense [*5*] separate steels into three groups by composition and estimate low-cycle fatigue behavior via a modified Coffin equation.

The purpose of this study was to establish the influence of microstructures produced by commercially feasible heat treatments on the room-temperature fatigue resistance of pressure vessel steels. The test specimen was chosen to simulate pressure vessel service conditions in both section size and type of loading.

Experimental Procedure

Steels and Heat Treatment

Table 1 is a listing of the compositions of the steels. Three low-alloy steels were included with a plain carbon grade in both the fine (FG) and coarse grained (CG) conditions. Various cooling rates were applied to the plain carbon steel ranging from furnace cooling to spray quenching. The austenitization temperatures were selected from commercial practice. The cooling rates involved in the range of treatments are tabulated in Table 2. The low-alloy steels were all tested in both the normalized and the quenched and tempered conditions; all treatments are listed in Table 3. The tempering temperature for each steel was selected to produce the same tensile strength

[3] The italic numbers in brackets refer to the list of references appended to this paper.

in the quenched material as that obtained for the normalized condition. This necessitated selecting some temperatures higher than normally would be considered in industry. The steels were obtained as ¾-in. plate. Following heat treatment, specimens were cut from the plate with the longitudinal axis in the same orientation as the indicated rolling direction.

TABLE 1—*Compositions of the steels.*

Steel	C	Mn	P	S	Si	Ni	Cr	Mo
A-516, FG	0.29	0.73	0.013	0.024	0.21	NA[a]	NA	NA
A-516, CG	0.28	0.82	0.020	0.036	0.24	0.16	0.19	0.05
A-302	0.19	1.32	0.022	0.024	0.25	NA	NA	0.43
A-387B	0.12	0.56	0.010	0.037	0.20	NA	1.09	0.46
(HY-80) A-543	0.18	0.24	0.010	0.015	0.21	2.26	1.20	0.25

[a] NA = not analyzed.

TABLE 2—*Cooling rates.*
Midsection of ¾-in. plate over 1650 to 860 F range

Treatment	Cooling Rate, deg F/min
Spray quench[a]	1200
Plate cool[b]	121
Air cool	61
Furnace cool (annealing treatment)	1.9

[a] Plate quenched within water spray; average spray rate of 0.3 in.^{3} of water per square inch of surface per side per second.
[b] Plate cooled between two massive slabs originally at room temperature.

Testing Apparatus and Specimen

The fatigue testing was performed using the Lehigh cantilever fatigue specimen and a constant deflection type of loading. The specimen is shown in Fig. 1. The specimen geometry is such that a 2:1 biaxial stress distribution is achieved at the center of the reduced section. A complete description of the test and test apparatus has been published elsewhere [*6*, *7*, *8*]. In accordance with standard procedure, a rate of 200 cpm was used at ambient temperatures.

TABLE 3—*Mechanical properties.*

Steel	Condition	Yield Strength, ksi	Tensile Strength, ksi	Yield Strength/ Tensile Strength, %	Reduction of Area, %	Elongation, %	BHN	Strain Hardness Exponent	Total Strain, % 5000 Cycles	Total Strain, % 100,000 Cycles
A-516, FG	norm	50.6	77.8	65.2	60.4	28.0	149	0.218	1.22	0.38
Austenite-1650 F	Q&T 1 h, 1300 F	51.6	77.6	67.0	71.6	32.5	146	0.191	1.21	0.33
	SQ	68.4	101.0	67.8	69.3	24.5	180	0.142	1.17	0.42
	A (FC)	35.4	70.6	50.2	72.7	31.5	132	0.235	1.34	0.36
	PC	53.1	80.0	66.4	65.0	29.0	158	0.198	1.25	0.37
A-516, CG	norm	49.4	83.6	59.0	56.7	27.0	156	0.174	1.20	0.43
Austenite-1650 F	Q&T 15 h, 1300 F	57.6	83.2	69.2	71.8	28.0	156	0.192	1.08	0.39
A-302	norm	54.3	87.8	61.8	60.6	26.0	191	0.168	1.02	0.48
Austenite-1650 F	Q&T 1 h, 1300 F	72.5	87.2	83.2	69.7	27.0	194	1.174	0.90	0.42
A-387B	norm	39.2	77.2	51.4	61.6	26.5	151	0.166	1.09	0.45
Austenite-1675 F	Q&T 2 h, 1375 F	62.5	80.7	77.5	74.3	28.0	163	0.147	1.00	0.42
HY-80 (A-543)	norm	80.2	125.1	64.2	60.0	21.5	229	0.129	1.10	0.57
Austenite-1600 F	Q&T 1½ h, 1150 F	112.5	125.0	90.0	74.6	21.5	234	0.087	1.01	0.50
	Q&T 1½ h, 850 F	156.0	166.0	94.0	62.2	16.0	332	0.091	1.18	0.63
	Q&T 5½ h, 1200 F	92.3	106.0	87.0	76.6	24.0	207	0.110	0.99	0.44

NOTE—Norm = normalized.
Q&T = Spray quenched and tempered.
SQ = as spray quenched.
A (FC) = annealed, furnace cooled.
PC = plate cooled.

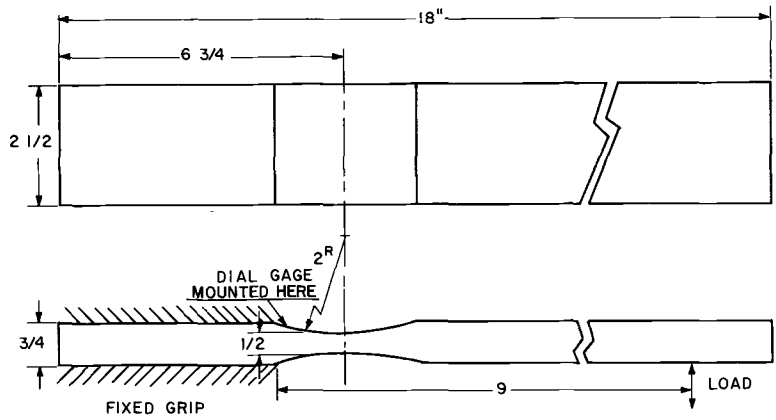

FIG. 1—*Lehigh cantilever fatigue specimen.*

Strain Measurements

Strain readings were obtained on each specimen with a Tuckerman optical strain gage having a nominal gage length of ¼in. The strain gage was applied to the specimen such that it straddled the midpoint of the reduced section and registered total strain over several complete cycles of reversed bending. Strain measurements were recorded after the tenth cycle to eliminate possible errors resulting from strain hardening effects [*6*].

Testing Criteria

Various total strain levels were applied to obtain fatigue failure over the range of 5000 to 100,000 cycles. Nine to twelve specimens were used to establish each fatigue curve. All specimens were run to final failure which was defined as the point at which the flexed section could no longer transmit a useful load to the fixed end. This point was determined by zero deflection, as registered by a dial gage mounted between the fracture zone and the stationary clamp (Fig. 1).

The tensile properties were evaluated using the standard 0.252-in.-diameter round specimen.

Results and Discussion

The tensile properties for the various heat treated conditions are listed in Table 3. In all cases, the objective of producing equivalent tensile strengths in both the normalized and the quenched and tempered conditions of each steel was met. This permits the study of the effect of differing microstructures at like strength levels. The range of cooling rates applied to the A-516 steel permits a comparison of the influence of tensile strength on the low-cycle

fatigue life of the plain carbon steel. The various tempering treatments applied to the HY-80 steel accomplishes the same end in an alloy steel. A comparison of the A-516, A-302, A-387B, and HY-80 steels can be made to ascertain the influence of alloy content on low-cycle fatigue resistance. A study of the influence of deoxidation practice cannot be made because of the higher than normal residual chromium in the coarse grained A-516 steel, the presence of which introduces an additional variable. In addition, the

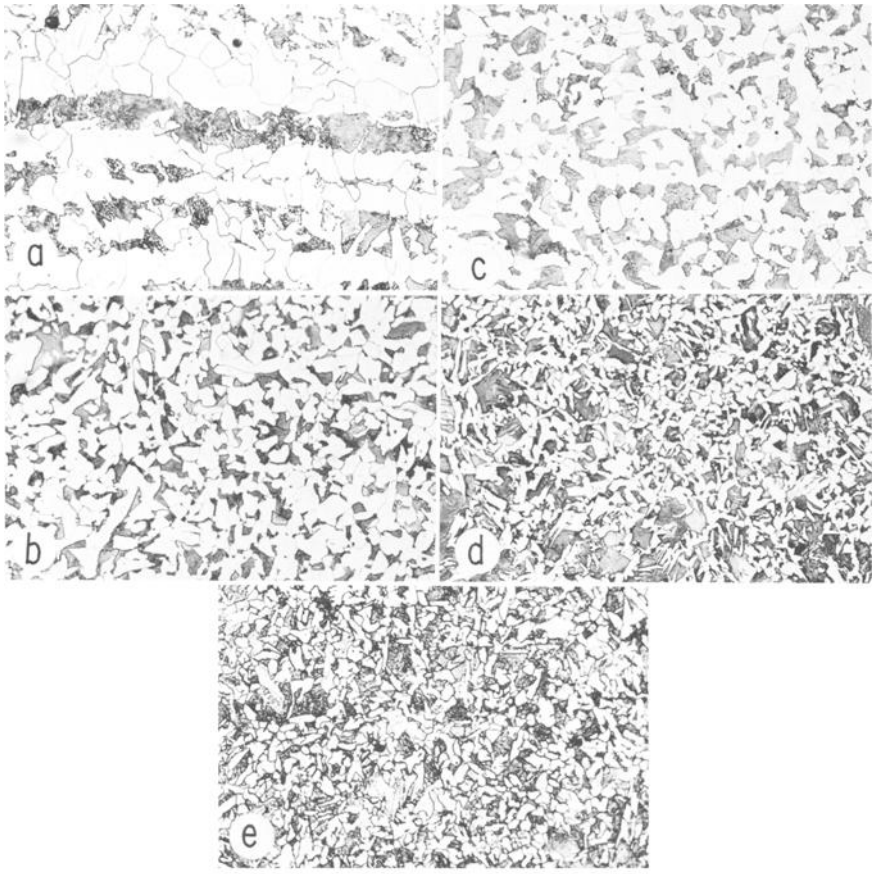

(*a*) Annealed. Cooling rate 1.9 F/min.
(*b*) Plate cooled. Cooling rate 121 F/min.
(*c*) Normalized. Cooling rate 61 F/min.
(*d*) Spray quenched. Cooling rate 1200 F/min.
(*e*) Spray quenched and tempered.

FIG. 2—*Microstructures of A-516, fine grained steel in various conditions of heat treatment. Nital etch.* (×*250*).

heat treatment response of this high residual level steel was such that an extreme tempering treatment of 15 h at 1300 F was necessary to achieve a tensile strength comparable to the corresponding normalized condition.

The microstructures obtained for the various conditions of heat treatment are shown in Figs. 2, 3, and 4. The normalizing treatment produced a ferrite-pearlite structure in all the steels except for the markedly finer ferrite-bainite structure of the HY-80 steel. The quenched and tempered structures ranged

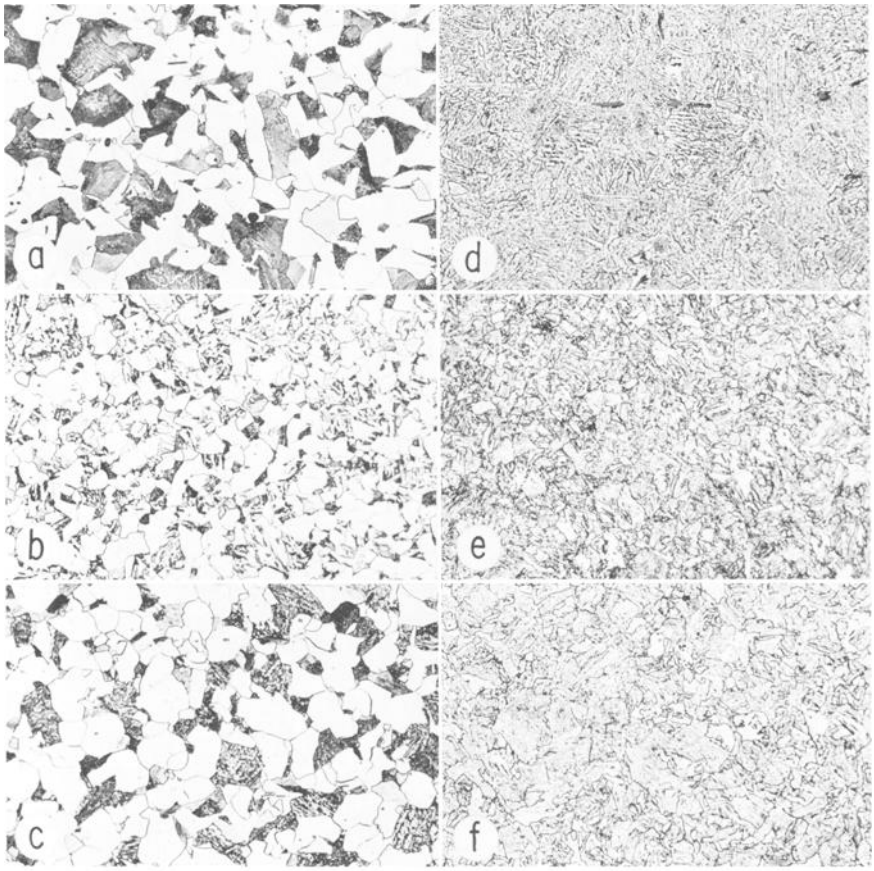

(*a*) Normalized. Coarse grained A-516.
(*b*) Normalized. A-302.
(*c*) Normalized. A-387B.
(*d*) Spray quenched and tempered. Coarse grained A-516.
(*e*) Spray quenched and tempered. A-302.
(*f*) Spray quenched and tempered. A-387B.

FIG. 3—*Microstructures of A-516 coarse grained, A-302, and A-387B steels. Nital etch.* (×250).

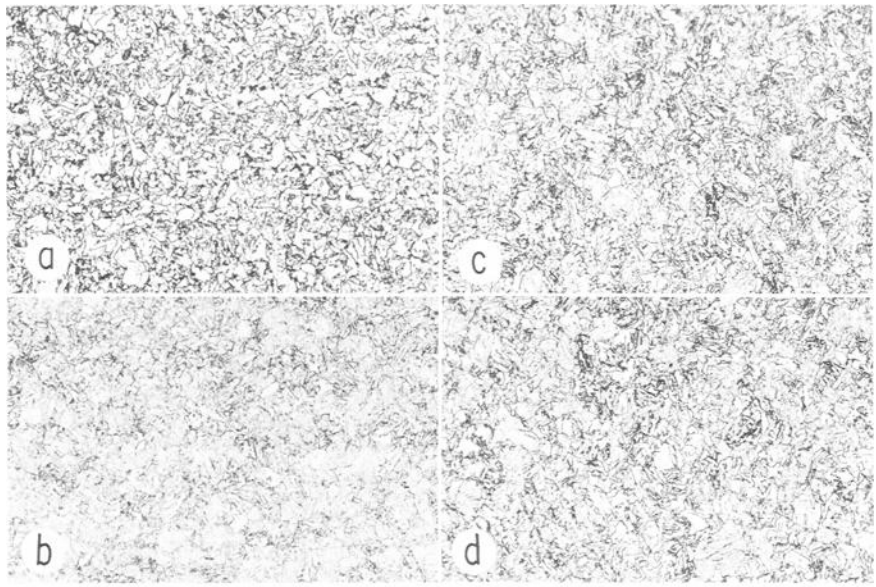

(*a*) Normalized.
(*b*) Spray quenched and tempered 1½ h at 850 F.
(*c*) Spray quenched and tempered 1½ h at 1150 F.
(*d*) Spray quenched and tempered 5½ h at 1200 F.

FIG. 4—*Microstructures of HY-80 steel in various conditions of heat treatment. Nital etch.* (×*250*).

from acicular ferrite-pearlite in the fine grained A-516 steel to almost 100 percent tempered martensite in the HY-80 steel.

Figures 5 through 9 compare directly the low-cycle fatigue behavior of the various steels in the normalized and the quenched and tempered conditions at equivalent tensile strengths. The correlation coefficients (r) for the least squares fits are listed for each curve and are quite high. For this reason, the log-log straight line is considered to represent the data satisfactorily. In actuality, one could expect some deviation from linearity in the region where the plastic component of the total strain becomes negligible when compared with the elastic component. Generally, this would occur at the high-cycle end of the lifetime range, and some "tailing-off" would be noted in the curves. However, the data in Figs. 5 through 9 do not, for the most part, justify drawing the curves differently from the way they are presented. Note that in every case, when considering total strain range as the test parameter, the normalized structure is superior to the quenched and tempered structure throughout the 5000 to 100,000 cycle range. The explanation for this lies in the fatigue crack propagation morphology. For every steel, the quenched

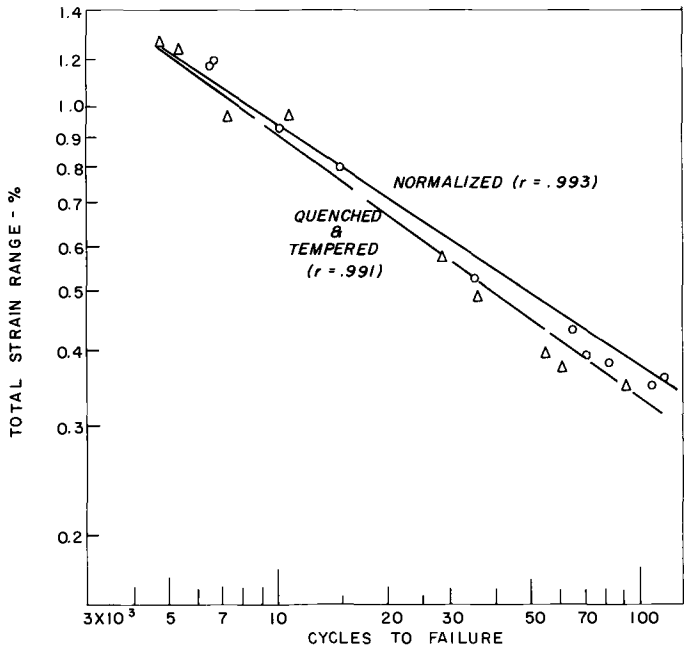

FIG. 5—*Low-cycle fatigue behavior of normalized and quenched and tempered A-516 FG steel.*

and tempered structure is more acicular than the normalized structure. A crack propagation study revealed a somewhat different crack path in the two types of structure. The more massive ferrite-pearlite mixtures of the normalized structures presented a potential crack with a widely spaced, discontinuous pathway. The cracks tend to favor pearlite areas and, therefore, had to traverse the larger, more ductile ferrite grains in their propagation. The acicular structures, however, permitted the cracks to follow the more closely spaced carbide particles which are somewhat aligned. This carbide alignment reduced the size of the ferrite areas confronting the cracks, thus forming a semicontinuous crack path of oriented fine carbides.

The total strain values taken from the fatigue curves for 5000 and 100,000 cycle fatigue life are listed in Table 3. Note that in general the 5000 cycle strains for the A-516 steel are higher than those for the alloy steels, while the 100,000 cycle strain values show the reverse. In other words, the lower strength, more ductile plain carbon steel is superior to the higher strength alloy steels under higher strain conditions, while beyond 15,000 to 20,000 cycles the opposite is true. This confirms a similar finding by Wood and Johnson [*9*] on vastly different steels.

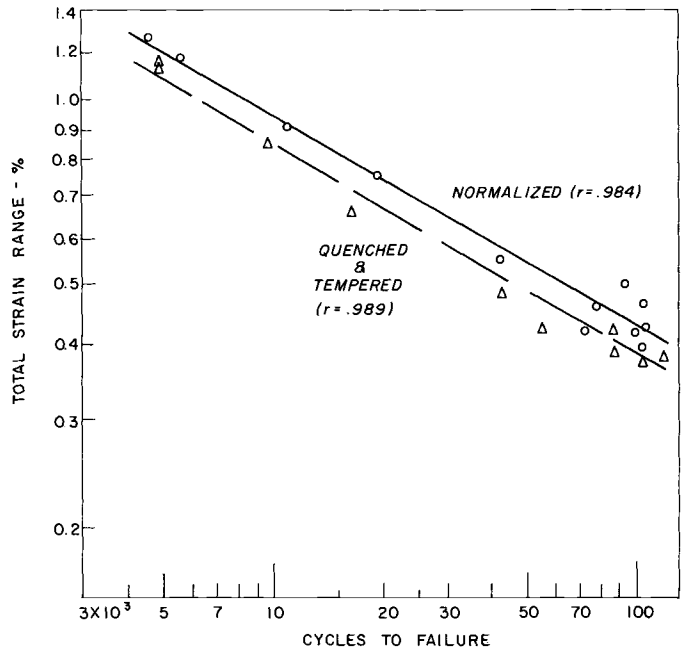

FIG. 6—*Low-cycle fatigue behavior of normalized and quenched and tempered A-516 CG steel having high residual alloy content.*

A more specific comparison can be made between the normalized and the quenched and tempered conditions of the A-516 FG and the A-387B steels where both tensile strength and type of structure are constant. Here too, the plain carbon steel is superior at 5000 cycle strain levels but inferior at the 100,000 cycle level. A similar relation exists even within the same steel, as shown in Fig. 10. The dashed lines define the band into which all the fine grained A-516 fatigue curves fall. The narrow band is a result of the low hardenability of the plain carbon steel which results in the minor response to varying the cooling rate after austenitization. However, within the narrow band the curves for the higher strength spray quenched and the more ductile annealed conditions cross as in the previous discussion.

Figure 11 shows the influence of tensile strength on the low-cycle fatigue behavior of HY-80 steel. Note that a change in strength level for similar microstructures produces a marked effect upon fatigue resistance throughout the 5000 to 100,000 cycle life. Increasing the tensile strength from 106 to 125 to 166 ksi raised the allowable 100,000 cycle total strain level from 0.44 to 0.50 to 0.63 percent, respectively.

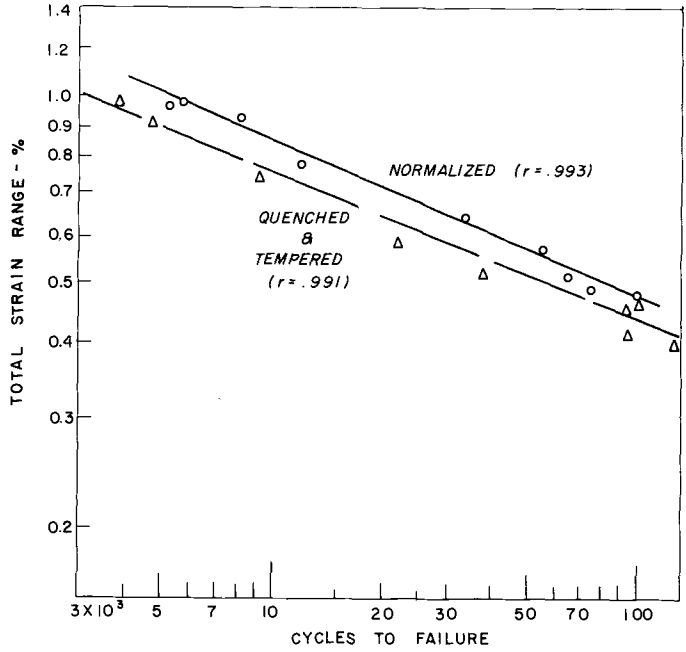

FIG. 7—*Low-cycle fatigue behavior of normalized and quenched and tempered A-302 steel.*

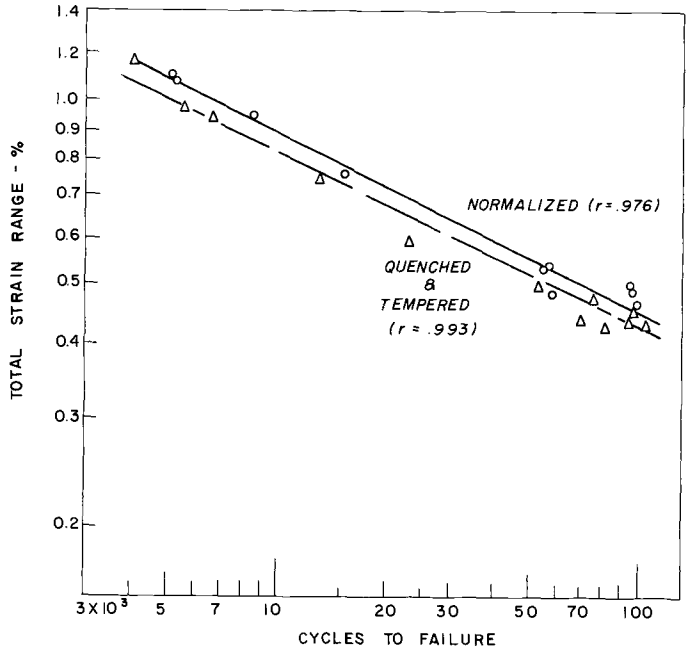

FIG. 8—*Low-cycle fatigue behavior of normalized and quenched and tempered A-387B steel.*

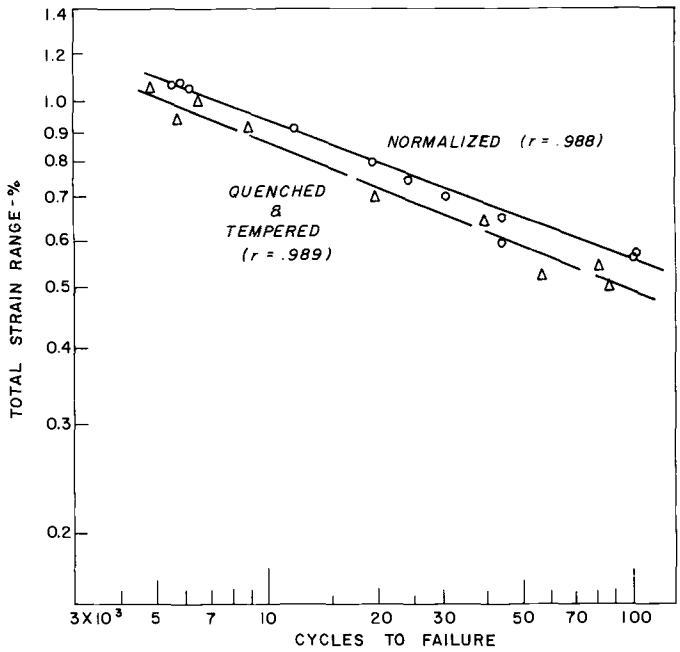

FIG. 9—*Low-cycle fatigue behavior of normalized and quenched and tempered HY-80 steel.*

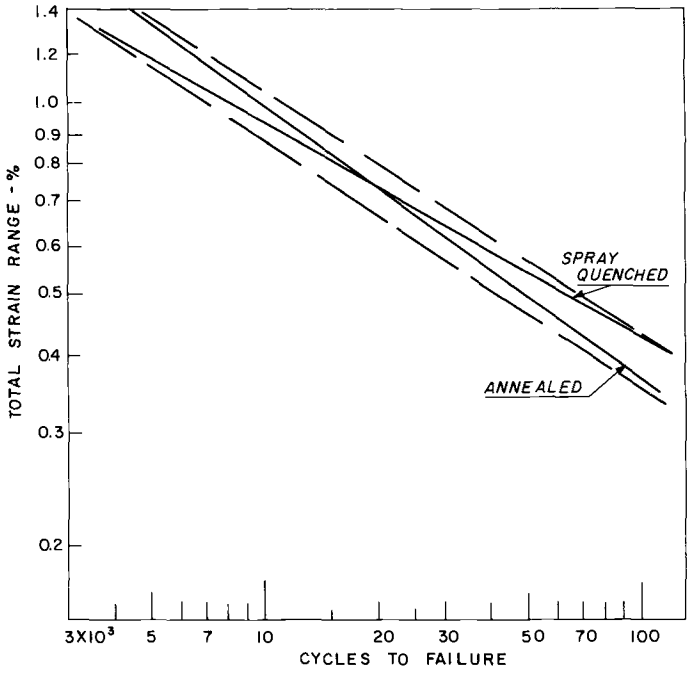

FIG. 10—*Influence of various cooling rates of low-cycle fatigue behavior of A-516 FG steel.*

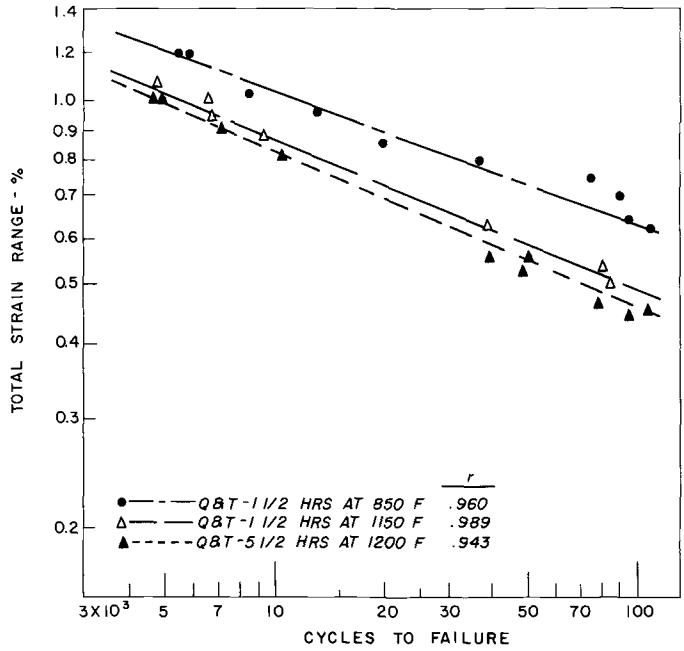

FIG. 11—*Influence of tensile strength on low-cycle fatigue behavior of quenched and tempered HY-80 steel.*

Conclusions

The following conclusions can be made concerning the low-cycle fatigue behavior of pressure vessel steels:

1. The ferrite-pearlite structure produced by normalizing a series of plain carbon and low-alloy steels possesses superior low-cycle fatigue resistance to that resulting from quenching and tempering to the same tensile strength when using total strain range as the test parameter.

2. High-strength steels, while proving to be superior at the lower strain levels, do not necessarily provide the optimum fatigue resistance over the entire 5000 to 100,000 cycle range.

3. Increasing alloy content reduces the slope of the total strain versus cycle fatigue curve over the 5000 to 100,000 cycle region such that plain carbon steels tend to be superior in the 5000 cycle range, while the low-alloy steels excel for fatigue lives greater than 20,000 cycles.

4. For a constant type of microstructure, namely, the quenched and tempered HY-80 structure, increasing tensile strength by varying the tempering treatment shifts the low-cycle fatigue resistance to higher allowable strain levels for any given life.

It should be pointed out that the above mentioned influences affect fatigue life at a given total strain range by, at most, a factor of three. The significance of these effects would have to be judged on the basis of the unique details and economics of the application involved.

Acknowledgment

The financial aid granted by the Materials Division of the Pressure Vessel Research Committee of the Welding Research Council made this work possible at Lehigh University.

References

[1] Cazaud, R., *Fatigue of Metals*, translation by Fenner, A. J., Chapman & Hall, London, 1953.

[2] Dolan, T. J. and Yen, C. S., "Some Aspects of the Effect of Metallurgical Structure on Fatigue Strength and Notch Sensitivity of Steels," *Proceedings*, American Society for Testing and Materials, Vol. 48, 1948, pp. 664–695.

[3] Sinclair, G. M. and Dolan, T. J., "Some Effects of Austenitic Grain Size and Metallurgical Structure on the Mechanical Properties of Steel," *Proceedings*, American Society for Testing and Materials, Vol. 50, 1950, pp. 587–618.

[4] Kooistra, L. F., "Effect of Plastic Fatigue on Pressure Vessel Materials and Design," *Welding Journal*, Vol. 36, No. 3, March 1957, p. 120.

[5] Stout, R. D. and Pense, A. W., "Effect of Composition and Microstructure on the Low-Cycle Fatigue Strength of Structural Steels," *Journal of Basic Engineering*, Vol. 87, No. 2, 1965, pp. 269–274.

[6] Gross, J. H., Gucer, D. E., and Stout, R. D., "The Plastic Fatigue Strength of Pressure Vessel Steels," *Welding Journal*, Vol. 33, No. 1, Jan. 1954.

[7] Tor, S. S., Ruzek, J. M., and Stout, R. D., "Repeated Load Tests on Welded and Prestrained Steels," *Welding Journal*, Vol. 31, No. 5, 1952, p. 238s.

[8] Gross, J. H., Tsang, S., and Stout, R. D., "Factors Affecting Resistance of Pressure Vessel Steels to Repeated Overloading," *Welding Journal*, Vol. 32, No. 1, 1953, p. 23s.

[9] Wood, D. S. and Johnson, E. R., "Effect of Irradiation on the High-Strain Fatigue Behavior of a Low-Carbon and a Low-Alloy Steel," *Journal of the Iron and Steel Institute*, Vol. 205, Part 3, March 1967, pp. 305–308.

L. J. Bartlo[1]

Effect of Microstructure on the Fatigue Properties of Ti-6Al-4V Bar

REFERENCE: Bartlo, L. J., **"Effect of Microstructure on the Fatigue Properties of Ti-6Al-4V Bar,"** *Fatigue at High Temperature, ASTM STP 459*, American Society for Testing and Materials, 1969, pp. 144–154.

ABSTRACT: Microstructure can have a significant effect on the mechanical properties of titanium alloys. The extent of this effect on the fatigue properties of the Ti-6Al-4V alloy in small diameter bar (0.625 in., 15.875 mm) was studied. Microstructural variations were produced by heat treating from 1550 to 1950 F at 100 F intervals. Three different cooling rates (furnace cooling, air cooling, and water quenching) were employed for each temperature. The room-temperature tensile, smooth, and notch-fatigue properties were evaluated for each thermal condition.

Thermal treatments that resulted in grain coarsening were found to lower the fatigue strength of the alloy. Beta quenching resulted in good tensile and fatigue strengths but low tensile ductility. Optimum tensile and fatigue properties occur in material consisting of fine grained alpha-beta structures or in material containing mixtures of fine primary alpha and martinisitic alpha.

KEY WORDS: fatigue (materials), titanium alloys, heat treatment, microstructure, evaluation, tests

The Ti-6Al-4V alloy has been referred to, on occasion, as the "workhorse" of the titanium alloys. The alloy exhibits excellent room- and elevated-temperature tensile, creep, notch-stress-rupture, and impact properties. The alloy also is known to have attractive fatigue properties; however, little information is available concerning the effect of various microstructural conditions on fatigue properties of the alloy.

The purpose of this work was to establish the effect of various microstructure types on the smooth and notched fatigue and room-temperature tensile properties of the alloy. Microstructural variations were produced by heat treatments that were aimed at producing fine grained alpha-beta, coarse grained alpha-beta, mixtures of primary alpha and transformed beta, and entirely transformed beta structures.

[1] Manager, Product Development Department, Reactive Metals, Inc., Niles, Ohio 44446.

Procedure

The material used for this study was 3.5-in. (88.9-mm) diameter bar stock. The bar was forged to 1.25 in. (31.75 mm) diameter at 1750 F (1228 K), conditioned, and hot rolled to 0.625 in. (15.875 mm) diameter at 1650 F (1172 K) to produce material for the entire program. A portion of the 3.5-in-diameter bar was retained for testing in the full section size.

Chemical analyses were obtained from a random selection of broken fatigue specimens. Both substitutional and interstitial elements were within the desired nominal composition. Results of the analyses are as follows:

C, %	N, %	Fe, %	Al, %	V, %	O, %	H, %
0.03	0.006	0.16	6.5	4.1	0.130	0.0039
0.02	0.005	0.14	6.2	4.2	0.120	0.0055

Specimens, 0.25 in. (6.35 mm) thick, were cut from the as-rolled bar for beta transus determination. The specimens were solution heat treated at various temperatures, quenched in water, and examined metallographically. The beta transus was based on the lowest temperature at which no primary alpha was visible in the microstructure. The beta transus of the material used in this investigation was established at 1840 F $\pm$ 10 F (1277 K $\pm$ 5.5 K).

Thermal treatments aimed at producing structural variations were based primarily on the beta transus temperature. Heat treatments were performed on specimen blanks from 1550 F (1116 K) to 1950 F (1338 K) at 100 F (311 K) intervals. Three different cooling rates (furnace cooling approximately 175 F (325 K) per hour, air cooling, and water quenching) were employed for each temperature.

Tension Testing

Standard 0.252-in. (6.4-mm) diameter tension specimens were prepared from each of the thermal conditions investigated. Tension tests were made on a Riehle testing machine at a uniform strain rate of 0.005 in./in./min up to the 0.2 percent offset yield strength. Crosshead speed then was increased to 0.2 in./min until failure occurred.

Fatigue Testing

Smooth and notched (K_t = 3.5) fatigue specimens were machined in accordance with the drawings shown in Fig. 1. The smooth specimens were polished carefully with 600 grit silicon carbide paper to avoid excess surface cold work [*1*].[2] The notched specimens were prepared by machining a 60 deg

[2] The italic numbers in brackets refer to the list of references appended to this paper.

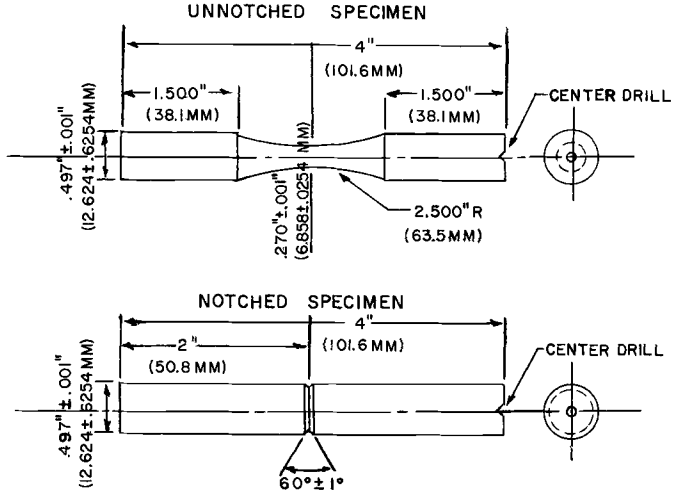

NOTCH DIMENSIONS
ANGLE – 60°±1°
DEPTH – .114±.001" (2.8956±.0254MM)
RADIUS – .010"±.001" (.254±.0254MM)

FIG. 1—*Unnotched and notched bar fatigue specimens.*

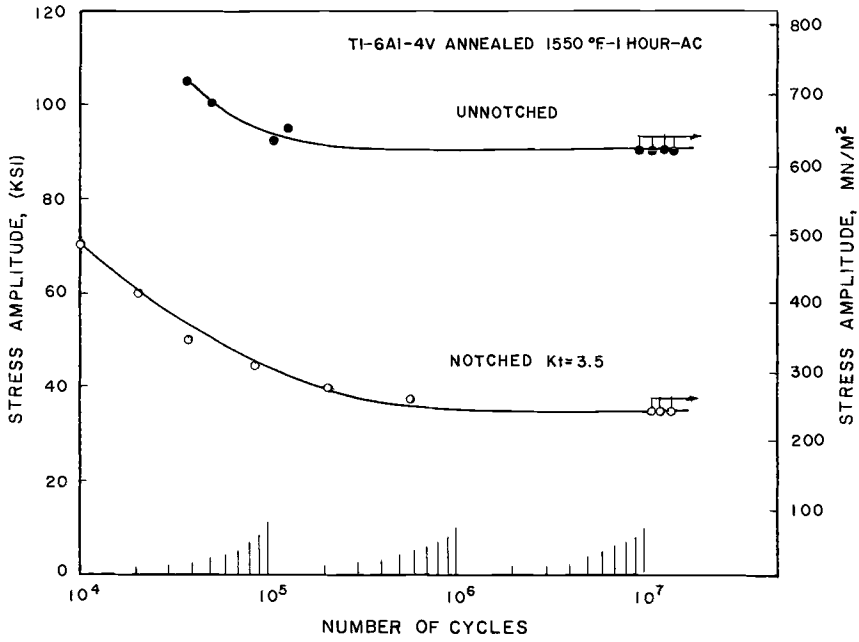

FIG. 2—*Typical* S-N *curves.*

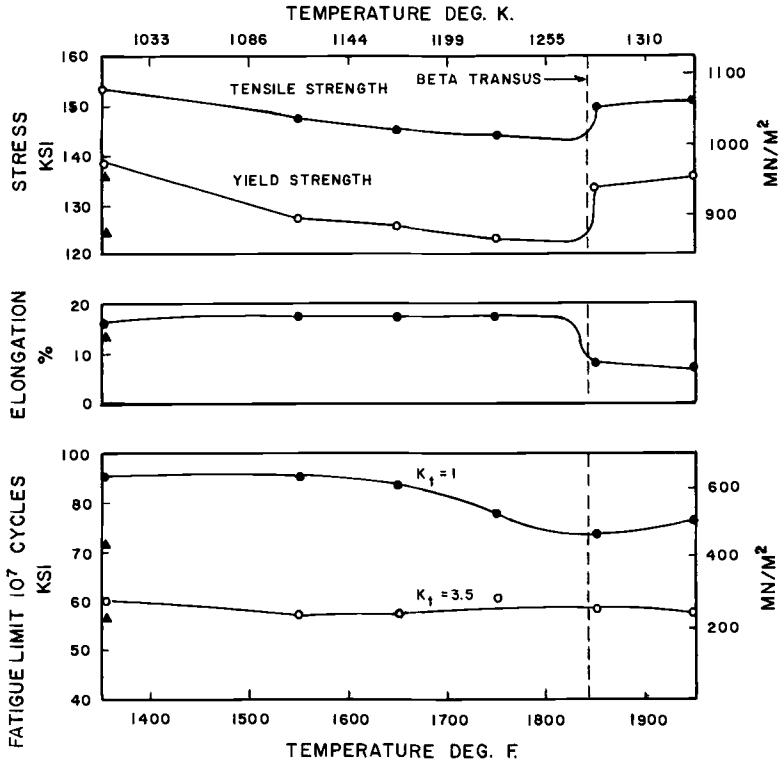

FIG. 3—*Effect of annealing temperature followed by air cooling on the properties of Ti-6Al-4V bar.*

V-notch with root radius of 0.01 in. (0.254 mm). The notched specimens were tested in the machined condition. Each specimen was tested on 200-in·lb capacity Krouse rotating beam fatigue machines at 8000 rpm.

Eight to twelve specimens were used to establish the conventional *S-N* curve between 10^4 and 10^7 cycles. The fatigue limit for 10^7 cycles was determined by the highest stress amplitude at which three specimens ran 10^7 cycles without failure. These values were determined to an accuracy of ± 1.0 ksi (6.9 MN/m^2). A typical *S-N* curve is shown in Fig. 2. Each of the *S-N* curves exhibited a fatigue limit.

Discussion

Room-temperature tensile properties are shown in Figs. 3 through 5 along with the corresponding fatigue properties for each of the thermal conditions investigated. Figure 3 illustrates the effect of annealing temperature followed by air cooling on these properties. Increasing the annealing temperature to just below the beta transus results in a slight decrease in both ultimate and

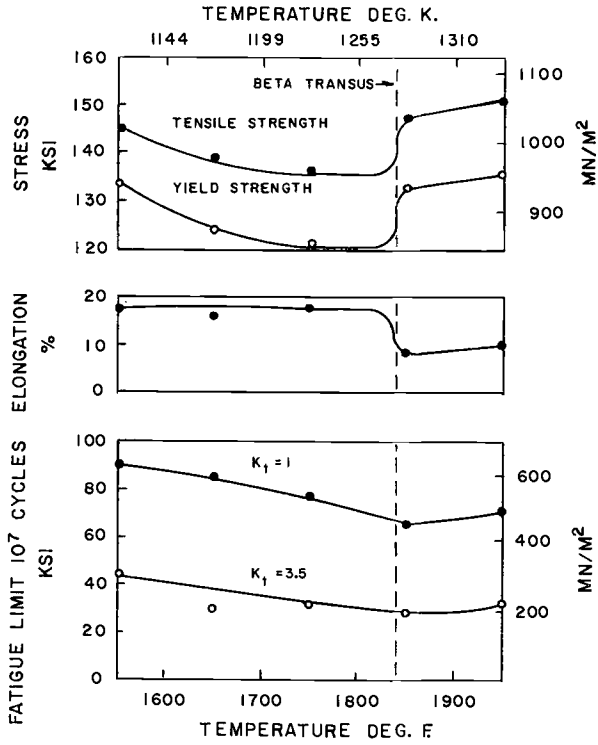

FIG. 4—*Effect of annealing temperature followed by furnace cooling on the properties of Ti-6Al-4V bar.*

yield strengths. A slight increase occurs when the beta transus is exceeded. This is possibly due to the formation of some martinsitic alpha (alpha prime), although this has not been verified. No noticeable change in ductility occurs until the beta transus temperature is exceeded. At that point, elongation decreased.

The notched and unnotched fatigue limits are illustrated in the lower portion of Fig. 3. The unnotched fatigue limit shows a slight decrease at the higher annealing temperatures, while the notched properties are not altered.

Figure 4 shows the effect of annealing temperature on tensile and fatigue properties when furnace cooling was used following annealing. Ultimate and yield strengths decreased at the higher temperatures and showed a slight increase in strength above the beta transus. Elongation remained unchanged but decreased when the beta transus was exceeded. Both unnotched and notched endurance limits decreased at the higher temperatures.

Figure 5 shows the effect of annealing followed by water quenching on the tensile and fatigue properties of the Ti-6Al-4V alloy. Ultimate and yield

strengths increased at the higher temperatures, while elongation decreased. The lower portion of Fig. 5 shows that the unnotched fatigue limit also increased at the higher temperatures but the notched properties essentially were unchanged.

The properties shown in Fig. 6 illustrate the effect of aging (1000 F for 4 h) on the tensile and fatigue properties of the alloy. Ultimate and yield strengths increased at the higher temperatures. Elongation was unchanged up to the beta transus and then decreased. The unnotched fatigue limit was high for all temperatures and showed a slight increase at the higher temperatures. The notched fatigue properties essentially were unchanged.

Figure 7 shows several photomicrographs which illustrate microstructural conditions which have the greatest influence on fatigue properties. Figure 7*a* shows a fine-grained alpha-beta structure which is indicative of high fatigue strength and good tensile ductility. Figure 7*b*, which was annealed at the

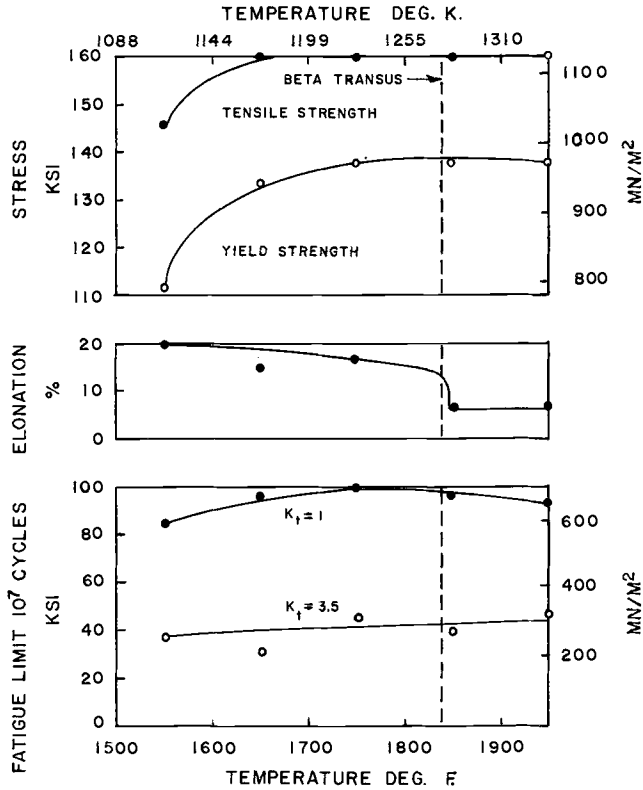

FIG. 5—*Effect of annealing temperature followed by water quenching on the properties of Ti-6Al-4V bar.*

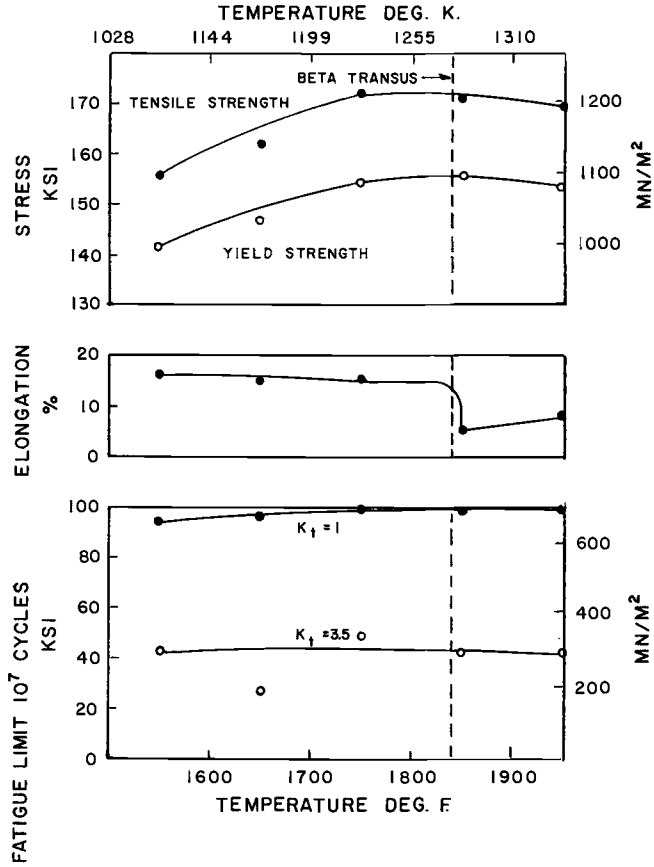

FIG. 6—*Effect of annealing temperature followed by water quenching and aging (1000 F, 4 h) on the properties of Ti-6Al-4V bar.*

same temperature as 7*a*, has a considerably coarser structure and exhibits low fatigue strength and medium ductility. The coarse structure was produced during fabrication of the 3.5-in.-diameter bar. Figure 7*c* consists of a mixture of fine primary alpha in a martinsitic alpha matrix (alpha prime). Such structures are typical of rapidly cooling the alloy from the alpha-beta phase field and results in high fatigue strength and good tensile ductility. Figure 7*d*, which consists entirely of martinsitic alpha (produced by rapid cooling from the beta phase field), has high fatigue strength and low tensile ductility. Figure 7*e* was produced by cooling slowly from the beta phase field. The structure consists of coarse plate-like alpha grains and resulted in low fatigue strength and low ductility. Figure 7*f* was produced by cooling slowly from the alpha-beta phase field. This structure exhibited low fatigue strength and good ductility.

a 250X
1350F - 2hrs-AC - 0.625-inch dia.
Fine grained alpha and beta
High fatigue strength

b 250X
1350F-2hrs-AC - 3.5-inch dia.
Plate-like alpha
Low fatigue strength

c 250X
1750F-1hr-WQ
Primary alpha and alpha prime
High fatigue strength

d 250X
1850F-1hr-WQ
Alpha prime (martinsitic alpha)
High fatigue strength

e 250X
1850F-1hr-FC
Plate-like alpha
Low fatigue strength

f 250X
1750F-1hr-FC
Equiaxed alpha
Low fatigue strength

FIG. 7—*Photomicrographs of various thermal treatments.*

Fatigue Strength-Tensile Strength Relationship

Figure 8 shows the ultimate tensile strength versus fatigue strength for the various thermal conditions investigated. The upper band shows the spread in endurance ratio (fatigue limit/ultimate tensile strength) for the unnotched test conditions. Endurance ratios varied from 0.42 to 0.62 for the unnotched condition. Several of the data points which make up the low side of the band represent slow cooling rates for the beta phase field. It should be pointed out that the data point representing the 1350 F treatment on the low side of the band was from material containing coarse plate-like alpha which was produced during fabrication. The structure (shown in Figure 7*b*) is similar to that obtained by cooling the alloy slowly from the beta field. This is further evidence that the coarse plate-like alpha structures lower the endurance ratio of the Ti-6Al-4V alloy [*2*]. It is therefore likely that heavy sections of Ti-6Al-4V, which contain coarse plate-like or even coarse equiaxed alpha, can be expected to have endurance ratios of 0.4 to 0.45. Fine grained alpha-beta

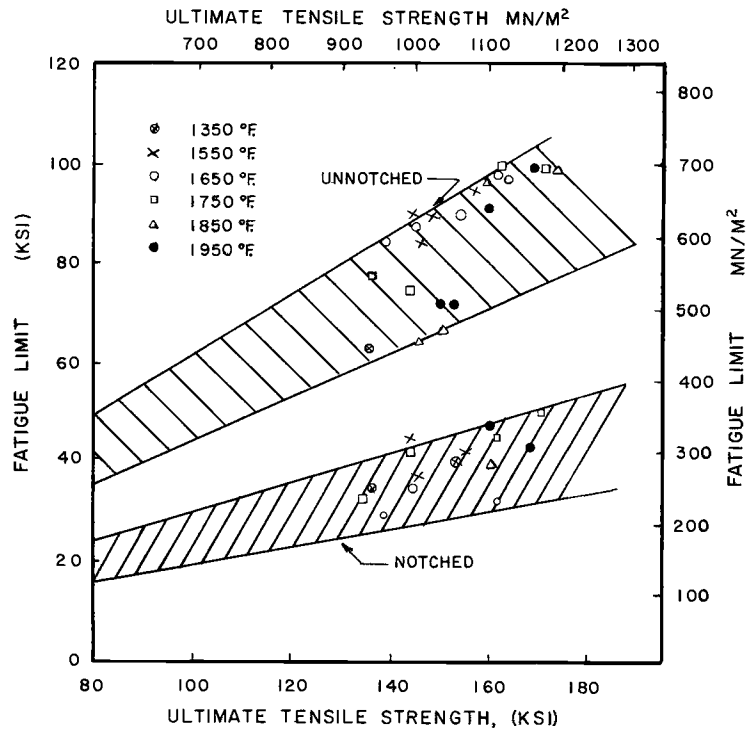

FIG. 8—*Ultimate tensile strength versus fatigue strength.*

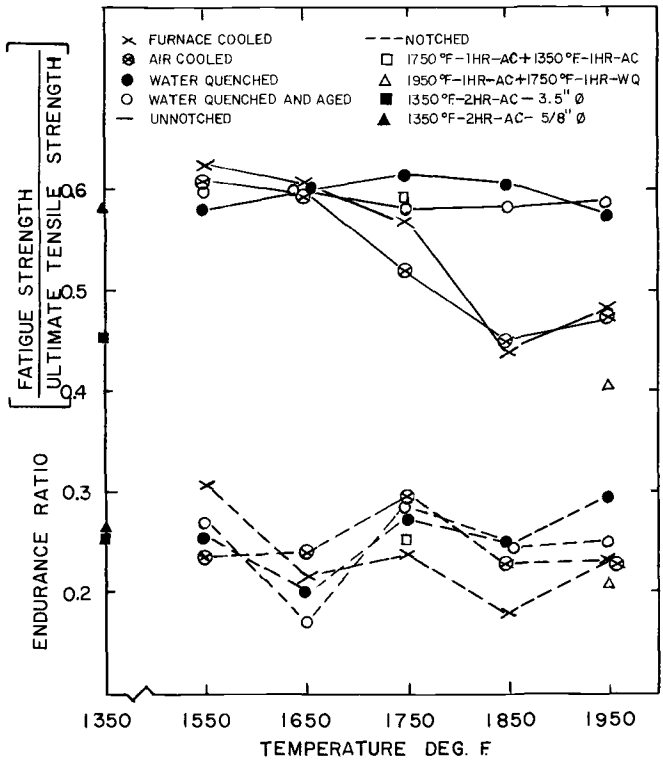

FIG. 9—*Effect of annealing treatment on endurance ratio.*

structures or structures produced by water quenching or quenching and aging can be expected to have endurance ratios between 0.55 and 0.62.

The data included in the upper band also show that fatigue strength generally increases with increasing tensile strength. Weinberg and Hanna [3] observed a similar trend in other titanium alloys. This trend does not appear to hold true for the notched condition as evidenced by the scatter present in the lower band. The notched endurance ratios varied between 0.17 and 0.3.

Figure 9 further illustrates the effect of thermal treatment on the endurance ratios of Ti-6Al-4V. As the temperature was increased from 1550 to 1750 F, the endurance ratio for all unnotched conditions remained quite high. Once the beta transus was exceeded, the endurance ratio of the air-cooled and furnace-cooled conditions dropped sharply to 0.45, while the water-quenched and age-hardened conditions remained at 0.59 to 0.60.

The notched condition again failed to show a trend or relationship of endurance ratio to thermal treatment.

Conclusions

Variations in microstructure were found to alter the tensile and fatigue properties of the Ti-6Al-4V alloy. The best combination of tensile and fatigue properties occurs in material with fine grained alpha-beta structures or in material with microstructures consisting of mixtures of fine primary alpha and martinsitic alpha. Thermal treatments that cause general grain coarsening lower both fatigue strength and endurance ratio (fatigue strength/ultimate tensile strength). Microstructures with martinsitic alpha as the principal phase (produced by beta quenching) exhibit good fatigue strength but have low tensile ductility.

The endurance ratios of all smooth specimens ranged from 0.40 to 0.62 with about 60 percent of the treatments having endurance ratios between 0.58 and 0.62. Beta treatments followed by air cooling or furnace cooling had endurance ratios on the low side of this range, whereas beta quenching, and the majority of the alpha-beta treatments, produced high fatigue strength and endurance ratios between 0.5 and 0.62.

The fatigue strength of the majority of the notched specimens ($K_t = 3.5$) was approximately 50 percent of the unnotched fatigue strength. No significant trends were observed in comparing the notched fatigue data and microstructures.

References

[1] Burklis, J. A., "Metal Removal by Electrochemical Methods and its Effects on Mechanical Properties of Metals," DMIC Report 213, Defense Metals Information Center, Jan. 1965.

[2] Ditmar, C. B., Bauer, G. W., and Evers, D., "The Effect of Microstructural Variables and Interstitial Elements on the Fatigue Behavior of Titanium and Commercial Titanium Alloys," WADC Technical Report No. 56-304, Wright Air Development Center.

[3] Weinburg, J. G. and Hanna, I. E., "An Evaluation of Fatigue Properties of Titanium and Titanium Alloys," TML Report No. 77, Titanium Metallurgical Laboratory, July 1957.